CARBON DIOXIDE SEQUESTRATION MONITORING AND VERIFICATION VIA LASER BASED DETECTION SYSTEM IN THE 2 μm BAND

by

Seth David Humphries

A dissertation submitted in partial fulfillment
of the requirements for the degree

of

Doctor of Philosophy

in

Engineering

MONTANA STATE UNIVERSITY
Bozeman, Montana

September, 2008

© Copyright

by

Seth David Humphries

2008

All Rights Reserved

APPROVAL

of a dissertation submitted by

Seth David Humphries

This dissertation has been read by each member of the dissertation committee and has been found to be satisfactory regarding content, English usage, format, citations, bibliographic style, and consistency, and is ready for submission to the Division of Graduate Education.

Dr. Kevin S. Repasky

Approved for the Department of Electrical and Computer Engineering

Dr. Robert C. Maher

Approved for the Division of Graduate Education

Dr. Carl A. Fox

STATEMENT OF PERMISSION TO USE

In presenting this dissertation in partial fulfillment of the requirements for a doctoral degree at Montana State University, I agree that the Library shall make it available to borrowers under rules of the Library. I further agree that copying of this dissertation is allowable only for scholarly purposes, consistent with "fair use" as prescribed in the U.S. Copyright Law. Requests for extensive copying or reproduction of this dissertation should be referred to ProQuest Information and Learning, 300 North Zeeb Road, Ann Arbor, Michigan 48106, to whom I have granted "the exclusive right to reproduce and distribute my dissertation in and from microform along with the non-exclusive right to reproduce and distribute my abstract in any format in whole or in part."

Seth David Humphries

September, 2008

ACKNOWLEDGEMENTS

I would like to thank Dr. Kevin Repasky for bringing me onto this project, for helping improve my writing skills, for his technical advice, personal example and helping me complete this project. He has put students first. Thank you!
I would also like to thank: Amin Nehrir and Paul Nachman, without both of whom this project would have been more difficult and much duller; Sytil Murphy, for being a big help in the lab; Jerome John Garcia for help getting through the longs days in the field; Erik Carlsten for help keeping my programming skills honed, especially all that MATLAB code; and Laura Dobeck for a superb job in managing and coordinating all the minutia of the field site.
I would also like to express much appreciation to my beautiful wife and our four children. They have given me a lot of their time and support.

Funding Acknowledgment

This work was kindly supported by the Department of Energy under Award No. DE-FC26-04NT42262. However, any opinions, findings, conclusions, or recommendations expressed herein are those of the author(s) and do not necessarily reflect the views of DOE.

TABLE OF CONTENTS

1. INTRODUCTION 1

CO_2 as a Contributor to the Greenhouse Effect 1
Carbon Sequestration 2
Sequestration Monitoring 5

2. THEORY 9

General Molecular Absorption 9
CO_2 Specific Molecular Absorption 13

3. CO_2 DETECTION BY DIFFERENTIAL ABSORPTION (CODDA) INSTRUMENT DETAILS 17

Laser Characteristics 18
Distributed Feedback (DFB) Laser Diodes 19
Diode Packaging 19
Laser Wavelength Tuning Rate 20
Laser Beam Divergence 21
Optical Power 22
Instrumentation 22
Laser Path 24
Data Acquisition 26
Data Analysis 27
CODDA Instrument Proof of Concept 29
Instrument Calibration 30
Instrument Conclusion 34

4. INITIAL OUTDOOR MEASUREMENTS 35

ZERT Field Specifications 35
Field Description 35
Investigated Techniques 37
Vertical Well Installation 38
ZERT Vertical Injections 38
First Vertical Well Injection 38
Second Vertical Well Injection 40
Initial Outdoor Conclusion 41

TABLE OF CONTENTS – CONTINUED

5. 2007 FIELD RELEASE 42

Instrument Improvements 42
Laser Mount 42
Laser Collimation 43
Detectors 48
Larger Optics 51
Moving Mirror Mounts 51
ZERT Horizontal Injections 2007 52
ZERT Horizontal Injection Well Description 52
ZERT Horizontal Injection, July 2007 53
ZERT Horizontal Injection, August 2007 54
Horizontal Release Conclusion 56

6. 2008 FIELD RELEASE 58

Instrument Improvements 58
Detector 59
Retro Reflector 59
Diode Mount 60
Data Collection Method 60
Background Measurements 61
Instrument Weatherization 62
ZERT Horizontal Injections 2008 64
Preliminary Measurements and Results 64
Measurements During the Injection 64
Horizontal Release Results 2008 68
Horizontal Release 2008 Conclusion 72

7. CONCLUSION 75

Instrument Results 75
Future Work 76

REFERENCES CITED 78

APPENDICES 84

APPENDIX A: Wedge Details 85
APPENDIX B: External Drawings and Schematics 89

TABLE OF CONTENTS – CONTINUED

APPENDIX C: Analysis Algorithms 104

LIST OF TABLES

Table Page

1 Molecular data from Hitran database. 15

2 Characteristics of the laser diode. Information provided by NanoPlus, GmbH. 18

LIST OF FIGURES

Figure Page

1 Plot of data analyzed from Antartica ice core samples. 2

2 Monthly average carbon dioxide concentration measurements taken continuously from 1958 to the present from several observatories around the globe. The black dots represent actual data measurements while the black lines are curve fittings to the data. The monitoring sites are located at the South Pole (SPO), Samoa (SAM), Christmas Island (CHR), Mauna Loa, Hawaii (MLO), La Jolla, California (LJO), and Point Barrow, Alaska (PTB)..... 3

3 Eddy covariance flux tower setup at a field site maintained by researchers at Montana State University. The picture is courtesy of graduate student Diego Riveros-Iregui of the Land Resources and Environmental Sciences (LRES) Department at MSU. 7

4 Transmission of light as a function of wavelength near 2 μm..... 14

5 Transmission of light as a function of wavelength at 2 μm. This is a version of fig 4, zoomed in at the desired operating wavelength. The line strength and line width values for each labeled absorption feature are found in table 1 on page 15. 16

6 Transmission as a function of laser path length (a) and as a function of ambient CO_2 concentration (b)..... 16

7 Tuning the 2 μm laser through a glass window to measure the temperature tuning rate. 20

8 Measurements made to calculate the laser beam divergence angle in both horizontal and vertical directions. 21

9 Voltage output of the reference detector as a function of laser drive current. 23

10 Picture of the CODDA Instrument optical and electronics setups. The picture was taken in the field during one of the controlled releases in the summer of 2007. The instrument is sitting in firing position, ready to take data. 23

11 Schematic of the CODDA Instrument layout and setup. 25

12 Transmission spectra through the 2 μm filters as a function of wavelength. Data taken with an FTIR by Dr. Laura Dobeck. 27

LIST OF FIGURES – CONTINUED

Figure Page

13 Laser scan taken after the instrument was first built. The measured data, the solid black line, is plotted with data from the HITRAN model, dashed red line, for comparison. The molecule that causes each particular absorption features is labeled. 29

14 Series of laser tuning scans taken over a few hours to demonstrate that the laser can be tuned repeatably yielding the same results in a lab environment. 30

15 The laser instrument was left over night in the lab to take data to test repeatability and robustness of the data taking method. 32

16 Schematic of the instrument calibration layout and setup. 32

17 Measured scans taken through the calibration chamber at three different CO_2 concentrations. 33

18 Calculated and measured concentrations as a function of transmission. ... 34

19 Satellite image of the field used by the ZERT experiment with well locations indicated. Courtesy of Dr. Laura Dobeck and google maps. 36

20 Picture of the field release site taken on the 28^{th} of September 2006. The tank containing the CO_2 used for the injection is visible in the background. In the center of the picture is the wood box containing the instrument, and also visible is the large shade used for protection from the sun. 39

21 Data measured on the 28^{th} of September 2006. Scans were captured with the laser passing over the well head and with the laser path rotated 90^o to the previous measurement. The analysis results from some of the absorption features are displayed. 39

22 Data taken on the 6^{th} of October 2006. Scans were captured with the laser passing over the well head and with the laser path rotated 90^o to the previous measurement. 41

23 Picture taken of the laser diode mounted to the optical breadboard in the bottom middle of the picture. Also visible is the structure used to hold the collimation lens. 43

24 A picture of the 2 μm laser beam taken by the pyro-electric camera at a distance of 24 cm from the instrument. The laser was collimated using the 20 mm, F/1 lens 44

LIST OF FIGURES – CONTINUED

Figure Page

25 A picture of the 2 μm laser beam taken by the pyro-electric camera at a distance of 69 cm from the instrument. The laser was collimated using the 20 mm, F/1 lens 45

26 A picture of the 2 μm laser beam taken by the pyro-electric camera at a distance of 474 cm from the instrument. The laser was collimated using the 20 mm, F/1 lens 46

27 A picture of the 2 μm laser beam taken by the pyro-electric camera. The laser was collimated using the 25.4 mm aspheric lens at a distance of 23 cm from the instrument box..... 46

28 A picture of the 2 μm laser beam taken by the pyro-electric camera. The laser was collimated using the 25.4 mm aspheric lens at a distance of 74 cm from the instrument box..... 47

29 A picture of the 2 μm laser beam taken by the pyro-electric camera. The laser was collimated using the 25.4 mm aspheric lens at a distance of 472 cm from the instrument box. 48

30 Detector responsivity as a function of wavelength. This responsivity was measured at Judson before the detectors were shipped to MSU. The responsivity of the three detectors used are assumed to be close enough to have only negligible differences. The approximate operating wavelength of the DFB laser is shown by the dashed vertical line. 49

31 A plot of laser diode scan taken with the two 0.5 mm diameter detectors from Judson. The scan (red dashed line) was taken in the lab and more closely matches the hitran model (black solid line) then did data collected using previous detectors. This is seen in figure 13 on page 29, figure 14 on page 30 & figure 15 on page 32 as a difference of over 5% and now less than 1%. 50

32 Results of analyzing the scan taken before, during and after the first release through the horizontal injection well. 54

33 A typical scan capture by CODDA for use in finding CO_2 in the air. This scan, while there is some noise, it is easily analyzed and gives good results. 55

LIST OF FIGURES – CONTINUED

Figure Page

34 The black line represents the results of analyzing the scans taken over the well before, during and after the seconds release through the horizontal injection well. The dashed red line is results of the data taken away from the injection well. 55

35 Photo of the CODDA instrument in the lab showing the translation stage used to direct the laser beam in two alternating directions for the 2008 field experiment. 61

36 Plot of the CO_2 measured raw data prior to the controlled release experiment. 63

37 Plot of the H_2O measured raw data prior to the controlled release experiment. The H_2O concentration results are used to validate instrument functionality and multi-direction independency. 63

38 Photo of the CODDA instrument in measurement location for the ZERT field CO_2 injection of 2008. 65

39 Plot of the CO_2 measured raw data immediately prior to the controlled release experiment. 65

40 Data taken during the release experiment in 2008. The data is plotted with rain marked as the light blue vertical lines. Thanks to Jennifer Lewicki for the rain information 67

41 Smoothed data, using a +/-40 point moving average, taken during the release experiment in 2008. The data is plotted with rain marked as the light blue vertical lines. Thanks to Jennifer Lewicki for the rain information 69

42 Plot of the CO_2 measured smoothed data and weather information around the time the CO_2 injection was started. 70

43 Plot of the CO_2 measured smoothed data and weather information during the CO_2 injection. 70

44 Plot of the CO_2 measured smoothed data and weather information during the CO_2 injection. 71

45 Plot of the CO_2 measured smoothed data and weather information around the time the CO_2 injection was stopped. 71

LIST OF FIGURES – CONTINUED

Figure Page

46 Plot of scan measured over the injection well suring the controlled release. These demonstrate that the large changes in measured CO_2 concentrations are real events. 72

47 Data taken during the release experiment in 2008 with the moving average applied. Note that during the entire release the water vapor concentrations in both directions, over the injection pipe and away from the pipe, are the same. This measurement is closer to the ground, about 10 cm, than the weather station, about 1.5m, so the water vapor concentration measured by CODDA is higher 73

48 Detailed drawing of incident light transmission through and reflections off of a glass wedge. 87

49 Drawing of the TO-8 can holding the DFB laser diode which is mounted on the TEC 91

50 Drawing of the laser mount used to hold the laser diode. The mount has an internal TEC that holds the temperature of the DFB laser diode more stable. 92

51 Drawing and specifications for the Judson 2.2 μm detector mount. 94

52 Drawing and specifications for the TEC controller that is mounted with the Judson 2.2 μm detector. 95

53 Judson 2.2 μm detector sapphire window coating information. 96

54 Drawing of the mount for the focusing lens. 97

55 Drawing of the mount for the filter. 98

56 Manufacturer information about the first 5 inch retro-reflector. 100

57 Manufacturer information about the second 5 inch retro-reflector. 101

58 Anti-Reflection coatings on spherical, F/1, 20 mm collimation lens. 103

59 MATLAB GUI screenshot performing a scan. 106

60 MATLAB GUI screenshot performing a scan. 106

61 MATLAB GUI screenshot performing a scan. 107

62 MATLAB GUI screenshot of a completed scan. 107

LIST OF FIGURES – CONTINUED

Figure Page

63 MATLAB GUI screenshot of a completed scan. 108
64 MATLAB GUI screenshot of a completed scan. 108
65 MATLAB GUI screenshot of a completed scan. 109
66 MATLAB GUI screenshot of plotted temperature measurements. 109
67 MATLAB GUI screenshot of plotted CO_2 concentration measurements. 110
68 MATLAB GUI screenshot of plotted CO_2 concentration measurements. 110

ABSTRACT

Carbon Dioxide (CO_2) is a known contributor to the green house gas effect. Emissions of CO_2 are rising as the global demand for inexpensive energy is placated through the consumption and combustion of fossil fuels. Carbon capture and sequestration (CCS) may provide a method to prevent CO_2 from being exhausted to the atmosphere. The carbon may be captured after fossil fuel combustion in a power plant and then stored in a long term facility such as a deep geologic feature.

The ability to verify the integrity of carbon storage at a location is key to the success of all CCS projects. A laser-based instrument has been built and tested at Montana State University (MSU) to measure CO_2 concentrations above a carbon storage location. The CO_2 Detection by Differential Absorption (CODDA) Instrument uses a temperature-tunable distributed feedback (DFB) laser diode that is capable of accessing a spectral region, 2.0027 to 2.0042 μm, that contains three CO_2 absorption lines and a water vapor absorption line. This instrument laser is aimed over an open-air, two-way path of about 100 m, allowing measurements of CO_2 concentrations to be made directly above a carbon dioxide release test site.

The performance of the instrument for carbon sequestration site monitoring is studied using a newly developed CO_2 controlled release facility. The field and CO_2 releases are managed by the Zero Emissions Research Technology (ZERT) group at MSU. Two test injections were carried out through vertical wells simulating seepage up well paths. Three test injections were done as CO_2 escaped up through a slotted horizontal pipe simulating seepage up through geologic fault zones. The results from these 5 separate controlled release experiments over the course of three summers show that the CODDA Instrument is clearly capable of verifying the integrity of full-scale CO_2 storage operations.

INTRODUCTION

CO_2 as a Contributor to the Greenhouse Effect

A greenhouse gas is defined as a gas that allows short-wave radiation (visible light) to pass through it but absorbs long-wave radiation (thermal energy or infrared (IR) light). The concentration of carbon dioxide (CO_2), a known greenhouse gas [1, 2], in the atmosphere is $\sim$0.04% which is commonly written as $\sim$400 parts per million (ppm). Monitoring the changes to this small amount of CO_2 is very important in understanding the radiative forcings of the climate system resulting from natural and anthropogenic changes of atmospheric CO_2 concentration [2].

Atmospheric temperatures and concentrations of CO_2 can be calculated using sampling techniques involving ice cores taken from Antarctica [3, 4, 5]. This data tracks changes in CO_2 concentrations as well as changes in ambient temperatures for several hundred thousand years [6, 7]. Analysis of the ice core data shows a link to and a delayed effect on the average atmospheric temperatures due to changes in atmospheric CO_2 concentrations [8, 9]. Figure 1 on the following page is a plot of the CO_2 concentrations using the ice core data [10, 7].

In our own time period, the atmospheric concentrations of CO_2 have been continuously monitored since 1958 at the Mauna Loa Observatory in Hawaii [11]. The monthly average atmospheric concentration of CO_2 in the air has increased from 315 ppm in 1958 to 382 ppm in 2007, an increase of over 20%. Figure 2 on page 3 shows the atmospheric concentrations of CO_2 from several observation sites located around the globe. All the locations show the same upward trend in the concentration of atmospheric CO_2 [12]. The data in figure 2 on page 3 also show cyclic, seasonal variations superimposed on top of that steady increase. The link between increasing

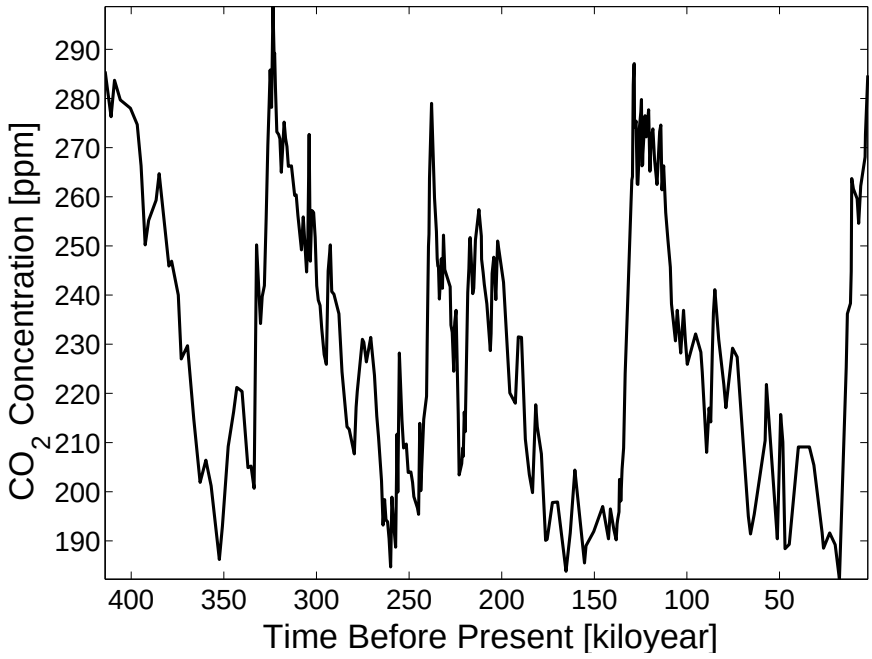


Figure 1: Plot of data analyzed from Antartica ice core samples [10].

atmospheric CO_2 concentrations and increased average temperatures established by the ice core data implies that the current increase in atmosphere CO_2 concentrations will lead to an increase in average global temperatures [13, 14, 15, 16].

Carbon Sequestration

The increasing concentration of CO_2 in the atmosphere is largely attributed to the burning of fossil fuels combined with deforestation [2, 17]. Annual total CO_2 emissions from burning fossil fuels increased from about 23.5 Gigatons of CO_2 per year ($GtCO_2$/yr) in the 1990s to about 26.4 $GtCO_2$/yr from 2000 to 2005, an increase of over 12% [18]. There is a large international movement of growing concern that the increase in CO_2 is significantly altering the global climate and environment [19, 20, 14, 13, 2, 17, 15, 6]. As a result, concerted efforts are now underway to curb

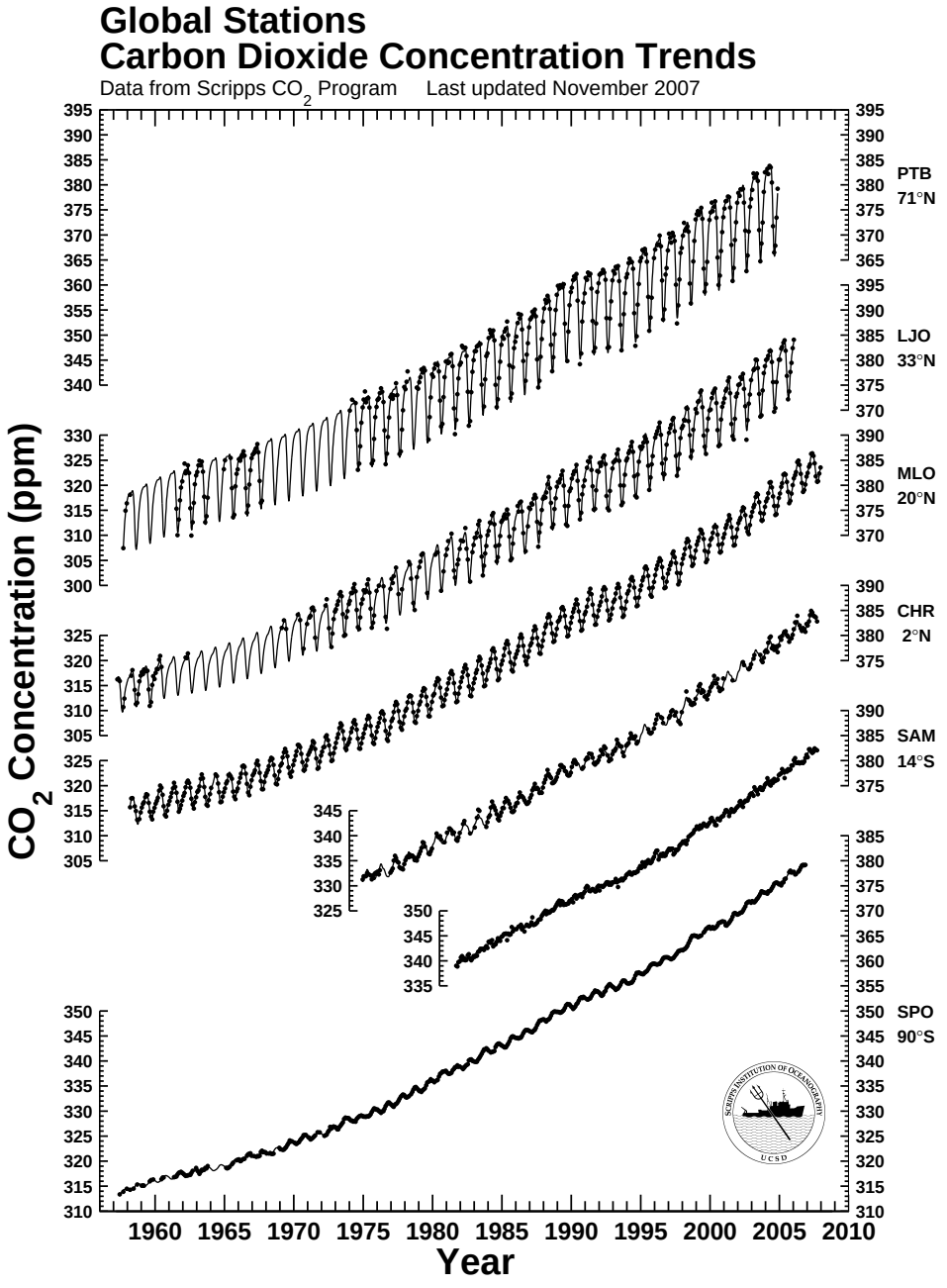


Figure 2: Monthly average carbon dioxide concentration measurements taken continuously from 1958 to the present from several observatories around the globe. The black dots represent actual data measurements while the black lines are curve fittings to the data. The monitoring sites are located at the South Pole (SPO), Samoa (SAM), Christmas Island (CHR), Mauna Loa, Hawaii (MLO), La Jolla, California (LJO), and Point Barrow, Alaska (PTB) [12].

the increase in CO_2 concentrations in the atmosphere. These efforts are in such fields as conservation and energy efficiency, development of renewable energy sources, development of nuclear energy, coal to gas substitution, and carbon capture and sequestration (CCS) [21, 22, 1, 23, 24].

The idea of carbon capture and storage is to capture the CO_2 that comes from the burning of fossil fuels before it is released into the atmosphere [23]. The CO_2 is then liquefied for pumping and storage. This process effectively removes the CO_2 from the atmosphere [1, 23, 24, 25]. Some of the best known sites for CCS are those that have already held fossil fuels for long periods of time [26] such as depleted oil wells, deep unmineable coal seams, or deep saline formations or aquifers [27]. Carbon storage potentials in geologic sites have been estimated to have a maximum capacity of 1680 Gt/CO_2 [23, 24, 25].

Initial experimental work in CCS is underway with three industrial scale projects. These projects include the Sleipner Saline Aquifer Storage Project [28, 27], the In Salah Gas Project [29, 27], and the Weyburn Project [30, 31, 27]. The Sleipner Saline Aquifer Storage Project stores 1 Mton/yr of CO_2 and stores it in a deep subsea brine-filled sandstone formation deep beneath the North Sea [28, 27]. The In Salah Gas Project, which began in 2004, is currently storing 1 Mton/yr of CO_2 in a depleted gas field in the Algerian desert [29, 27]. A third project, at the Weyburn oil field located in Saskatchewan, Canada, is using CO_2 injection for both enhanced oil recovery (EOR) and also for carbon storage [30, 31, 27]. The CO_2 used in this third project is captured by the Dakota Gasification Plant located in North Dakota which produces between 6 Mtons/yr to 10 Mtons/yr of CO_2 [30, 31, 27]. Several smaller pilot projects for CO_2 storage are also under investigation [1, 27].

Sequestration Monitoring

The temperatures and pressures associated with geologic sequestration cause the CO_2 to be in a supercritical state. In this state, the CO_2 is buoyant [32]. If the CO_2 leaks from storage sites, the benefits of CCS in terms of reduced levels of atmospheric CO_2 is lost [33, 34, 35]. The three main causes of leakage include leaking injection wells, leakage from improperly sealed abandoned wells, and leakage through geologic faults and fractures [36, 35, 32, 33]. Initial studies of geologic storage sites indicate that for carbon storage to be effective and realistic seepage rates must be between 0.1% and 0.01%/yr [36]. Thus an important issue for the successful storage of CO_2 is the ability to monitor geologic sequestration sites for leakage, to verify site integrity.

The concentration of CO_2 that is due to leakage from a sequestration site may be calculated. For this calculation the Weyburn project will be used. It is currently storing nearly 10 Mtons/yr of CO_2 [30, 31, 27]. Further, the calculation will use the assumption that the sequestration site allows the CO_2 to seep out uniformly over a single square kilometer and the smallest expected seepage rate. After a primary conversion from years and from tons this yields 28.81 g/(sec km^2).

Converting this result to cm^2 and using Avogadro's number to calculate the number of atoms yields 3.943×10^{13} atoms/(sec cm^2). Using Loschimdt's number the above result is converted to a diffusion speed, yielding 1.5904×10^{-4} (m atm)/sec.

This is the diffusion speed of the carbon dioxide molecules as they diffuse away from the soil surface. The diffusion rate is assumed to be the same as the ambient wind. An average ambient wind at the soil surface is about 1.0 m/s (about 2.2 mph). Using this value and converting yields 1.5904 ppm.

This is the concentration of CO_2 expected above a 10 Mton/yr sequestration site with a seepage rate of 0.01%. The Weyburn site is a small-scale sequestration site,

with full-scale sequestration sites expected to store as much as 1 Gton/yr. If the larger seepage rate is also assumed, a worse scenario, the resulting CO_2 concentration over a uniform square km is 1590.4 ppm.

Due to heterogeneity of the subsurface geologic formation and of the soil, it is not likely that the CO_2 seepage will be uniform. What is more likely is that the CO_2 will emerge in concentrated plumes. Thus the concentrations calculated above should be considered as lower bounds on what concentrations to expect.

Several instruments and techniques have been proposed for monitoring carbon sequestration sites. Some of those techniques involve tracers, satellite observations, soil CO_2 flux, eddy covariance, soil resistivity, soil permeability, water table sampling, carbon isotope tracking, plant stress through hyperspectral and multispectral imaging and differential absorption. Some of these techniques are based on direct detection of CO_2 using optical techniques. Optical detection techniques are based on the fact that CO_2 absorbs light at specific wavelengths and the amount of absorbed light can be used to determine the CO_2 concentration. Instruments measuring CO_2 that are based on optical detection techniques include soil gas chambers [37], satellite technology [37], eddy-covariance measurements [38, 39, 40], flux chamber measurements [41], and tunable laser differential absorption measurements [42].

Each detection method has advantages and disadvantages in terms of implementation on the kind of scale needed for sequestration site monitoring. Soil gas chambers are point sensors and the data between chamber measurements must be assumed. Heterogeneity of the soil, even within the same field, can cause large errors in those assumptions leading to an incorrect picture of CO_2 concentrations as a function of position [37]. Eddy covariance flux towers, such as the one seen in figure 3 on the next page, have a foot print that is dependant on the height of the tower, wind speed and wind direction [37]. These towers measure an integrated amount of the CO_2 inside the

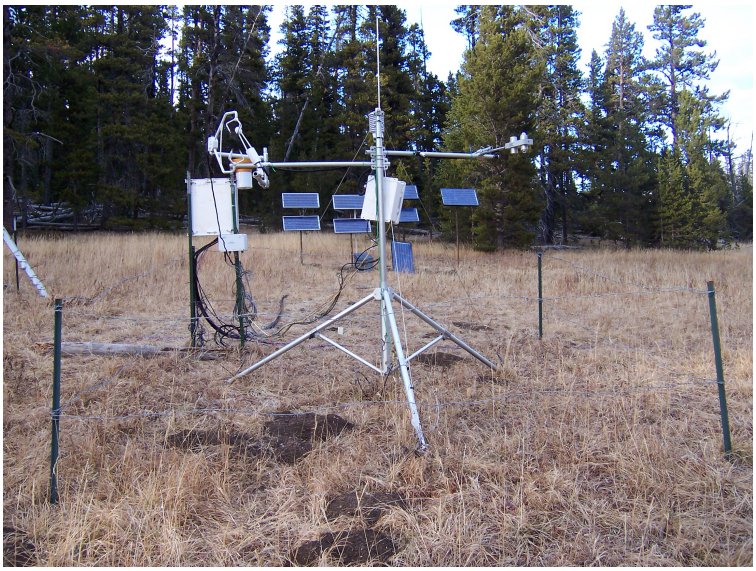


Figure 3: Eddy covariance flux tower setup at a field site maintained by researchers at Montana State University. The picture is courtesy of graduate student Diego Riveros-Iregui of the Land Resources and Environmental Sciences (LRES) Department at MSU.

footprint. Issues associated with ground slope, vegetation canopy heterogeneity, and wind velocity can cause errors in the calculations [37]. Satellite-based measurements yield details on a kilometer or larger scale, but the details of changes on a smaller scale are lost [37]. A new type of sensor is needed that can accurately cover a large detection range or area (1 km^2) while not losing the small scale (1 m range) information.

A differential absorption instrument was built and tested at Montana State University (MSU) that measures CO_2 molecular concentrations in the atmosphere. It has been named the CO_2 Detection by Differential Absorption (CODDA) Instrument. The instrument directs the laser along an open air path to a corner cube mirror, which reflects the light back to the instrument. From the normalized ratio of the returning optical power to the outgoing optical power, the molecular concentration of a given species is calculated. This instrument is capable of accurately measuring path-integrated CO_2 concentrations along the laser path.

This dissertation will discuss details and characteristics of the CODDA Instrument starting with theoretical considerations regarding molecular absorption and specifically CO_2 absorption. Discussion will then center on specifics to the instrument, how measurements are made, instrument operation and laboratory calibration. Incremental steps of the instrument from initial stages to field development and then field deployment will be discussed in the latter chapters in this dissertation. Field deployments at the controlled release test facility operated by the Zero Emissions Research Technologies (ZERT) group and results from those measurements will be presented. The results from the ZERT facility are important to establish the sensitivities of the instrument for monitoring injection well locations. The measurements from the CODDA Instrument will be compared with results from other instruments that have taken CO_2 concentration measurements at the controlled release field site. This dissertation will then conclude with remarks about the results and possible directions for future work with this system.

THEORY

General Molecular Absorption

The CO_2 Detection by Differential Absorption (CODDA) Instrument will be used to measure the normalized atmospheric transmission as a function of wavelength as the laser source is tuned across CO_2 absorption features. The normalized atmospheric transmission measurements can then be used to determine the atmospheric concentration of CO_2. Presented in this section is the theory used to connect the normalized transmission measurements with the atmospheric CO_2 concentrations [43].

A model has been developed by the U.S. Air Force Research Lab (AFRL) to describe, at high spectral resolution, molecular transmission through the atmosphere, which is named HITRAN [44]. The HITRAN model accurately describes absorption by various atmospheric molecules, including CO_2. Throughout this section and in this dissertation, measured data and results will be compared to this model.

The normalized optical transmission, T, for monochromatic light passing through a given path length, L, can be found using

$$T = \frac{I}{I_0} = e^{-\alpha L} \tag{1}$$

where I is the optical intensity after traveling a path of length L, I_0 is the optical intensity at the beginning of the path, and α is the absorption per unit length, which is also referred to as the linear absorption coefficient and has units of [1/cm].

Each individual absorption feature is described by a unique linear absorption coefficient, α, that can be written as

$$\alpha = S\ N(T_a, P)\ g(\nu - \nu_0) \tag{2}$$

where S is the molecular line intensity and includes information about the partition function of the molecule, the quantum mechanics of the state transition and the Boltzmann population factor. Values for the line intensity, S, with units of length per molecule [cm/molecule], are listed in the HITRAN database for many molecules of interest [44]. N is the number density of the molecule of interest with units of [molecule/cm^3] and is a function of both ambient temperature and barometric pressure. $g(\nu - \nu_0)$ is the normalized lineshape and has units of length [cm]. The ν is the optical wavenumber in cm^{-1} and ν_0 is the optical wavenumber at line center for a specific absorption resonance [44].

There are three different types of lineshapes. The first lineshape type accounts for pressure broadening and is Lorentzian. This is described by

$$g_p(\nu - \nu_0) = \frac{\gamma_p/\pi}{\left[(\nu - \nu_0)^2 + \gamma_p^2\right]} \tag{3}$$

where γ_p is the half-width at half-maximum (HWHM) of the absorption feature. Pressure broadening is the widening in frequency of the molecular transition from a sharp transition, delta function, due to collision of the species molecule with molecules in the air. For example, from the HITRAN database the transition for CO_2 due to pressure broadening at 2003.5 nm is found to be 28.9 pm, or 2.16 GHz, wide at half-width at half-maximum (HWHM) [44]. HITRAN actually provides values of $2 * \gamma_p$, the full-width at half-maximum (FWHM).

The second lineshape type accounts for Doppler broadening and has a Gaussian profile described by

$$g_D(\nu - \nu_0) = (1/\gamma_D)\left(\frac{\ln 2}{\pi}\right)^{0.5} e^{\left[-ln(2)\left(\frac{\nu-\nu_0}{\gamma_D}\right)^2\right]} \tag{4}$$

where γ_D is the HWHM of the absorption feature associated with Doppler broadening. This accounts for the broadening due to the thermal movements of the molecules and at temperature of interest (275 to 310 K) the HWHM is about 125 MHz for transitions near 2 μm. Since this is much less than the broadening due to the pressure, the Doppler broadening effect will not be considered hereafter. As a side note, the frequency *shift* due to a Doppler shift for a 30 MPH (13.4 m/s) wind is less than 7 MHz, so this effect is also negligible.

The third lineshape type is a Voigt profile and is a composite or convolution of the two previous profiles. Since the Doppler broadening is negligible here compared to the pressure broadening, the convolution of the two will essentially yield just the pressure-broadened profile. Hence, in further equations and treatments only the equation describing the pressure broadening (eq. 3 on the preceding page) will be used.

If the calculation is restrained to the wavelength where the maximum absorption occurs, $\nu = \nu_0$, then equation 3 on the previous page becomes

$$g_p(\nu = \nu_o) = \frac{1}{\pi\gamma_p} \tag{5}$$

Due to this restriction, T is defined as the optical transmission at line center of the molecular absorption feature, which is the minimum transmission.

The factor $N(T_a, P)$, from equation 2 on page 9, scales with temperature and pressure and may be written as

$$N(T_a, P) = N_L \; P_a \; \frac{T_s}{T_a} \tag{6}$$

where N_L is Loschmidt's number which has the value of $2.479{\times}10^{19}$ and has units of molecules per (cm^3 atm). P_a is the partial pressure [atm] of the molecule of interest. T_s is equivalent to 296 Kelvin [K] and T_a is the ambient temperature in Kelvin.

The total number density of all molecules in the air may be written as

$$N(T_a, P)_{total} = N(T_a)P_t \tag{7}$$

where P_t is the total barometric pressure [atm]. Using the same idea, the number density, $N(T, P)$, of the molecules of interest can be written as $N(T_a, P) = N(T_a)P_a$ where P_a is the partial pressure of the species of interest [atm]. Thus the concentration of the molecule of interest, in units of parts per million [ppm], can be written as

$$C = 10^6 \ \frac{N(T_a, P)}{N(T_a, P)_{total}} = 10^6 \ \frac{P_a}{P_T} \tag{8}$$

It is desired to have the concentration, C, as a function of transmission, T. Equation 8 may then be solved for T by several substitutions. Solving equation 1 on page 9 for α yields

$$\alpha = \frac{-\ln(T)}{L} \tag{9}$$

Substituting equation 9 into equation 2 on page 9 and solving for $N(T_a, P)$ yields

$$N(T_a, P) = \frac{\ln(1/T)}{S \ g_p(\nu = \nu_0) \ L} \tag{10}$$

Substituting equation 6 on the previous page into equation 10 and solving for P_a leads to

$$P_a = \frac{\ln(1/T)}{S \ g_p(\nu = \nu_0) \ L \ N_L \left(\frac{T_s}{T_a}\right)} \tag{11}$$

Finally the molecular concentration of interest, equation 12, may be found by substituting equation 11 into equation 8. Then substituting into equation 5 on the preceding page and simplifying yields

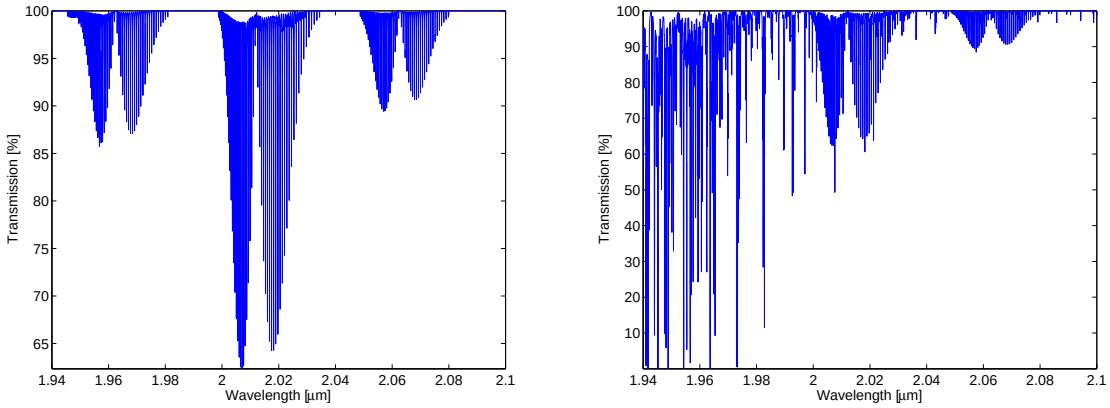
$$C = \frac{10^6 \ \pi \ \gamma_p \ T_a \ \ln(1/T)}{T_s \ L \ N_L \ P_T \ S} \tag{12}$$

Equation 12 on the previous page is used to calculate single species concentrations from a measured transmission spectrum at line center. The calculated concentration per species is dependent on the ambient temperature, barometric pressure and the path length. Independent measurements of T_a, P_T and L should be made prior to performing the calculation.

CO_2 Specific Molecular Absorption

Strong absorption bands for the CO_2 molecule corresponding to different vibrational transitions are found around 2 μm, 5.6 μm, and 10 μm [45, 46]. The band around 2 μm, seen in figure 4 on the following page, was chosen for this application largely because of the desired line strength (amount of transmission for a given path length) and also the lack of overlapping absorption features from other molecules. A laser in this range was found that operates at a nominal wavelength of 2.004 μm and can be tuned over several CO_2 absorption features. The CO_2 absorption features near 2 μm are plotted in figure 4(b). Absorption due to all atmospheric molecules for the same wavelength range as used in figure 4(a) are plotted in figure 4(b). The CO_2 absorption features near the operating wavelength of the tunable laser used for the CODDA Instrument are plotted in figure 5(a) on page 16, while the absorption features for all molecules in this same wavelength range are plotted in figure 5(b).

To understand how the inputs into α in equations 1 & 2 on page 9 affect the total transmission and thus the resulting CO_2 concentration, two plots were made. The first plot is to show the effect that changing the total path length has on the overall transmission. This was done for the CO_2 absorption lines at the wavelengths of 2.00110 μm, 2.00402 μm, and 2.00496 μm. For this a total pressure of 1 atm, an ambient temperature of 296 K, and a concentration of 381 ppm were assumed.



(a) Absorption from only CO_2

(b) Absorption from all molecules

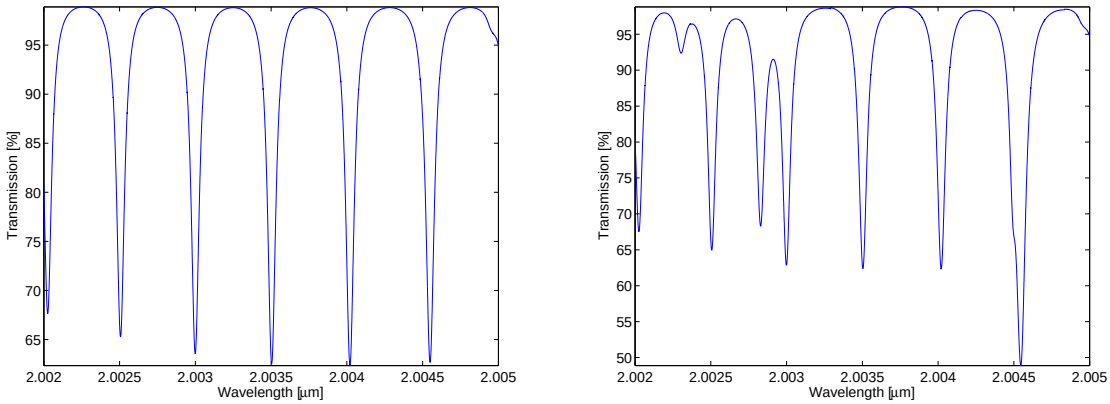
Figure 4: Transmission of light as a function of wavelength near 2 μm.

Using the values given in table 1, a value for the absorption per unit length, α, of 8.89×10^{-4} m^{-1}, 1.36×10^{-3} m^{-1}, and 1.99×10^{-5} m^{-1} were calculated, respectively, for the absorption features [47]. The results are shown in figure 6(a) on page 16.

The second plot, figure 6(b) on page 16, shows the effect that changing the CO_2 concentration has on the total transmission. This is to demonstrate the accuracy that will be needed by the instrument relative to changes in CO_2 concentration. This calculation was performed for the single absorption feature at 2.00402 μm and for three different path lengths (100 m, 200 m, and 500 m). A total pressure of 1 atm and an ambient temperature of 296 K were assumed. The plot in figure 6(b) on page 16 shows that when the carbon dioxide concentration changes from an initial ambient concentration of 381 ppm to 391 ppm, for the 500 m path length, a 1% decrease in transmission will result. For the 200 m path this change is to 398 ppm for the same 1% decrease in transmission and 399 ppm for the 100 m path. This indicates that if the instrument is capable of measuring changes in transmission of 1%, an instrument sensitivity of 11 ppm for a 500 m path length, 17 ppm for 200 m, and 18 ppm for 100 m will result [47].

Table 1: Molecular data from Hitran database.

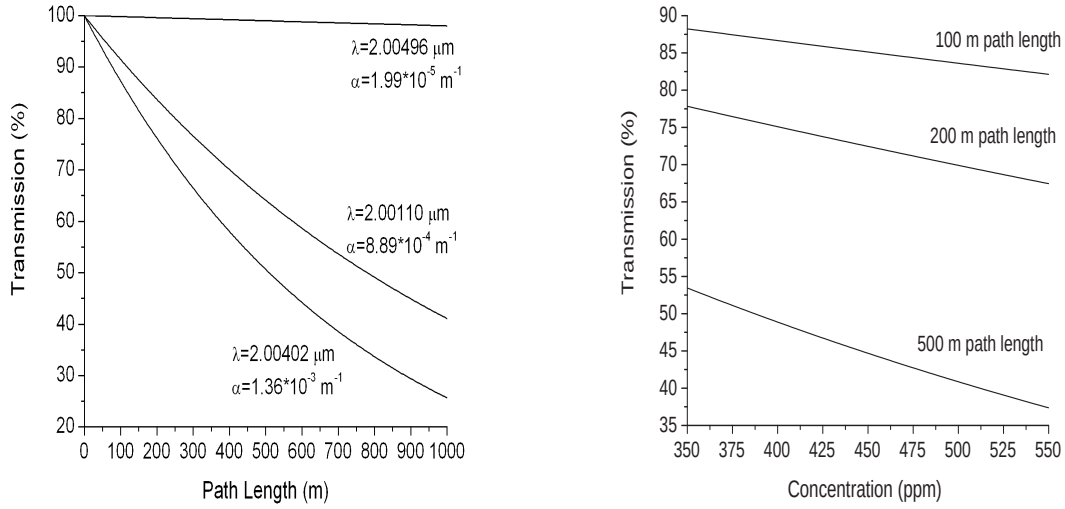
Molecule	Feature labeled in figure 5(b)	Wavelength λ [μm]	Line Intensity S [cm/molecule] $\times 10^{21}$	Normalized Lineshape $g_p(\nu = \nu_0)$ [cm]
CO_2		2.00110	0.81120	5.59420
H_2O		2.00122	0.01370	5.26567
H_2O		2.00128	0.00066	21.93728
H_2O		2.00133	0.00023	22.58318
CO_2		2.00156	0.93160	5.55515
CO_2	a	2.00203	1.04800	5.50233
H_2O	b	2.00230	0.00976	3.65663
CO_2	c	2.00251	1.15300	5.45518
H_2O	d	2.00283	0.04490	5.11341
CO_2	e	2.00300	1.24100	5.38595
H_2O		2.00347	0.00071	6.25363
CO_2	f	2.00350	1.30200	5.31846
CO_2	g	2.00402	1.33200	5.23106
CO_2		2.00449	0.01618	5.66892
H_2O	h	2.00449	0.01909	6.65433
H_2O		2.00453	0.00608	6.81971
H_2O	h	2.00454	0.02319	4.64347
CO_2		2.00455	0.01463	5.67903
CO_2	i	2.00455	1.32200	5.13817
CO_2		2.00494	0.01969	5.64379
CO_2		2.00497	0.01796	5.65382
CO_2		2.00509	1.27000	5.03655
H_2O		2.00527	0.00584	4.57671
CO_2		2.00540	0.02162	5.63879
CO_2		2.00541	0.02350	5.61393
H_2O		2.00553	0.00175	4.38746
CO_2		2.00564	1.17300	4.92740



(a) Absorption from only CO_2

(b) Absorption from all molecules

Figure 5: Transmission of light as a function of wavelength at 2 μm. This is a version of fig 4, zoomed in at the desired operating wavelength. The line strength and line width values for each labeled absorption feature are found in table 1 on the previous page.



(a) Transmission vs Path Length

(b) Transmission vs Concentration

Figure 6: Transmission as a function of laser path length (a) and as a function of ambient CO_2 concentration (b).

17

CO_2 DETECTION BY DIFFERENTIAL ABSORPTION (CODDA) INSTRUMENT DETAILS

Given the theory of molecular absorption from Chapter 2 on page 9, an instrument may be built that utilizes a particular absorption feature to detect a given molecular species. This has been done previously by measuring the amount of absorption at line center of the absorption feature and then measuring the absorption away from the feature. This technique is sometimes used in lidar systems and is referred to as a Differential Absorption Lidar (DIAL) System. Work using DIAL systems has been done at Montana State University for range-resolved atmospheric measurements of water vapor [48].

While this technique is useful and also yields range information, it is not suitable for the requirements of carbon sequestration monitoring. For the monitoring and well integrity verification a measurement is needed that is horizontal to the ground and for this purpose concentration information is much more important than range information. Since the ranging information is not necessary, a non-pulsed or continuous-wave (cw) laser may be used and the molecular concentration along the laser path will be integrated or averaged in a measurement. Using a cw laser to measure molecular concentrations has been done previously using various techniques such as frequency modulation [49, 50]. However, these techniques may not be suitable to the rugged field environment needed to make measurements for the monitoring of sequestration sites.

A simpler technique is required. The simpler method is to use a continuously and widely tunable laser source to measure several absorption features. The result is a near copy of the molecular model such as the HITRAN model data seen in figure 5(b). The

Table 2: Characteristics of the laser diode. Information provided by NanoPlus, GmbH [51].

Parameter	Symbol	Unit	min	typical	max
Wavelength	λ	nm	2003	2004	2005
Side mode suppression		dB	32	35	40
Optical output power	P_{opt}	mW	1	3	10
Forward current	I_f	mA	40	50	100
Threshold current	I_{th}	mA	20	25	50
Beam divergence parallel		deg.	25	30	35
Beam divergence perpendicular		deg.	45	50	60
Emitting area	WxH	μm		5x1.5	
Slope efficiency	e	mW/mA	0.08	0.12	0.15
Current tuning rate	C_I	nm/mA	0.01	0.02	0.03
Temperature tuning rate	C_T	nm/K	0.18	0.2	0.22

amount of absorption may be measured from the resulting spectrum. This technique may now be implemented as mode-hop free, widely tunable laser diodes are currently available at various center wavelengths.

At Montana State University, an instrument has been built to measure the absorption spectrum of CO_2 and hence measure the concentration of CO_2 in the air. This chapter describes in detail the CODDA Instrument and how carbon dioxide concentration measurements are made.

Laser Characteristics

The laser source in use in the CODDA Instrument is a distributed feedback (DFB) laser diode operating at a wavelength of 2004 nm. The laser is continuous-wave (cw), has mode-hop free tuning and operates at a single frequency. Some of the specifications given by the manufacture, Nanoplus GmbH, have been placed into table 2 for reference. In further subsections some of the laser characteristics are discussed and verified.

Distributed Feedback (DFB) Laser Diodes

Laser diodes are available in many shapes and sizes and with a wide assortment of characteristics. The type of diode laser in use for this instrument, a distributed feedback or DFB laser, was chosen because of its tuning characteristics. In 1971 Kogelnik and Schank wrote a paper describing a phenomenon that had been seen by several other researchers [52]. They called this phenomena, for the first time, distributed feedback. It was reported that periodic structures in the gain medium cause optical feedback that further stimulates emission. The spacing of the periodic structures determines the particular wavelength at which feedback occurs, thus controlling the DFB laser operating wavelength.

Particular periodic structures may be built or etched into a diode structure as part of the laser gain medium [53]. When the period of the internal structures change size a different optical wavelength is fed back into the gain medium causing the operating wavelength to change. Thus thermal expansion, or contraction, may be used to change the operating wavelength of the laser [53]. This has been applied to DFB laser diodes ranging from 760 nm to 2500 nm [53].

Diode Packaging

The laser diode in the CODDA Instrument is packaged on a single-stage thermoelectric cooler (TEC), also known as a peltier cooler, and sealed inside a TO-8 can. A schematic drawing of the can, mounting of the TEC and laser diode is available from the manufacturer and is seen in figure 49 on page 90 [51]. The can, as seen in the schematic, is 14 mm in diameter and has a flat window to seal the can. The six leads on the can allow control of the diode drive current, diode temperature via TEC current, and measurement of the TEC temperature via an internal thermistor.

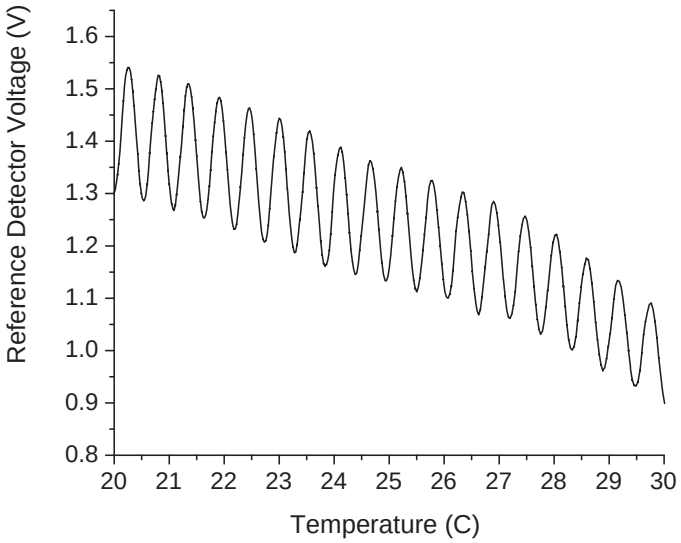


Figure 7: Tuning the 2 μm laser through a glass window to measure the temperature tuning rate.

Laser Wavelength Tuning Rate

The first of the laser diode characteristics to be tested was the temperature tuning rate. Light from the laser diode is incident on a piece of glass of known thickness and with a known index of refraction. Light passing through the glass is then incident on a detector. The laser diode operating temperature was changed and the detector output was recorded at each temperature step. Figure 7 shows the results of this experiment. The horizontal axis of the plot is the diode temperature in degrees Celsius and the vertical axis is the detector direct output voltage. The glass window acts as a Fabry-Perot etalon with a free spectral range (FSR) of

$$FSR = c/2nL \tag{13}$$

where c is the vacuum speed of light, L is the thickness of the glass that was measured to be 0.9525 cm, n is the index of refraction that is assumed to be 1.53 at this

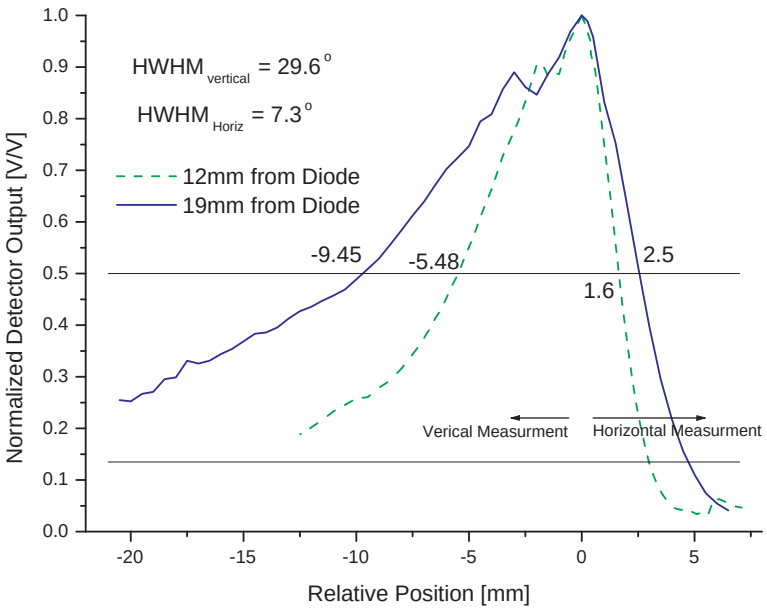


Figure 8: Measurements made to calculate the laser beam divergence angle in both horizontal and vertical directions.

wavelength. Using these values, a FSR of 10.3 GHz was calculated for the glass window. From figure 7 on the preceding page, one period, which corresponds to one free spectral range, may be measured per unit temperature. This yields an overall tuning rate of 18.9 GHz/^{o}C which in wavelength units is 0.253 nm/K. This is slightly larger than the maximum tuning rate quoted by the manufacturer in table 2 on page 18.

Laser Beam Divergence

Laser beam divergence angles were measured by moving a detector in front of the laser in two orthogonal directions, horizontal and vertical, at two different distances away from the DFB laser. To minimize the angular dependence of the measurement, two razor blades were placed in front of the detector forming a narrow slit perpendicular to the detector direction of travel. The half width at the half maximum

(HWHM), the beam radius at half maximum power, was calculated at the two lateral positions using the measured data. The HWHM values and a plot of the data from the measurements may be seen in figure 8 on the preceding page. The HWHM divergence angle of the laser was measured to be 29.6^o in the vertical direction and 7.3^o in the horizontal direction. According to the manufacturer, table 2 on page 18, the HWHM divergence should be 50^o for vertical and 30^o for horizontal directions.

Optical Power

Optical output of the laser was measured on a detector as a function of laser drive current. The temperature of the laser diode was set to 22.0 ^{o}C or 11.2 kΩ in equivalent TEC resistance, while the drive current was changed. The measured detector voltage as a function of laser drive current may be seen in figure 9 on the following page. From the plot in figure 9 on the next page the lasing threshold is seen as the intersection of a linear regression to the two portions of the plot. This is measured to be about 17.5 mA which differs from the minimum specifications of 20 mA given by the manufacturer in table 2 on page 18. Since the threshold drive current does vary with laser diode temperature it is not surprising to find a difference from the manufacturer's specifications. Another explanation for the deviation from the manufacturer's specifications is that the diode was not new when this data was taken in September 2007. The age of the diode may change the threshold current or the slope of the sloping drive current and may be an indication of imminent failure.

Instrumentation

The equipment for the CODDA Instrument is mounted onto a portable optical breadboard. The breadboard measures 2 feet by 4 feet and is 2 inches thick. The

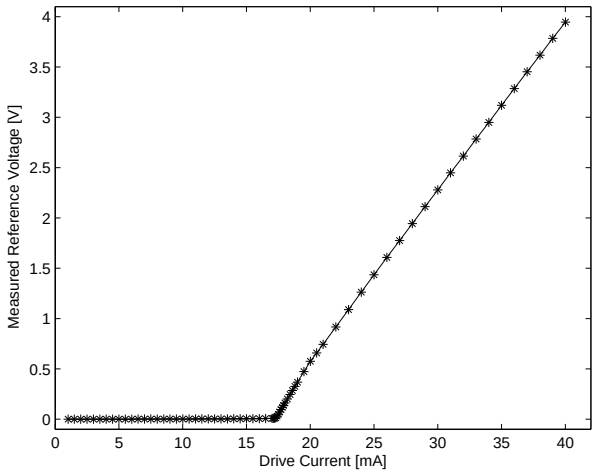


Figure 9: Voltage output of the reference detector as a function of laser drive current.

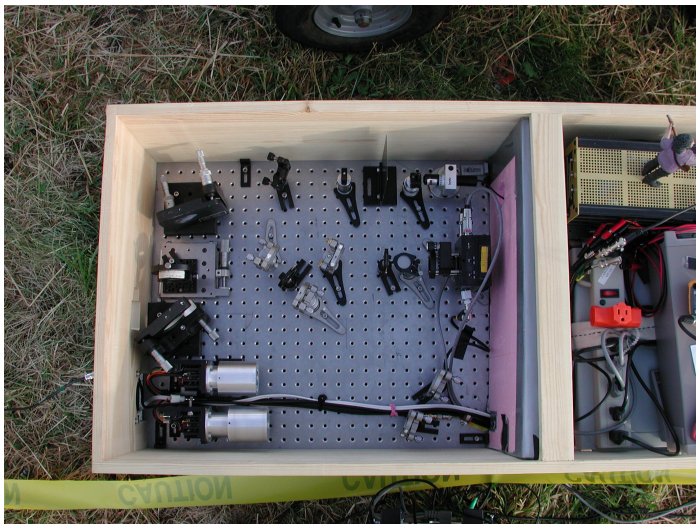


Figure 10: Picture of the CODDA Instrument optical and electronics setups. The picture was taken in the field during one of the controlled releases in the summer of 2007. The instrument is sitting in firing position, ready to take data.

board is divided into two sections using 1 inch thick thermal insulation. The first and larger section contains the laser, optics, and detectors. The other section contains all the electronic equipment. The separation serves to thermally isolate the laser diode and optical equipment, which are temperature sensitive, from the heat produced by the electronic equipment. This separation is seen as the wood cross piece and pink insulating foam in figure 10 on the previous page.

A pine box fits just on the edge of the optical breadboard. This box is 12 inches tall and has removable tops that act as lids for the separate sections mentioned above. The box serves to enclose the instrument, prevent extraneous light from reaching the detectors and prevent dust from falling onto sensitive equipment.

The electronic equipment consists of a computer, laser diode current driver and temperature controller, and data acquisition (daq) system to measure output signals from the detectors, power supply for the detectors and visible laser power source. A laser diode current and temperature controller, model 3702b, was purchased from ILX Lightwave, Inc. This controller has remote communication capability via a general purpose interface bus (GPIB) connection to a computer through which the laser diode temperature may be set or read. The daq system will be discussed in later sections.

Laser Path

Figure 11 on the following page is a schematic drawing of the CODDA Instrument. Due to the wide divergence angles of the laser diode a lens is employed to achieve a best collimation to the laser light. The output of the laser is collimated using a 25.4 mm diameter, F/1 lens. This lens has an anti-reflection (AR) coating appropriate for near infrared (NIR) telecommunication purposes. This lens is positioned in front of the laser diode at a distance that yields a maximum detected signal 100 meters away.

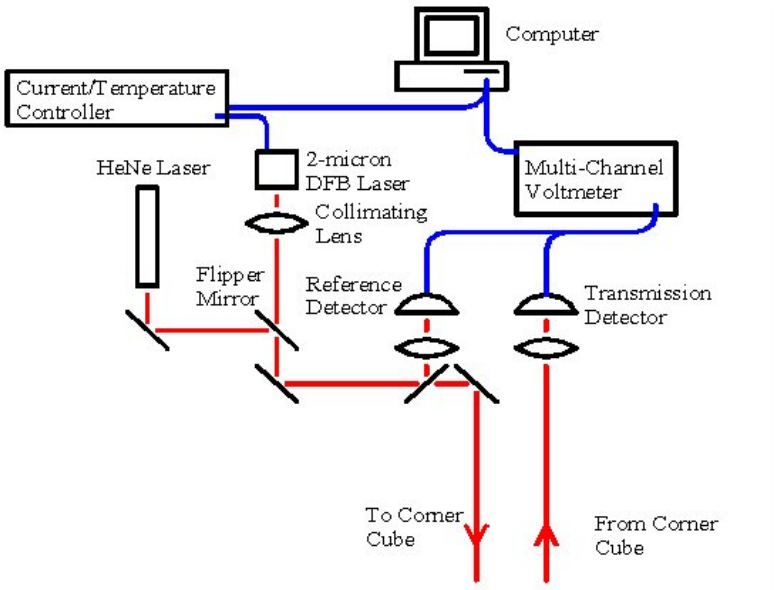


Figure 11: Schematic of the CODDA Instrument layout and setup.

After passing through the collimation lens the laser light is incident on a glass wedge. The wedge used is made of plain BK-7 glass having about a 3^o angle between the two flat surfaces. The wedge does not have any AR coatings and reflects about 4% of incident optical intensity in the visible spectrum. A section of the Appendix on page 86 describes in detail how light is reflected off of and through the wedge and at what angles. The light reflected off the front surface of the wedge is directed towards a detector and is focused onto the detector through a lens to capture the incoming light. This signal is used as a reference measurement of the output optical power and is called the reference signal. Since the output power changes as a function of laser operating wavelength and laser drive current, it is important to measure the laser diode optical output power.

The remaining light passing through the wedge is directed out of the instrument box. The output laser light is incident on a retro-reflector or corner cube. A corner

cube is a set of three mirrors that are mutually orthogonal. Light incident on a corner cube is directed anti-parallel back to the source.

The light that is returned to the instrument from the retro-reflector is directed to a detector. The light is focused through a lens onto the detector. This is a measurement of the amount of light that passes through the atmosphere from the source. This measurement of the returning optical power is referred to as the transmission signal.

To reduce background light, narrow band filters are employed at each detector. Two filters, one for each detector, were purchased from CVI. The transmission through the filter was measured by a Fourier Transform Infra-Red (FTIR) Spectrometer in Prof. Lee Spangler's lab by Dr. Laura Dobeck in December of 2005. The transmission measurements plotted versus wavelength are shown in figure 12 on the next page. The filters unfortunately have parallel surfaces; therefore they cause a Fabry-Perot etalon type of effect with the light transmitted though them. The effect due to the filters is more than 10% of the normalized transmission data. For short paths, less than 20 meters, this can be as large as the absorption features. The filters were thus not used.

A laser in the visible spectrum is co-aligned with the 2 μm laser via a flip mounted mirror. Since the 2 μm beam is hard to monitor, the co-aligned visible laser is used for coarse field alignment.

Data Acquisition

A computer is connected to the laser diode temperature controller via a GPIB connection and a diode temperature is set. The laser diode temperature is recorded along with voltages from both the detectors forming a single data point. The temperature of the laser diode is then changed and the process continues until a series of data points is measured. One series of data points is referred to as a scan.

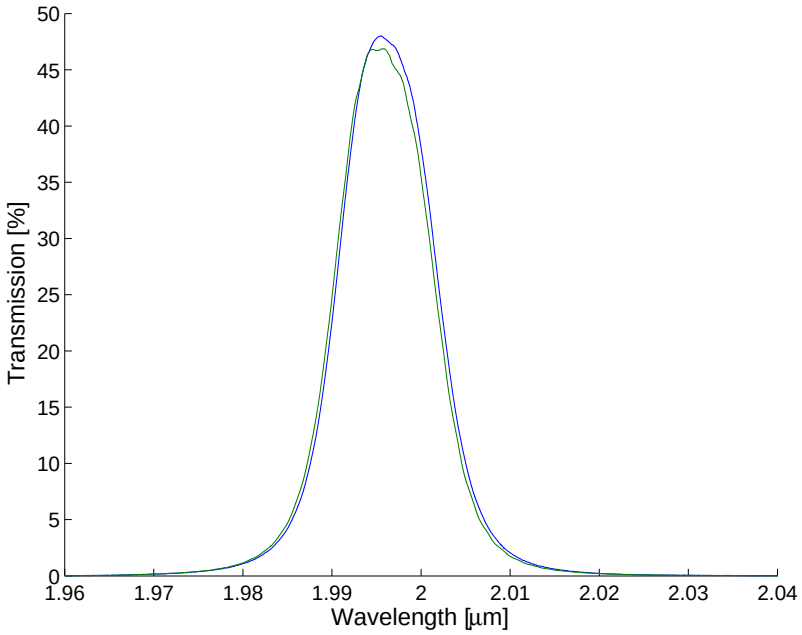


Figure 12: Transmission spectra through the 2 μm filters as a function of wavelength. Data taken with an FTIR by Dr. Laura Dobeck.

The instrument is controlled from the computer via a program written in Matlab. This program communicates with equipment, records data, performs analysis and displays results. This program uses the Graphical User Interface (GUI) Development Environment (GUIDE), Data Acquisition Toolbox, Instrument Control Toolbox and the Signal Processing Toolbox in Matlab. The code for the entire program and the MATLAB figure are included as Appendix C on page 101.

Data Analysis

The data analysis portion of the CODDA Instrument presents a difficult problem as it is necessary to find the center of each absorption feature with its corresponding transmission value. Each of the features must be identified uniquely as the line strength and line width values will be different for each feature. The challenge arises

from the fact that the temperature around the laser diode changes the operating wavelength, shifting the features with respect to the laser diode set temperature.

The method developed for robust absorption feature detection is seen as code in the Appendix on page 101 and is described in this paragraph. The scan is transformed from transmission to percent absorption. Data in the scan is then smoothed using a 7-point moving average (± 3 data points). The resulting smoothed data is then raised to the fourth power. The reason for the power is to make the absorption features stand out against noise in the scan. The four peaks or features are identified in this new data using a thresholding method. Using these points, peaks are located in the original transmission data using a search window around the peaks. The background transmission value between each feature is calculated as an average of 10 points exactly between two adjacent features. The two background levels on either side of the features are averaged to give a background level for each feature. The total transmission for each feature is found by subtracting the transmission at each peak from this background level.

Once the features are identified and the amount of transmission is calculated for each feature the concentration is calculated using equation 12 on page 12. This process uses values for the barometric pressure from a local weather station, ambient temperature measured by the instrument, and both line strength and line width values from the HITRAN database [44]. The actual code for this process is in the Appendix on page 101 in the Matlab function called CalcPPM.

Analysis is performed on each scan immediately after the scan is completed. The concentrations for a water vapor line, and three CO_2 lines are calculated. The atmospheric concentration from the two CO_2 lines farthest in wavelength from the water vapor line are averaged together for a single CO_2 concentration value per scan. The CO_2 feature closest to the water vapor line is not used in the averaging because of

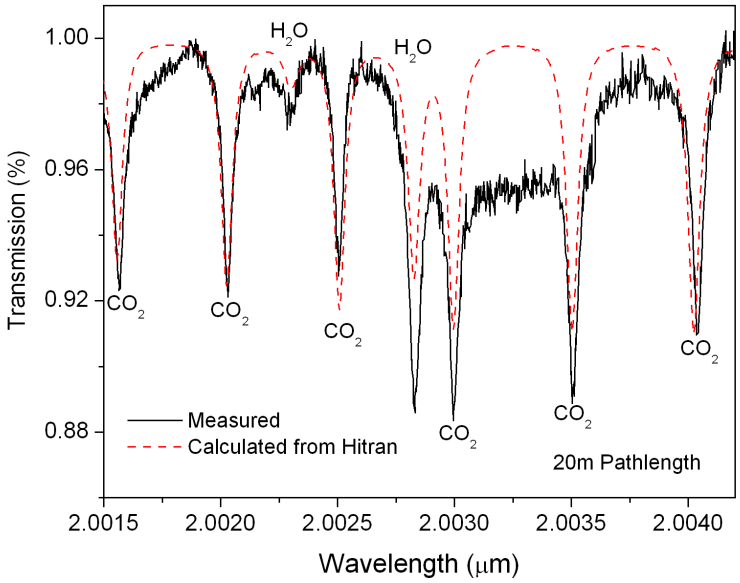


Figure 13: Laser scan taken after the instrument was first built. The measured data, the solid black line, is plotted with data from the HITRAN model, dashed red line, for comparison. The molecule that causes each particular absorption features is labeled.

the difficult nature of finding the background transmission level with the overlapping H_2O absorption features. The water vapor concentration is calculated and compared against concentration levels calculated from relative humidity measurements from the local weather station. This comparison provides the user with a confidence that the instrument and calculations are functioning properly.

CODDA Instrument Proof of Concept

The CODDA Instrument idea was first brought to reality in the summer of 2005. Data was taken to verify that tuning the laser was possible and to determine how it was to be accomplished. In other words, the instrument was put together as a proof of concept. Some of the first data taken with the instrument is seen plotted along with data from the HITRAN model in figure 13.

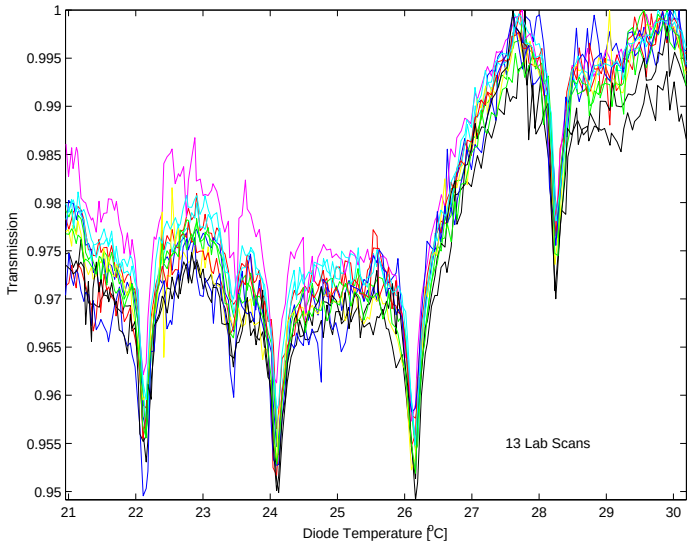


Figure 14: Series of laser tuning scans taken over a few hours to demonstrate that the laser can be tuned repeatably yielding the same results in a lab environment.

The next step was to test the repeatability of scans measured by tuning the laser in this manner. This was done in the lab and 13 scans were recorded during one afternoon. These scans are plotted in figure 14 as a function of diode temperature. The scan repeatability was later tested in the lab over night. The temperature in the lab changes about 10 ^{o}C from day to night. A series of 72 consecutive scans were recorded at an interval of 15 minutes between scan times. These scans are plotted in figure 15 on page 32. These two figures, 14 and 15, demonstrate that the data taking process is repeatable and that the laser can be tuned reliably.

Instrument Calibration

With any instrument it is important to know the noise sources, accuracy and resolution. Therefore, capabilities and accuracy of the CODDA Instrument were measured in the lab. The calibration yields best-case-scenario accuracy.

Inputs, P_T and T_a, for equation 12 need to be measured by instrumentation co-located with a CO_2 measurement instrument. For field work this is a weather station [54] located in the same field as the CODDA Instrument. The measurement accuracy of the barometric pressure sensor is ± 0.5 mbar [54]. Out of the nominal 850 mbar this is $\pm 0.05\%$ accuracy in the CO_2 concentration calculation. The measurement accuracy of the temperature sensor is ± 0.2 K [54]. Out of the nominal air temperature of 280 K leads to $\pm 0.07\%$ accuracy in the CO_2 concentration calculation. Thus both the error associated with measuring temperature and barometric pressure are negligle.

The laser instrument was calibrated using an optical chamber. The optical chamber is a sealed cylinder that can withstand vacuum pressures. The ends of the cylinder contain rugged windows that are placed at an angle with reference to the optical axis so that they form a Brewster's angle. The chamber has a length of 1.4 meters and the total path length of the light from source to transmission detector was 2 meters.

The chamber and all the plumbing was evacuated using a roughing pump. A cold trap was used with the roughing pump to prevent oil vaporized by the pump from entering into the chamber. A pressure detector, model 6100 from the Mensor Corporation with rated accuracy of 0.01% of full signal (FS) and a specified precision of 0.003% FS. This has a full scale range of 0 to 200 psi, yielding an absolute accuracy of 0.02 psi or $\sim$1.3 mbar and a precision of 0.006 psi or $\sim$0.41 mbar, which is about 410 ppm. The chamber was evacuated to approximately 1 μbar or about 750 mtorr. This was measured using a pressure detector meant to measure vacuum pressures. Once evacuated, the chamber was opened briefly, via a needle valve, to a tank containing CO_2 and the change in total pressure in the optical chamber was measured. The chamber was sealed and the ductwork plumbing leading to the tank was again evacuated. The chamber was then opened to a tank containing N_2 and the cell filled until a total pressure approximately equal to ambient pressure was obtained.

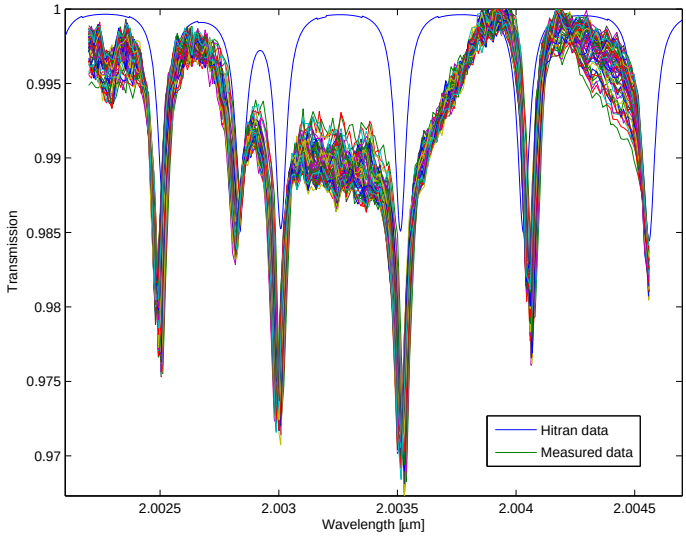


Figure 15: The laser instrument was left over night in the lab to take data to test repeatability and robustness of the data taking method.

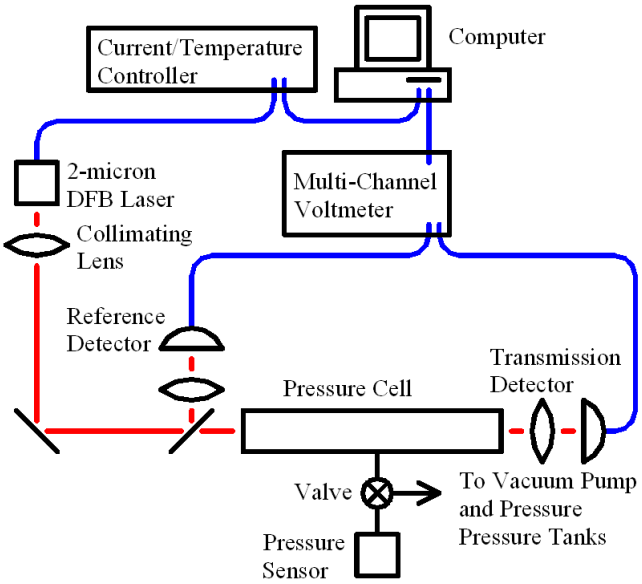


Figure 16: Schematic of the instrument calibration layout and setup.

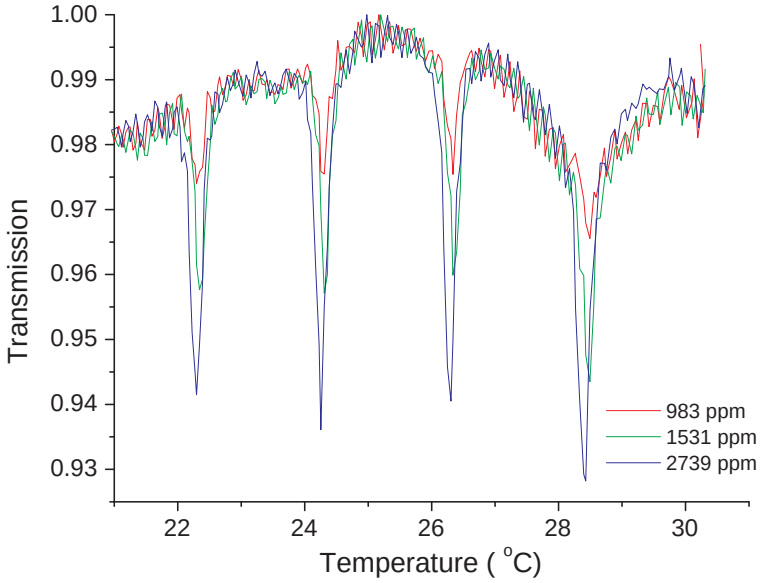


Figure 17: Measured scans taken through the calibration chamber at three different CO_2 concentrations.

Ambient pressure at nearly 1524 m (5000 ft) above sea level is about 845 mbar. The chamber now containing only CO_2 and N_2 simulates ideal operating conditions in the atmosphere with no absorption from water vapor or other undesirable molecules. The chamber conditions also prevent broadening or narrowing effects that can occur at higher or lower total pressures, respectively.

At this point, the laser passing through the chamber is temperature tuned and a scan captured. Figure 17 has three scans that were typical of the data measured through the chamber. The CO_2 pressure is divided by the total chamber pressure and multiplied by $\times 10^6$ for a concentration in units of Parts per Million (ppm). From each measurement scan, CO_2 concentrations are calculated and compared to those concentrations calculated from measurements of the pressure detector output. A plot of transmission as a function of CO_2 concentration is shown in figure 18 on the following page. The solid line indicates the expected transmission from a known

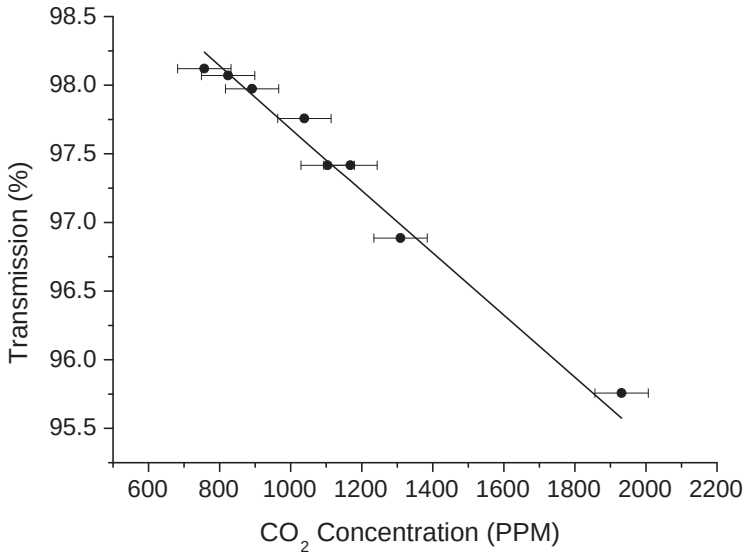


Figure 18: Calculated and measured concentrations as a function of transmission.

CO_2 concentration using data and the HITRAN database. The solid circles represent the measured values of CO_2 concentration measured using the pressure sensor and the transmission using the CODDA Instrument. The error bars shown in the figure, which are associated with the measured values, are attributed to the accuracy of the pressure sensor. There is good agreement between the measured and predicted values.

Instrument Conclusion

The concept of the CODDA Instrument has been shown to be feasible in the lab. CO_2 concentration measurements may be can and the instrument has been tested to determine reliability and accuracy. To continue to assess the performance of the instrument, it must be tested in an outdoor environment

INITIAL OUTDOOR MEASUREMENTS

The goal of this project is to evaluate the CODDA instrument for use at carbon sequestration sites to monitor and verify well integrity. To meet this goal the instrument has been developed with consistant and repeatable operation demonstrated in the lab, as discussed in Chapter 3. To test the feasibility of using the CODDA Instrument for detection of elevated CO_2 levels initial outdoor experiments were performed in 2006. The field site and initial outdoor results are presented in this chapter.

ZERT Field Specifications

The Zero Emissions Research and Technology (ZERT) group at MSU has been established to develop the technology needed to conduct research on geologic sequestration of carbon dioxide generated from fossil fuel consumption. For carbon sequestration to be successful, storage locations must be continuously monitored to verify storage integrity. A field site has been selected by ZERT that best suits the needs of releasing carbon dioxide with the purpose of testing sequestration monitoring techniques. This field site is described in this section.

Field Description

The 30 acre ZERT field site is located near the MSU-Bozeman campus in Bozeman, Montana. The field is at an elevation of approximately 1500 m above sea level and has thick sandy gravel and cobble deposits which are overlain by several meters of topsoil made of a mixture of silts and clays. The water table is at or just below the surface until about mid summer. The ground water gradient is 17 degrees west of north and summer winds are predominant out of the southeast but with a lot of

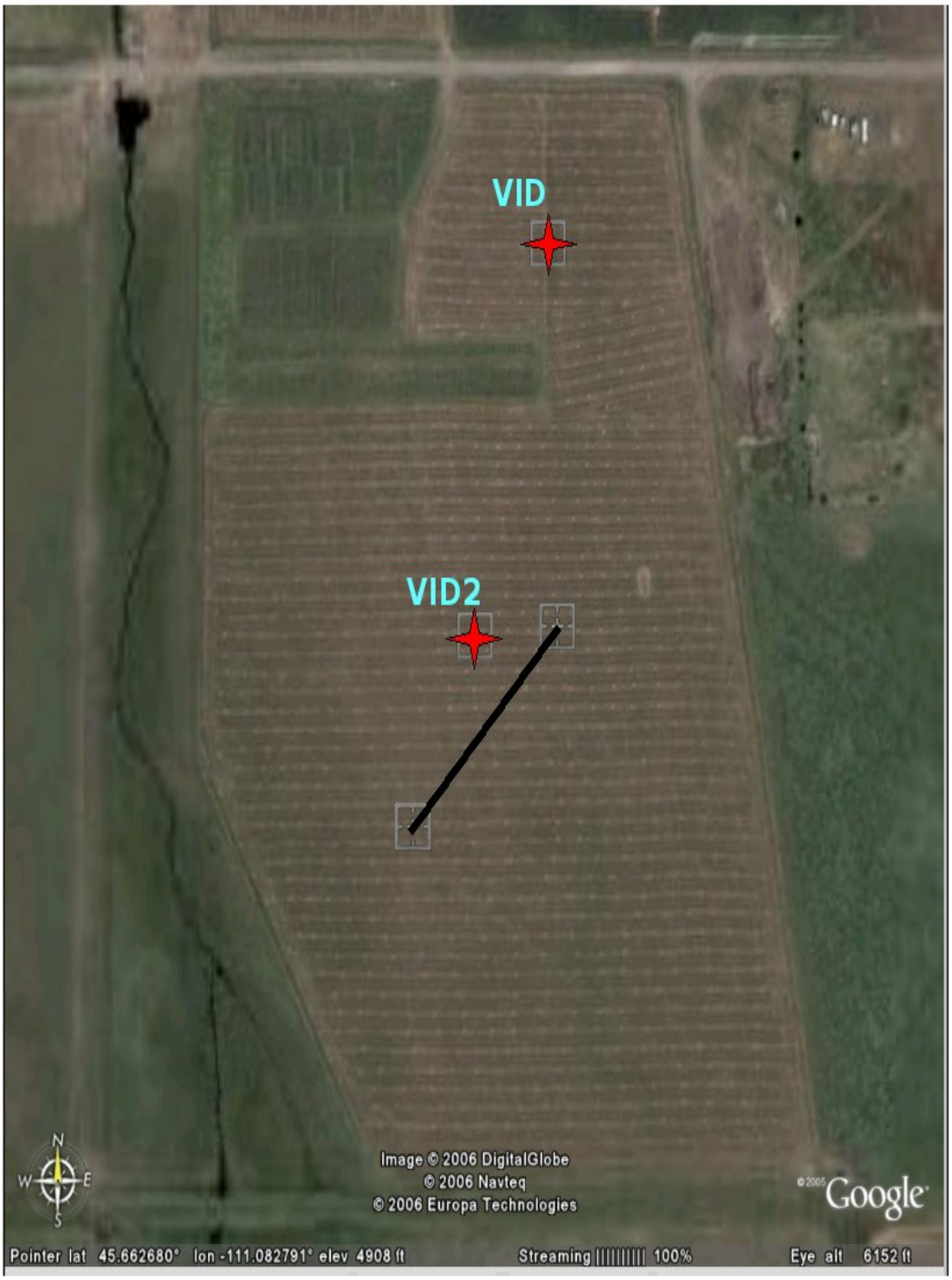


Figure 19: Satellite image of the field used by the ZERT experiment with well locations indicated. Courtesy of Dr. Laura Dobeck and google maps.

variability. Figure 19 on the previous page shows an aerial photograph of the field site with approximate injection well locations identified [55].

Investigated Techniques

At the field site, various monitoring techniques are tested on a small scale to determine feasibility and also scalability. The techniques tested at the field site are listed below in alphabetic order. Some of these techniques were not used for all test injections.

⇒ CO_2 Detection by Differential Absorption (CODDA) instrument for above-surface measurements by Kevin Repasky and Seth Humphries from MSU.

⇒ CO_2 Detection by Differential Absorption (CODDA) instruments for below-surface measurements by Kevin Repasky, Amin Nehrir and Jamie Barr from MSU.

⇒ CO_2 Flux by James Amonette and Jon Barr from Pacific Northwest National Lab (PNNL).

⇒ Eddy Covariance CO_2 Flux by Jennifer Lewicki from Lawrence Berkeley Lab (LBL) and Thom Rahn from Los Alamos National Lab (LANL).

⇒ Hyperspectral Imaging by Kevin Repasky and Charlie Keith from MSU.

⇒ Carbon isotopes in soil, water, and canopy by Julianna Fessenden from LANL.

⇒ Microbial Concentrations by Bill Inskeep and Rich Macur from MSU.

⇒ Multispectral Imaging by Joe Shaw and Josh Rouse from MSU.

⇒ Plant Stress by Bill Pickles and James Jacobson from University of California at Santa Cruz (UCSC).

⇒ Soil Gas CO_2 Flux Chambers by Jennifer Lewicki from LBL.

⇒ Soil Permeability by Al Cunningham and several graduate students from MSU.

⇒ Soil Resistivity by Rick Hammack and Garret Veloski from the National Energy and Technology Lab (NETL).

⇒ Tracers and CO_2 Flux by Brian Strasizar, Rodney Diehl, Art Wells, and Dennis Stanko from NETL.

⇒ Water Sampling by Henry Rauch from West Virginia University (WVU) and Kadie Gullickson from MSU.

Vertical Well Installation

Two vertical injection wells were installed in the field in 2006. The bottom 22 inches of each vertical well is made of a porous material called Schumasoil. The standpipe above the porous media for each well is solid PVC. The bottom of the first well is 3.4 m below the surface and the bottom of the second vertical well is 3.1 m below the surface. A picture of the setup used for injection is seen in the background in figure 20 on the following page. On the ground in figure 20 is the CODDA instrument .

ZERT Vertical Injections

First Vertical Well Injection

For the first injection, a flow rate of 0.86 liters per minute (lpm) was used. This flow rate equates to 0.003 pounds per day or equivalently 1.3×10^{-6} tons of CO_2 per day. Compared to a car getting 20 mpg of gasoline which emits 1 pound of CO_2 per mile, the amount of CO_2 being injected into the ground per day was small.



Figure 20: Picture of the field release site taken on the 28^{th} of September 2006. The tank containing the CO_2 used for the injection is visible in the background. In the center of the picture is the wood box containing the instrument, and also visible is the large shade used for protection from the sun.

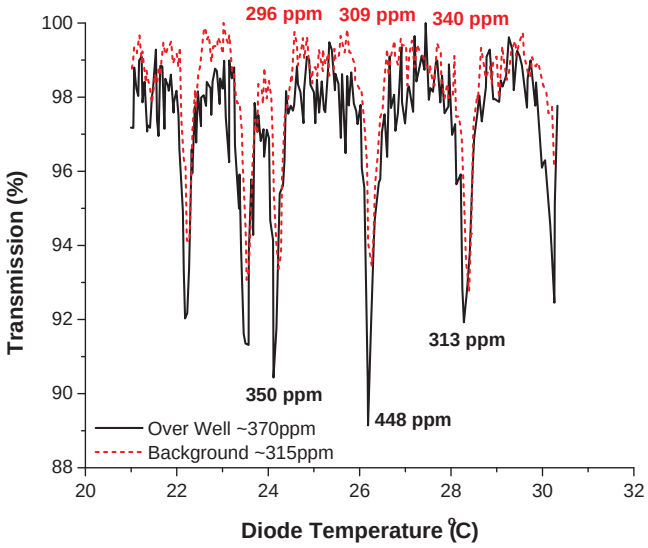


Figure 21: Data measured on the 28^{th} of September 2006. Scans were captured with the laser passing over the well head and with the laser path rotated 90^o to the previous measurement. The analysis results from some of the absorption features are displayed.

On September 28^{th} 2006, during the injection into the first vertical well, the instrument was taken to the field and laser tuning scans were captured. Transmission data as a function of diode temperature is plotted in figure 21 on the previous page. In the plot, the solid black line is data captured with the laser passing adjacent to the well head. Additional data was captured with the instrument rotated approximately 90^o to obtain background measurements. This data is plotted as a red dashed line in figure 21. Data was captured through the late morning into the early afternoon. The concentration of CO_2 for each of three CO_2 absorption features was calculated and are labeled on the plot. Clearly evident is the difference between the amount of light absorbed between the two firing positions of the laser.

Second Vertical Well Injection

The second injection used a flow rate of 1.6 lpm or equivalently 2.4×10^{-6} tons of CO_2 per day. The instrument was again taken into the field for the release. Data scans were taken in a similar manner as with the first release, adjacent to the well head and the away from the head. A plot of two scans taken at the field are plotted in figure 22 on the following page. The red dashed line in the figure is the scan taken away from the well and the black line was taken with the laser passing adjacent to the well head. A concentration of 337 ppm was calculated from the data over the well and 318 ppm calculated from the data as a background concentration. It is clear from the plots that there are different amounts of absorption from differing CO_2 concentrations and from the measured scans.

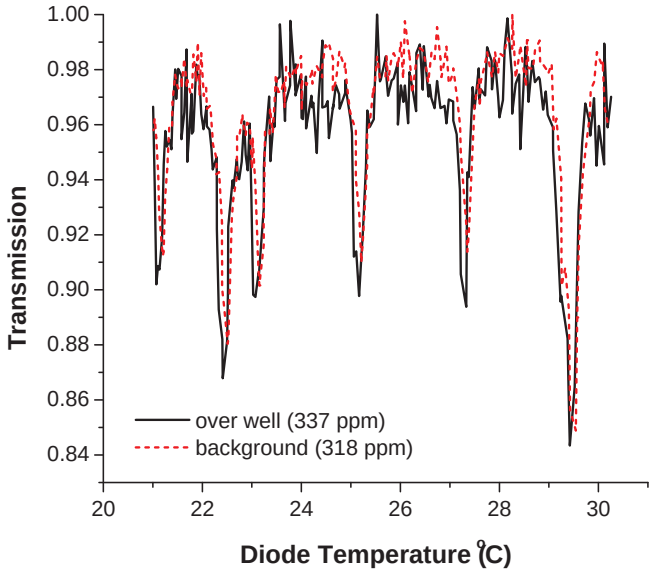


Figure 22: Data taken on the 6^{th} of October 2006. Scans were captured with the laser passing over the well head and with the laser path rotated 90^o to the previous measurement.

Initial Outdoor Conclusion

Measurements obtained by participation in the two vertical release experiments show that the CODDA Instrument is functional outdoors. CO_2 concentrations were obtained that also demonstrate that this technique can distinguish between a natural background level of CO_2 and any deviation from the natural background level. However, there are also changes that can be made to improve the performance of the instrument.

2007 FIELD RELEASE

The results from the 2006 field experiments, as discussed in Chapter 4 on page 35, show that the CODDA instrument is functional in the field and can yield good results. It is also clear that some changes to the instrument could be made to improve system performance. This chapter will discuss some issues with the instrument and how each issue is addressed and overcome prior to the next controlled release experiments. The description of the setup for a horizontal controlled release will then follow and the chapter will conclude with results measured by the improved CODDA instrument.

Instrument Improvements

Laser Mount

The absolute operating wavelength of the laser diode may change with respect to a given laser diode set temperature. This is evident from early field measurement data and mentioned in sections on page 27. In brief, despite a given constant set temperature on the laser diode, temperatures external to the diode mount may still affect the absolute diode operating wavelength. This is evident in data as a lateral shift in the absorption features for the same measured diode temperature. Since it is known that the absorption features do not shift significantly with respect to the width of the feature due to either changes in temperature or in pressure [44], the effect must be due to changes in the operation of the laser diode.

To better isolate the laser diode from ambient temperature changes, another stage of temperature control was added to the instrument. A TCDLM9 laser diode mount, with a built-in TEC, was purchased from Thor Labs, Inc. The mount holds a laser diode mounted in a T5.6 or TO-9 can. The laser-containing can is then mounted

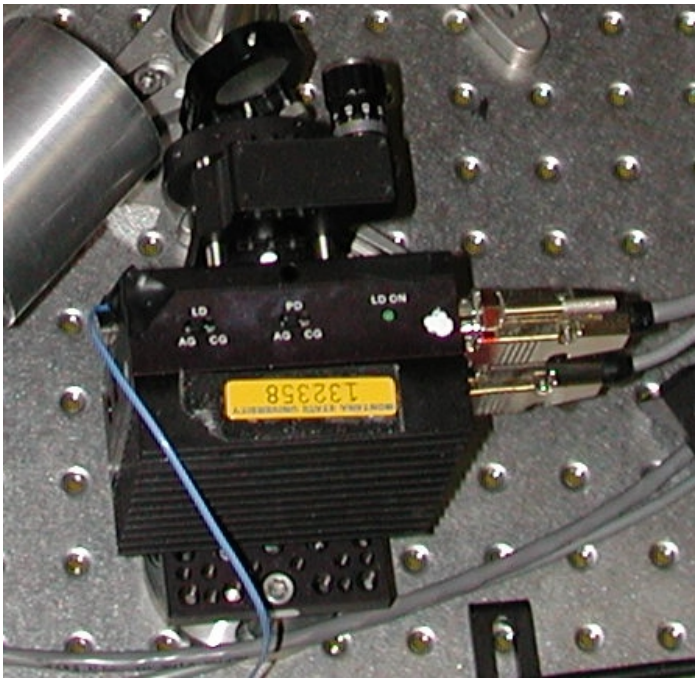


Figure 23: Picture taken of the laser diode mounted to the optical breadboard in the bottom middle of the picture. Also visible is the structure used to hold the collimation lens.

onto a pair of thermoelectric coolers (TEC) and bolted in place with an aluminum ring. However, the DFB laser diode used in the CODDA instrument is in a TO-8 can (see the manufacture drawing in figure 49 on page 90 for specifications). The can is a lot larger than either the TO-5.6 and TO-9 cans. The off-the-shelf (OTS) diode mount was modified in house so it would hold our laser diode. The temperature of this mount is set to a constant temperature and controlled by a separate temperature controller purchased from ILX Lightwave, Inc.

Laser Collimation

The divergence angle of the laser light leaving the instrument is critical. If the light diverges too fast the signal, as a function of path distance, decreases rapidly

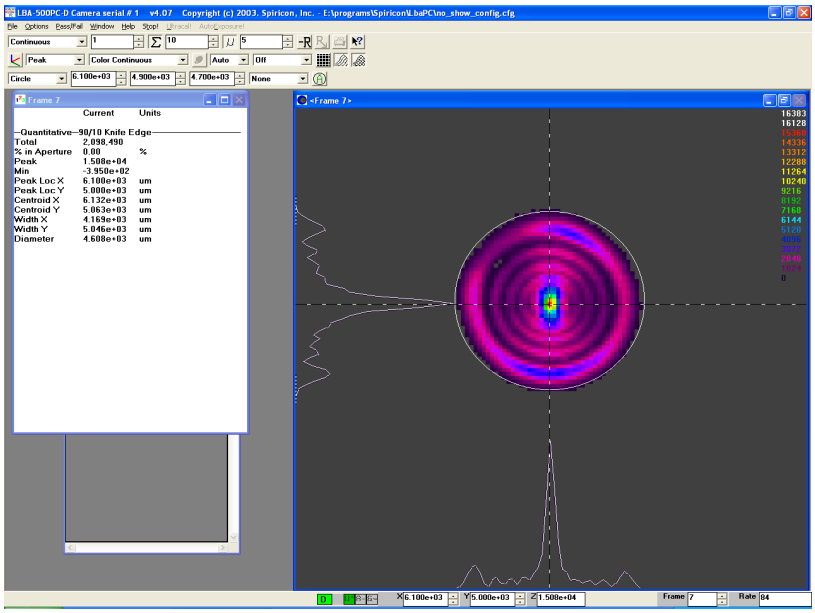


Figure 24: A picture of the 2 μm laser beam taken by the pyro-electric camera at a distance of 24 cm from the instrument. The laser was collimated using the 20 mm, F/1 lens

making it hard to make long distance measurements. Thus a good collimation of the laser is important to achieve.

To assist in the collimation of the laser beam, a pyro-electric camera was purchased from Spiricon, Inc. in December of 2006. The camera is a 124 by 124 pixel array of small pyro-electric detectors. The small detectors have a good response over a wide range of visible to infrared light so a 1.4 μm to 2.5 μm interference filter is used. The camera provides two crucial capabilities. First is the ability to find the 2 μm beam in the lab. This allows the instrument pieces and optics to be moved and placed quickly and more accurately. Secondly, laser beam collimation was laborious and time consuming previously. Figures 24 through 29 show screen shots of laser beam captured by the pyro-electric camera using the capture software provided with the camera.

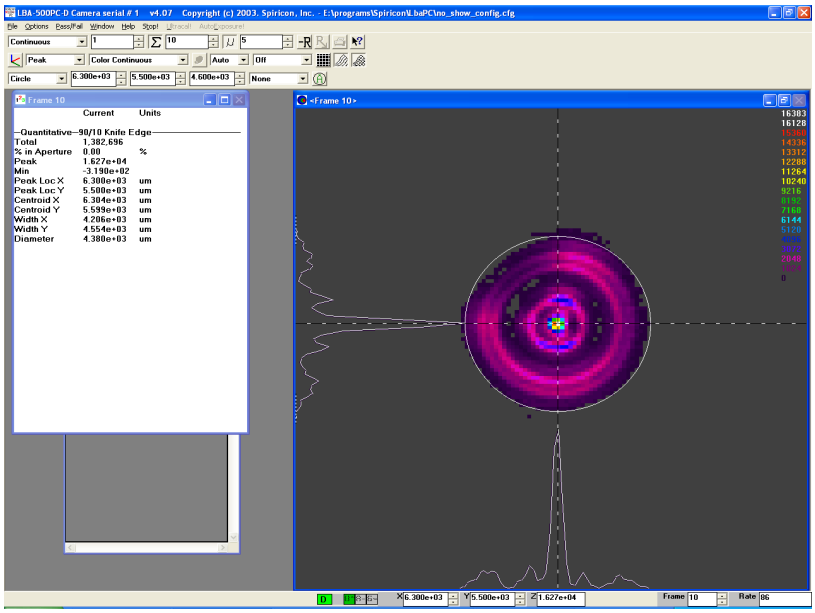


Figure 25: A picture of the 2 μm laser beam taken by the pyro-electric camera at a distance of 69 cm from the instrument. The laser was collimated using the 20 mm, F/1 lens

This lens originally used in the system (see the section on page 24) was replaced prior to the vertical injection tests with a lens that has an AR coating specifically made for 2 μm wavelength. This lens was purchased from the Rocky Mountain Instrument Company (RMI). The optical transmission through the lens and the coatings may be seen in Appendix B as figure 58 on page 99. The spherical lens is 20 mm in diameter and has a focal length of 20 mm. Pictures of the laser beam taken using the Pyrocam with this lens as the collimator are seen in figure 24 through figure 26. The light coming out of the laser is rapidly diverging (see table 2 on page 18) and therefore the light incident on the lens is not at near-normal incidence. A large amount of spherical aberration is thus induced by the laser beam passing through this lens. This effect is seen in figure 24 on the previous page through figure 26 on the following page as concentric circular rings.

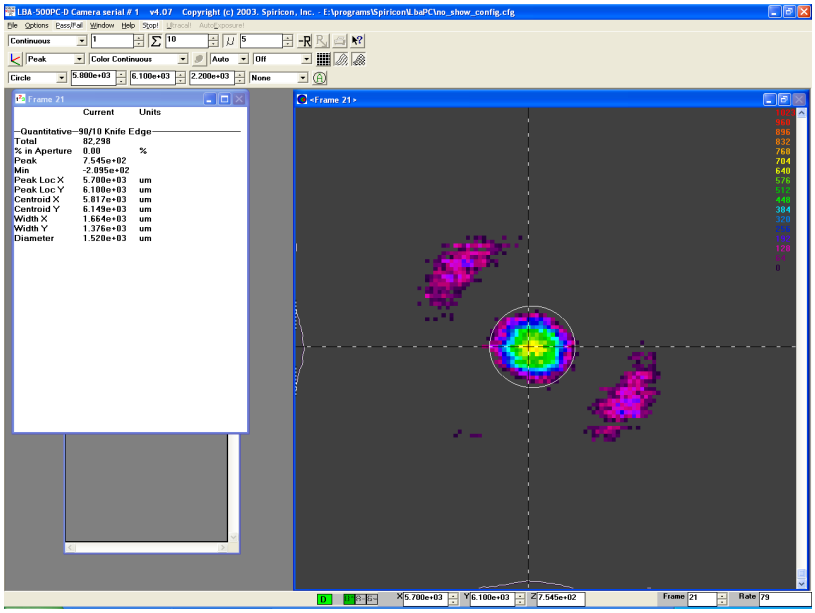


Figure 26: A picture of the 2 μm laser beam taken by the pyro-electric camera at a distance of 474 cm from the instrument. The laser was collimated using the 20 mm, F/1 lens

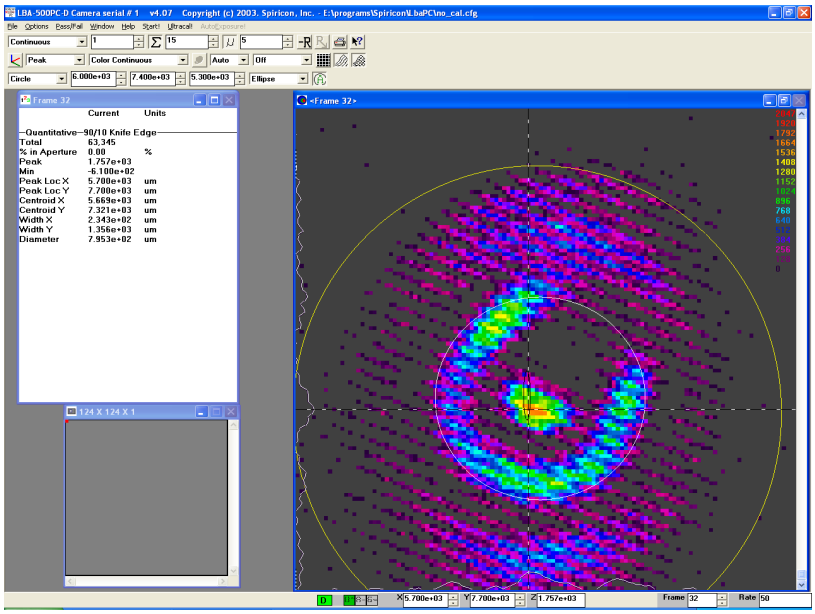


Figure 27: A picture of the 2 μm laser beam taken by the pyro-electric camera. The laser was collimated using the 25.4 mm aspheric lens at a distance of 23 cm from the instrument box.

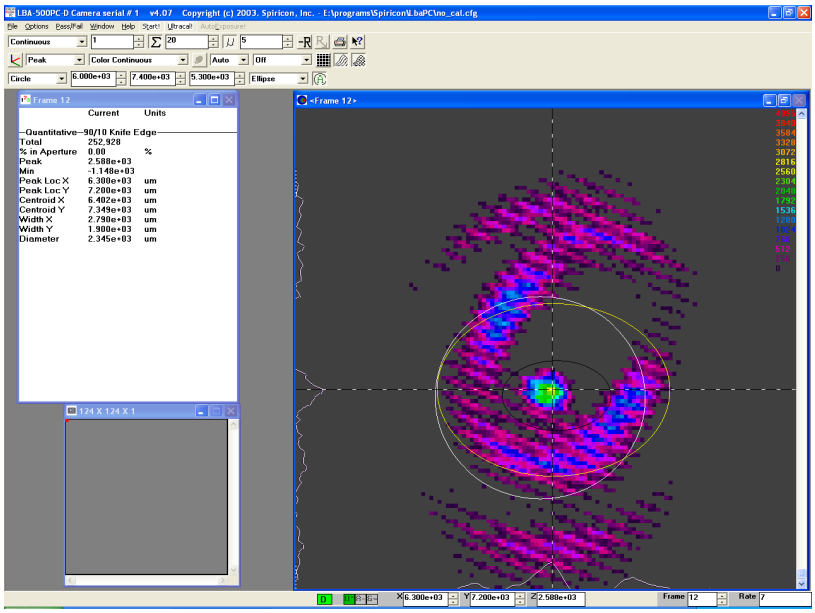


Figure 28: A picture of the 2 μm laser beam taken by the pyro-electric camera. The laser was collimated using the 25.4 mm aspheric lens at a distance of 74 cm from the instrument box.

To improve beam quality and return signal an aspheric collimation lens was purchased from Melles Griot. The uncoated aspheric lens is 25.4 mm diameter and has an equivalent focal length of 25.4 mm. Pictures of the laser beam using the aspherical lens as a collimator are seen in figure 27 through figure 29. Despite the odd laser beam shape, simply using this lens significantly increased the amount of optical power received by the transmission detector, with no other changes to the instrument. The output signal of the transmission detector changed from about 200 mV to 4 V over the same eighty meter path an increase in signal-to-noise ratio (SNR) of over 20 dB_V.

Also, to yield easier adjustments and better alignment between the collimation lens and the diode output, the lens is mounted directly to the structure that holds the laser diode. The section on page 42 describes the mounting structure and figure 23 on page 43 shows the collimation lens in place on the mount.

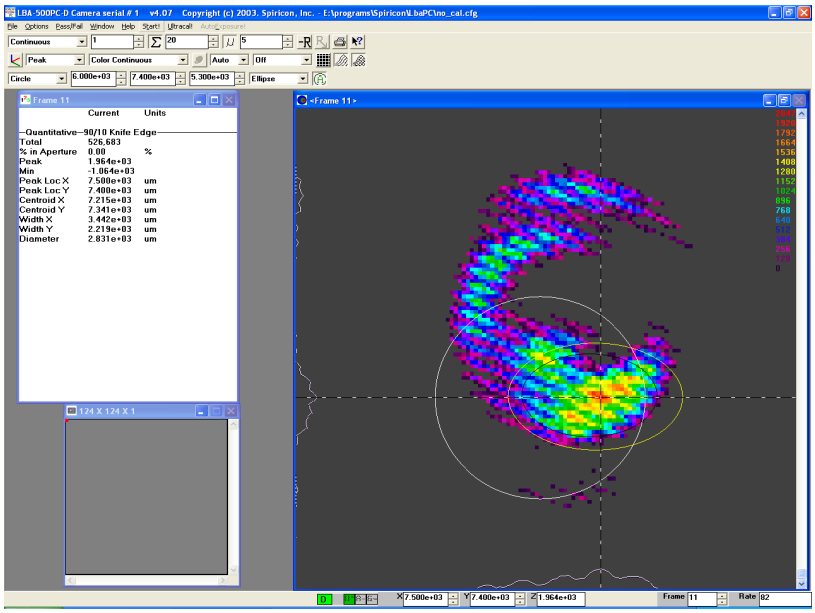


Figure 29: A picture of the 2 μm laser beam taken by the pyro-electric camera. The laser was collimated using the 25.4 mm aspheric lens at a distance of 472 cm from the instrument box.

Detectors

The detectors used are photo-diodes made from Indium-Gallium-Arsenide (InGaAs) that has been doped such that it is called "extended InGaAs". The photo-diodes have an operational peak responsivity at 2.2 μm. The detectors used in the system until after the vertical injections were purchased from New Focus (model 2034). Data captured using these detectors did not match the expected results from the HITRAN model. There is a transmission difference of over 5% as seen in figure 13 on page 29. This is also evident in figures 14 and 15 on page 32.

Through trial, error, and research it was discovered that the cause of the discrepancy between the expected and measured spectra is attributable to the windows of each mounting can that holds the photodiodes. The windows have flat, parallel surfaces and these surfaces act as a Fabry-Perot etalon. As the laser is tuned the interference pattern changes and the measured signal changes. This effect is similar

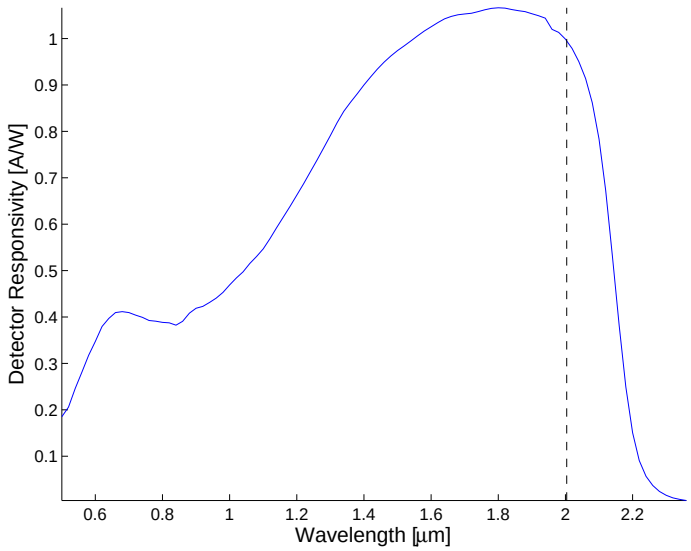


Figure 30: Detector responsivity as a function of wavelength. This responsivity was measured at Judson before the detectors were shipped to MSU. The responsivity of the three detectors used are assumed to be close enough to have only negligible differences. The approximate operating wavelength of the DFB laser is shown by the dashed vertical line.

to the process described on page 20 to measure the tuning rate of the DFB laser diode.

The etaloning, or signal variation, due to the detector window is slightly different on each detector, perhaps because the windows are of slightly different thicknesses. Also, this effect changes with temperature as the windows thermally expand or contract. The measured scans using these detectors are usable but for automated analysis they present a difficult problem.

A window with a sufficient wedge angle to it will make a suitable solution. New Focus was contacted for assistance and they replied that they simply purchase the detectors from Judson Technologies, LLC (Judson). Judson offers customizable detector solutions and they offered us detectors packaged in a can with a window wedge angle of approximately 4^o. The optical windows of each can are AR coated sapphire (Al_2O_3). A plot of the transmission through the coatings as a function of wavelength

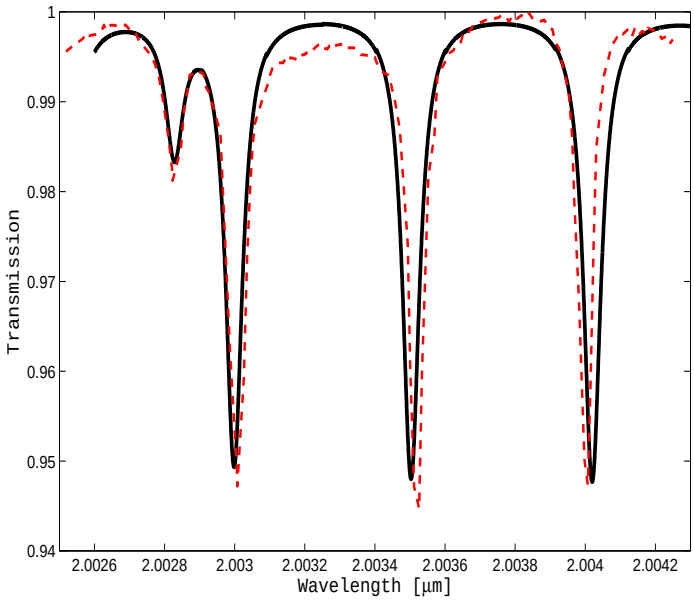


Figure 31: A plot of laser diode scan taken with the two 0.5 mm diameter detectors from Judson. The scan (red dashed line) was taken in the lab and more closely matches the hitran model (black solid line) then did data collected using previous detectors. This is seen in figure 13 on page 29, figure 14 on page 30 & figure 15 on page 32 as a difference of over 5% and now less than 1%.

is seen in figure 53 on page 94. The responsivity of these detectors was given to us by Judson and is plotted as a function of wavelength in figure 30 on the previous page. The temperature of each detector is held at a steady -40^o Celsius by a triple-stage TEC inside the can.

Two detectors, each with an active area diameter of 0.5 mm, were purchased. These detectors were put into the instrument and used for data collection in the field experiments in the summer of 2007. Data taken with these detectors may be seen in figure 31, where the data matches very closely to the HITRAN model.

Originally a focusing lens was simply mounted to the bread board in front of each detector to focus the light onto the active area. This provided a simple and easy setup but extraneous light often caused large changes in the signal during field experiments. Shadows from clouds, people, etc. falling on the instrument caused

changes in the signal by as much as 150%. When the detectors from Judson were received, a large aluminum tube was made into which a lens may be placed. This tube is mounted to the structure that holds each photo diode acting as a light-tight box. See figure 51 on page 92 for a schematic of the detector mounting structure. By blocking the extraneous light, the signal-to-background ratio (SBR) was improved.

Larger Optics

Several changes were made to the instrument to decrease the amount of large variations within each scan that arise from localized fluctuations in the index of refraction in the air. Two inch steering mirrors replaced the 1 inch mirrors that direct the laser beam returning to the instrument onto the transmission detector. Also, a 2 inch diameter lens replaced the smaller lens previously used to focus the transmitted light onto the transmission detector. In addition to these two changes, the focusing lens was moved from being mounted directly in the light-tight box onto a manual, single-axis translation stage. This was done so that the transmitted signal could be maximized by moving the lens closer to or away from the detector surface.

Moving Mirror Mounts

Perhaps the largest source of thermally introduced noise in the data captured in initial outdoor experiments was the mirror mounts themselves. The mounts used are simple kinematic mounts and are made from aluminum but have brass threads. It was shown in the lab that when heated, a mirror mount actually moves due to the mismatched expansions of the threaded materials. This simple lab setup also showed that when cooled the mirror mount did not return to the original position, thus producing large historesis. In the field, as the mounts heat up, due to incident solar radiation and heat from the electronics, the beam walks off of the transmission

detector. Manual adjustments to the steering mounts had to be made about every ten to twenty minutes on a hot day or data was quickly corrupted. To counter this effect, mounts made entirely of stainless steel, which has a coefficient of thermal expansion less than 10 times that of aluminum, were purchased from Thor Labs. The mounts were shown to be more stable for a much longer time without needing user intervention.

ZERT Horizontal Injections 2007

ZERT Horizontal Injection Well Description

The general field layout is described in the section on page 35. A horizontal injection well was put into the field for an injection simulating sequestered CO_2 seepage up through a geologic fault line. The to be injected CO_2 originated from an Alberta natural gas field. The field manager for the ZERT field location, Dr. Laura Dobeck, described the horizontal pipe and installation of the pipe in the following manner:

> The horizontal well was sited on the field 45^o east off of true north. This orientation was chosen to allow resolution of vector components perpendicular to the well of potential CO_2 transport both in ground water and by wind. In order to disturb the formation as little as possible, horizontal directional drilling was chosen as the method of installation over more aggressive, albeit easier and less costly, methods such as trenching. The well casing is 98 meters of 10.16 cm diameter Schedule 40, 304L stainless steel pipe. Fifteen meters and 12 m on the northeast and southwest ends, respectively, is solid casing. The remaining central 70 meters is slotted with a 20-slot pattern and has an open area of 0.55%. Directed Technologies Drilling Incorporated installed the well in early December of 2006. A biodegradable drilling fluid manufactured by Cetco called Cleandrill that is composed largely of cornstarch, guar gum, and xanthan gum was used as a lubricant and later flushed with enzyme breaker in the well development stage. To preserve the connectivity with the surrounding formation use of bentonite as a drilling fluid was avoided. Although effective in the installation process, bentonite would have left an unacceptable impermeable annulus around the well casing.

> Cobble in the gravel layer presented very difficult drilling conditions, and it was not possible to install the well screen without some deflection off of a level straight path. Vertical location (accuracy of +/-5% of the absolute depth) of a sonde in the drilling head was done every 4.6 meters along the length of the well during installation. Thus, depth below ground surface and the location on the surface directly above the well is known at intervals of 4.6 meters. The average depth of the slotted section of the well is 1.8 meters below ground putting most of it in the sandy gravel layer and below the water table at the time of the 2007 CO2 releases.

Refer to figure 19 on page 36 for the location of the horizontal pipe with respect to directions and other parts of the field.

The slots in the horizontal pipe are large enough to prevent an even distribution of injected CO_2 along the pipe. To improve the chances of getting an even distribution of CO_2 along the length of the pipe and to increase the flexibility of the system, the well is partitioned by a system of packers into 6 isolated and independent zones. Because each zone is plumbed separately and has a dedicated mass flow controller, CO_2 flow in each zone may be controlled independently [55]. The mass flow controller and packer (zoning) systems were provided by Sally Benson from Stanford, Ray Solbau and Paul Cook from LBL.

ZERT Horizontal Injection, July 2007

A controlled release using the horizontal injection well was conducted from the 9^{th} to the 19^{th} of July 2007. A flow rate of 0.1 tons CO_2 per day was used for the duration of the release. The gas was delivered to the zones at roughly ambient air temperature and at a pressure of less than 34.5 kPa (5 psi) above atmospheric pressure which is about an absolute pressure of 84 kPa (12.2 psi) [55].

Figure 32 on the next page shows the daily average CO_2 concentration measured directly over the well. It is not clear from the data when the injection started and

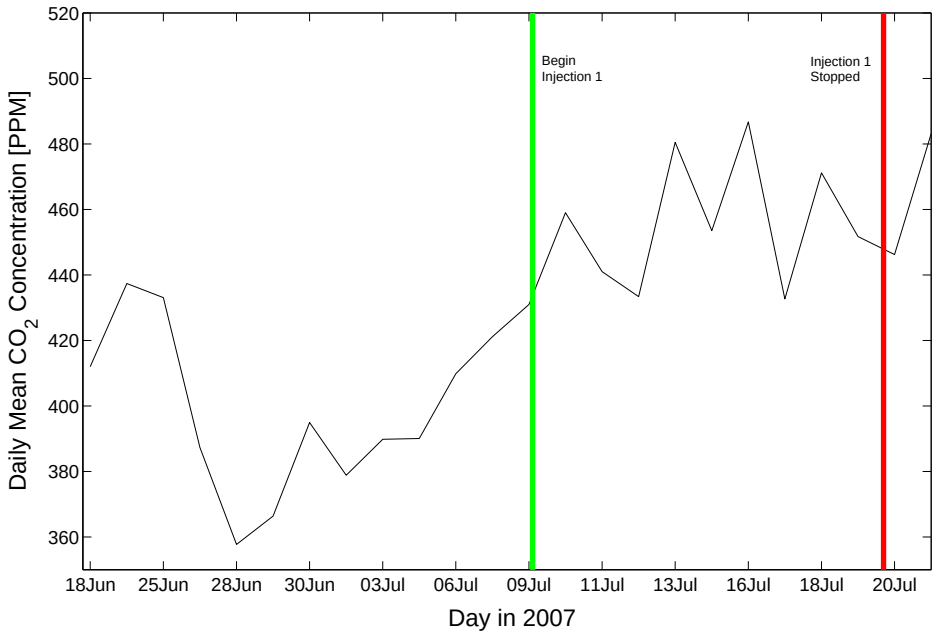


Figure 32: Results of analyzing the scan taken before, during and after the first release through the horizontal injection well.

stopped. Figure 33 shows a typical captured scan used for calculations of CO_2 concentrations. There is a need to measure the concentrations of CO_2 above the field away from the release zone for comparison with concentrations directly above the release.

ZERT Horizontal Injection, August 2007

In August of 2007 a uniform flow rate was delivered to the six zones for a total release rate of 0.3 tons CO_2/day. This is the same amount of CO_2 released from driving 600 miles per day at 20 mpg. The CO_2 injection lasted for an eight day period starting August 3^{rd} through the 10^{th}. The gas was again delivered to the zones at roughly ambient air temperature and pressure [55]. During this release the depth of the water table was approximately 1.6-1.7 m, as measured from the ground surface.

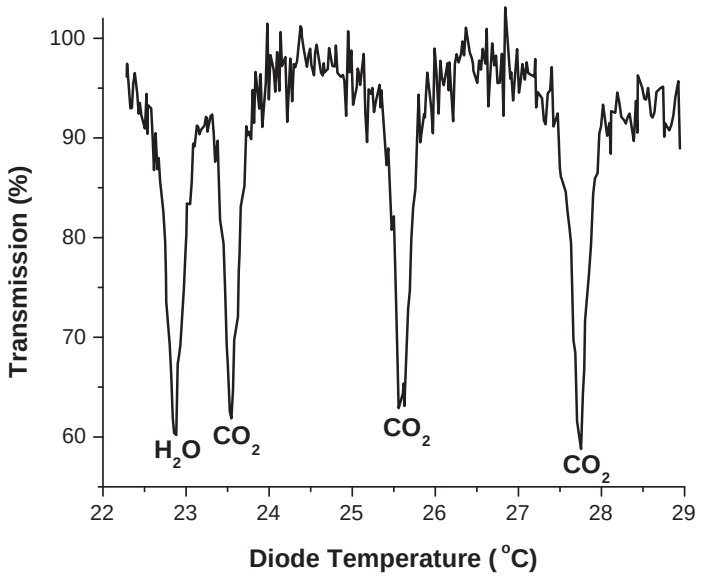


Figure 33: A typical scan capture by CODDA for use in finding CO_2 in the air. This scan, while there is some noise, it is easily analyzed and gives good results.

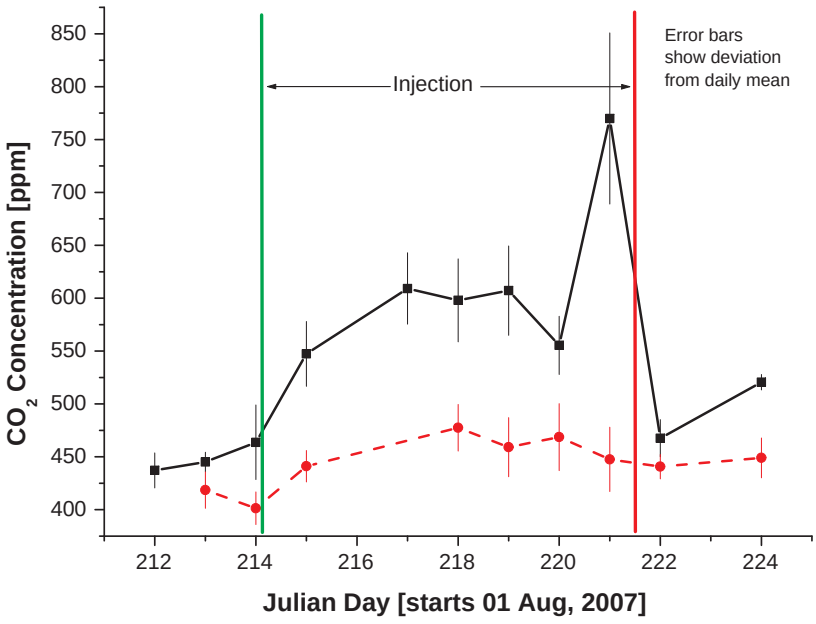


Figure 34: The black line represents the results of analyzing the scans taken over the well before, during and after the seconds release through the horizontal injection well. The dashed red line is results of the data taken away from the injection well.

During the second release, the instrument was setup for the laser to pass directly over the horizontal well at about 10 cm above the surface of the ground. This was done in the early morning and scans were captured until about 9 AM. The scans were analyzed and the concentration results for two CO_2 absorption features were averaged together for a single concentration per scan. The concentration results per scan were then averaged with the results from noisy scans being removed for a single daily average number. Daily standard deviations were also calculated.

Because data from the previous horizontal release was inconclusive, after scanning the laser over the injection pipe the instrument was moved about two hundred meters away from the eastern end of the injection well. The laser was scanned over the same path length in this new location at about 70 cm above the ground. The grass was taller and to avoid having to cut the grass the instrument was raised to about 60 cm above the ground.

Figure 34 on the preceding page shows the daily average CO_2 concentration measurements made both over the well (black line) and away from the well as a background (red dashed line). Also shown in the figure are the daily standard deviations which are shown as the vertical lines for each data point. The CO_2 plume effluent from the injection is evident and easily distinguished from the background CO_2 concentrations in measured data from this release.

Horizontal Release Conclusion

Measurements obtained by participation in from the first horizontal release are not conclusive due to the lack of background measurements. This shows at least two measurements must be made for comparison. This was done for the second horizontal release and the CO_2 effluent from the release is evident compared to the background

data. The two horizontal releases show that the CODDA Instrument functions well outdoors and is capable of distinguishing differences in CO_2 concentrations. However, in the heat of the day the CODDA instrument did not work well. Changes to the instrument to improve the measurements are discussed in the next chapter.

2008 FIELD RELEASE

The results of the 2007 field experiments show marked improvement over measured results from 2006. The data demonstrates the capabilities of the CODDA instrument and shows how it may be used in a monitoring scenario for carbon sequestration site verification. However, the instrument did not perform perfectly and some improvements to the instrument could be made to improve and enhance its capabilities. This chapter will discuss those issues with the instrument and how each issue is addressed and overcome prior to the next controlled release experiments. The setup of the horizontal well controlled release experiment will then be reviewed and the chapter will conclude with results measured by the CODDA instrument prior to, during and after the controlled injection. The injection started on the 9^{th} of July at 2:45 PM and ended on the 7^{th} of August at 10:00 AM.

Instrument Improvements

The measurement of the light transmitted from the instrument and back to it, as seen in the plotted data in figure 33 on page 55, is noisy and on a hot afternoon the captured signal quality decreases rapidly. It is believed that the noise is partly caused by beam steering and also by scintillation. Scintillation is caused by changes in air temperature and pressure which change the index of refraction of the air. The steering, due to thermal movement of the mirror mounts, moves the beam onto or off of optics in the path. This vignettes the beam. This is seen as sharp increases or decreases in the output voltage measured of the detector. As this section discusses, the improvements to the instrument are designed to address these issues and improve the signal quality.

Detector

It is thought that one way to reduce this noise is to have a larger active area detector to measure the return transmission signal. A detector with an active area diameter of 3 mm, 6 times the diameter as previously used, was purchased from Judson Technologies and delivered in October 2007. The detector has a coated, wedged sapphire window, with the same responsivity as the previous detector. The new detector is also held at the same constant temperature, -40^o Celsius, as previous detectors. This detector provides a larger surface over which the focused returning light may vary without changing the measured signal. This detector was used as the transmission detector for the field release experiments in the summer of 2008.

Retro Reflector

Light leaving the instrument box is returned to the instrument using a retro-reflector. This is also known as a corner-cube which is made of three mutually orthogonal mirrors. Light reflected from the corner cube is anti-parallel to the incident light regardless of the orientation of the corner cube with respect to the incident angle of the incoming light. For use with this instrument, the mirrors are made of gold and have a protective coating which provides improved reflectivity at 2 μm.

Data taken prior to the 2008 experimental season used a corner cube with a diameter of 2 inches. For the 2008 measurement season, two new 5 inch diameter retro-reflectors were purchased from PLX, Inc. The larger size is intended to prevent laser light being vignetted on the edges of the retro-reflector or receiving optics.

The manufacturer measured specifications for the two large retro-reflectors are given in figure 56 on page 97 and figure 57 on page 98 respectively.

Diode Mount

For the data collected in the 2007 measurement season, the diode mount was held in place using a single, low profile mounting pedestal. This mount was susceptible to movement due to the vibrations of moving the laser to and from the field each day. These vibrations caused slight rotations to this mount, misaligning the laser with the optics. To fix this for the 2008 season, the diode mount is mounted using a flat plate, multiple bolts and a wide stainless steel base. This locks in place the mount, preventing rotation and vibrational movement. The mount may be seen bolted in place in the instrument in figure 23 on page 43.

Data Collection Method

To measure and record detector output voltages with a computer, a digital multimeter (DMM) with remote communication capabilities was used as part of the instrument. The device used, through the 2007 season, was a Keithley 2000DMM. It is useful in collecting data on multiple channels and for noise filtering, especially noise at 60 Hz. The DMM has a maximum sample rate of about 200 Hz. However, communication with the instrument via GPIB can be slow, reducing the sampling rate to about 3 Hz. Using this DMM, a typical laser temperature tuning scan takes longer than 4 minutes to complete.

To improve data taking and increase the speed of the data acquisition, a portable USB data acquisition (DAQ) system, model USB-6210, was purchased from National Instruments (NI) to replace the DMM. The DAQ has sample rates up to 250,000 samples per second and 8 analog input channels. Repeatable temperature tuning scans of the laser may be made in about 25 seconds. This is a marked improvement over the 4 minutes previously required for a scan. The length of time it takes to

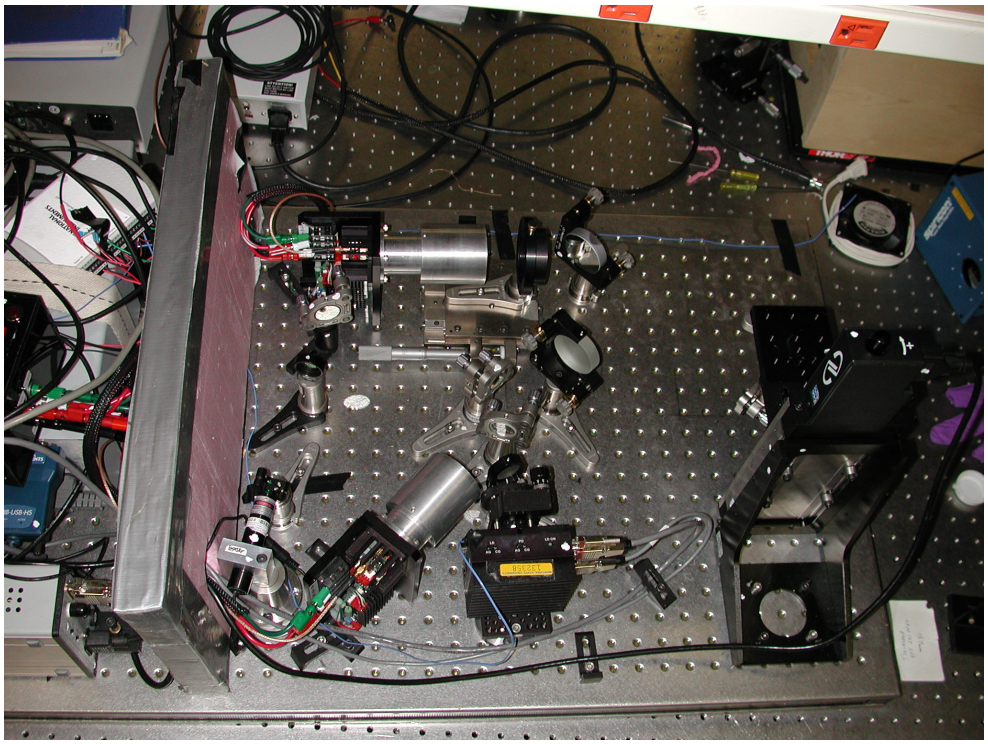


Figure 35: Photo of the CODDA instrument in the lab showing the translation stage used to direct the laser beam in two alternating directions for the 2008 field experiment.

capture a scan is now limited by the repeatability of the temperature tuning of the laser diode and not by the data acquisition system. This is, however, still a longer time scale than scintillations caused by changes in the index of refraction of the air.

Background Measurements

In all previous field deployments the instrument was physically moved from a location for the laser to pass over the injection well to another location to measure the background plant and microbial respiration. The difference between these two measurements is the effluent CO_2 from the injection. However, the time correlation of the measurement was not accurate. Moving the instrument also caused other problems as discussed previously in the section on 60. To solve these issues, a motorized

linear translation stage with mounted turning mirrors was put into the system for the 2008 measurement season. The linear translation stage, mounted to move veritcally, may be seen on the right of figure 35 on the previous page. For the 2008 season, the system captured scans as follows. One laser scan was captured with the laser passing directly over the well. The turning mirrors were then lowered into place via the motorized translation stage to point the laser perpendicular (or orthogonal) to the direction of the horizontal injection well. A laser scan was then captured. The mirrors were then be moved out of the way to take a measurement with the laser pointing over the well, repeating the process. This process, for the two scans, took less than 2 minutes. This provided excellent temporal correlation of the data in the two cases without having to move the instrument.

Instrument Weatherization

During previous field deployments weather events have been a large issue. For example, in the case of rain the instrument had to be quickly moved to a sheltered environment. In the ZERT field, that presents the problem of needing to rapidly cart the instrument across the uneven field, more than 100 meters, at a moments notice.

So that the laser instrument can be left in the field regardless of the weather conditions, a water-tight shipping container large enough to hold the CODDA instrument was purchased. Two six inch diameter PVC flanges were mounted to the container through which the laser in the two different directions may easily pass without being clipped. This container prevents water from entering and possibly damaging the system and also allow data measurements during the night. In the case of *severe* weather, each port flange may quickly be capped to be water tight without moving the system.

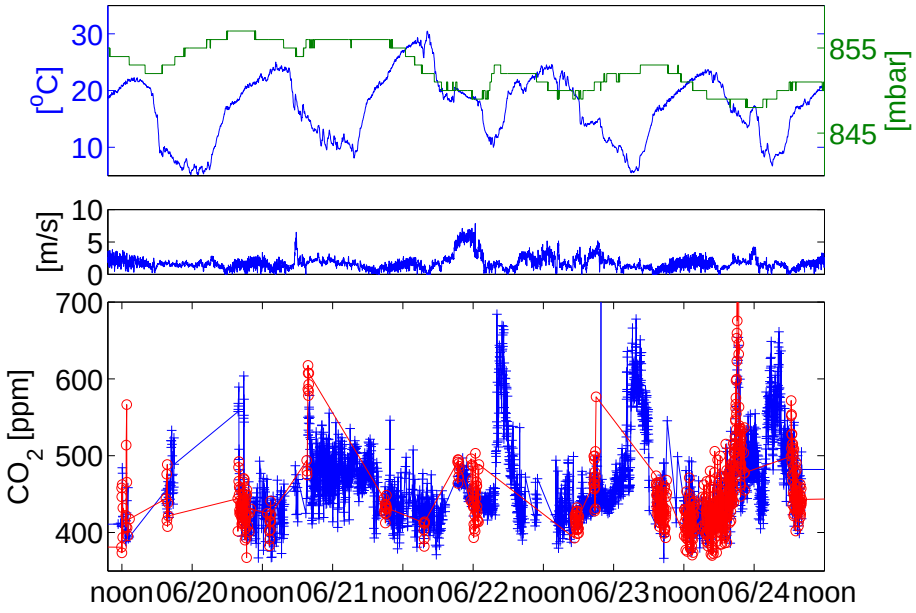


Figure 36: Plot of the CO_2 measured raw data prior to the controlled release experiment.

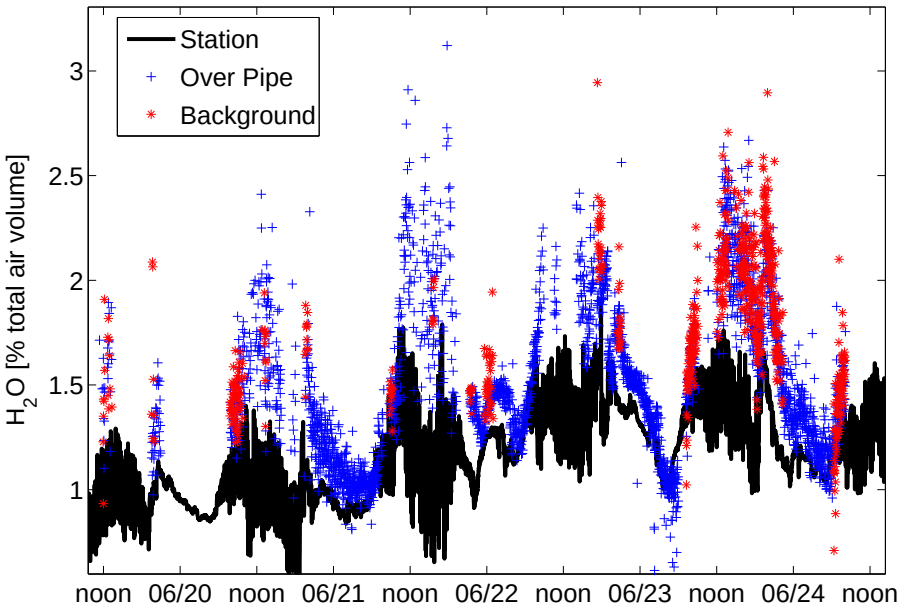


Figure 37: Plot of the H_2O measured raw data prior to the controlled release experiment. The H_2O concentration results are used to validate instrument functionality and multi-direction independency [54].

ZERT Horizontal Injections 2008

For the test injection experiment in 2008, the same field and the same setup as in 2007 are used again. The field setup is described on page 38. The horizontal well setup is described on page 52.

Preliminary Measurements and Results

To test the instrument and prepare for the injection, the CODDA instrument was setup on the edge of the ZERT field for several days prior to the injection. The edge of the field was used for this because a suitable path for the laser was found adjacent to the fence and the rest of the field was yet unmown. Data was taken using scans taken in both directions starting on the 19th and then operated continuously from the 20^{th} to the 24^{th} of June. The results of the measurements may be seen in figures 36 and 37.

The data collected prior to the injection show that there is a large diurnal cycle of CO_2 concentrations. It also clearly shows that the concentrations in the two directions are the same and change together. The water vapor plot is shown to verify that the instrument is working correctly.

Measurements During the Injection

Once the field was mown by the farming crew, the CODDA instrument was setup in place to pass the laser directly over the well and also away from the well. To anchor the instrument container in place and to provide a solid base on which the instrument could be operated, it was placed on four aluminum cylinders. These cylinders are four inches in diameter and are six inches in height. These cylinders were placed in the ground so that the top of each was just over 1 cm above the ground



Figure 38: Photo of the CODDA instrument in measurement location for the ZERT field CO_2 injection of 2008.

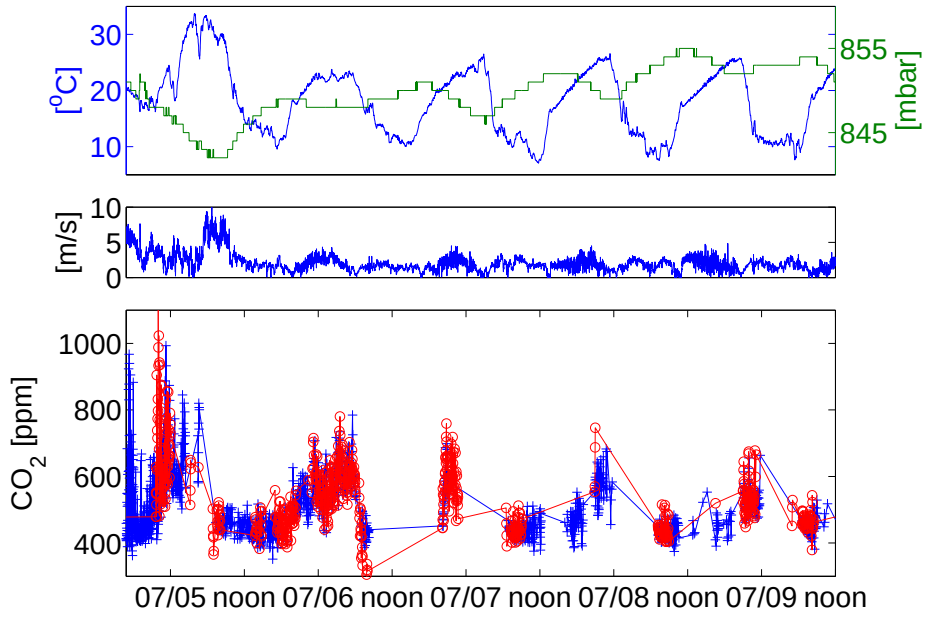


Figure 39: Plot of the CO_2 measured raw data immediately prior to the controlled release experiment [54].

surface. This results in the laser passing about 10 to 12 cm above the ground surface for the measurement. To further secure the instrument, tent stakes were placed at each corner and ropes firmly anchored the container through the handles to the stakes. The CODDA instrument container in place for the field experiment is seen in figure 38 on the preceding page.

In the measurement location, data was captured for a week prior to the start of the injection. Figure 39 on the previous page shows this data taken in place over the injection pipe and also perpendicular to the pipe. There is excellent matching in the measured CO_2 concentrations in the two directions as in the data measured previously on the side of the field.

During the release, data was taken continuously with some exceptions. Power outages, severe weather storms, extra hot days and technical issues are responsible for these outages.

Recorded scans were analyzed in a preliminary manner and results plotted in real time for CO_2 and H_2O concentrations to verify functionality. The data was postprocessed after the injection to improve the calculation. For the post processing, each captured scan was plotted and scans with unacceptable noise levels or that were unanalyzable were removed from the analysis process. The remaining data was then processed using air temperature (^oC) and absolute barometric pressure (mbar) information, unavailable real time in the field, from the weather station in the ZERT field [54]. The concentration results from the analysis for the entire range of the injection is seen in figure 40 on the following page and in figure 41 on page 69. Figure 41 has a ± 40 point, equal weight, moving average applied to the data. The vertical cyan lines in the figures represents rain events that were recorded by an Eddy Covariance Flux Tower operated by Jennifer Lewicki [56].

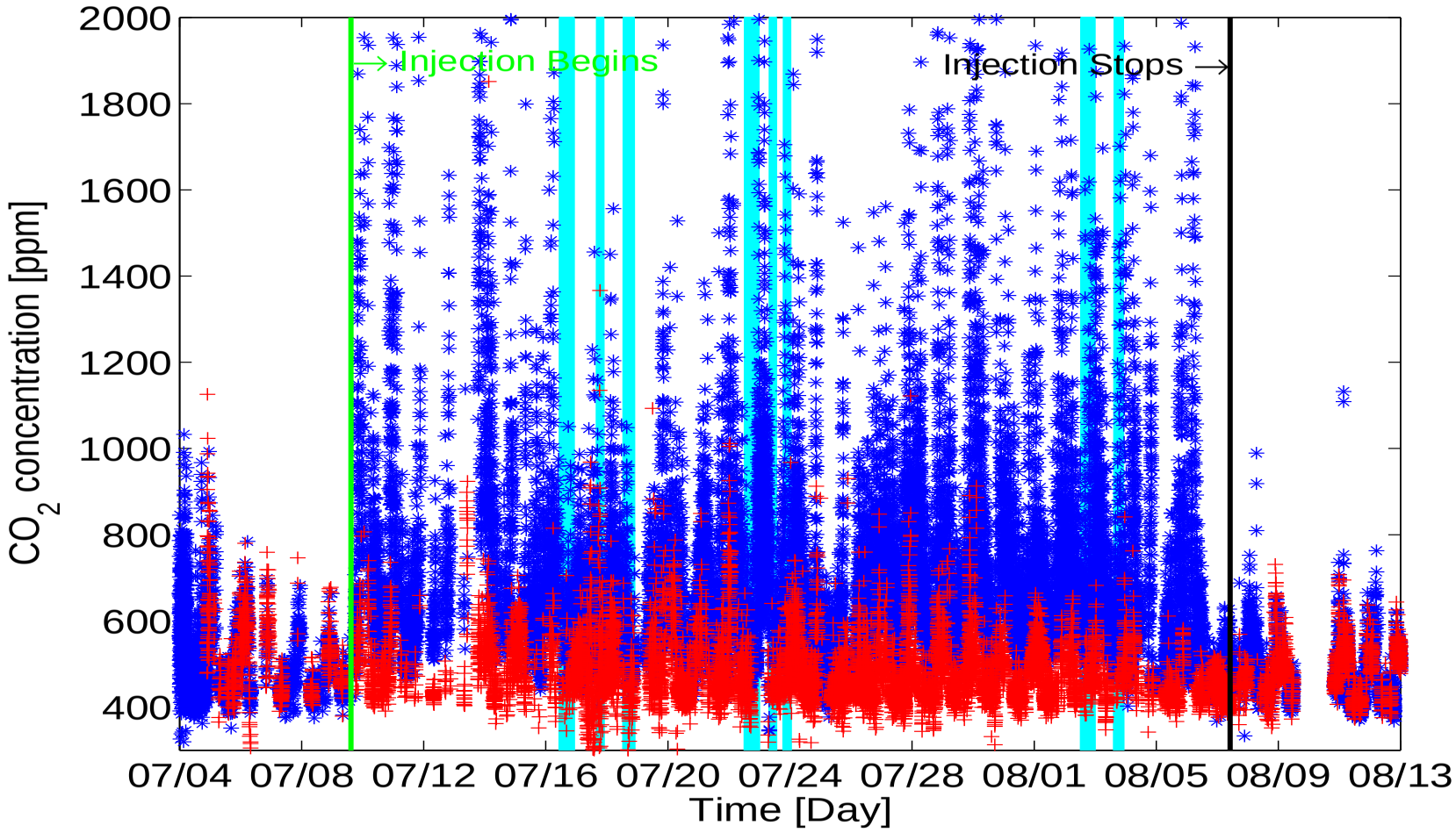


Figure 40: Data taken during the release experiment in 2008. The data is plotted with rain marked as the light blue vertical lines. Thanks to Jennifer Lewicki for the rain information [56].

Horizontal Release Results 2008

Figure 42 on page 70 show a range of data around the start of the injection. Plotted along with the CO_2 data is wind speed (m/s), air temperature (^oC) and absolute atmospheric pressure (mbar) data [54].

From the plotted data, it is evident that prior to the start of the injection, the CO_2 concentrations in the two directions closely match, while shortly after the injection started, a large difference between data from the two directions is seen.

Figure 43 and figure 44 show data from portions of time in the middle of the injection. From the data plots there does appear to be an anti-correlation between wind speed and CO_2 concentrations over the well. This makes sense as a stronger wind would cause the CO_2 to diffuse faster than at lower wind speeds.

Figure 45 are plots of data around the time when the injection was stopped. Some large changes in the measured CO_2 concentrations are evident in most of the plotted data in these and previous figures. However, in this data at the end of the injection, there is a distinct drop prior to the time when the injection was stopped. It is not clear why such large changes were measured but the data indicates that such events are real. Figure 46 on page 72 is a plot of the raw scans measured at various times from Aug 5^{th} through the 6^{th}. The timing of these scans start at the first peak in CO_2 concentration measured, seen in figure 45 on page 71, then they show the low in between the two peaks, the second peak and the low after the second peak.

The data plotted in figure 47 on page 73 is the water vapor concentration measured along with the CO_2 concentration in each captured scan. The concentrations are plotted with humidity information from the weather station in the field [54] to

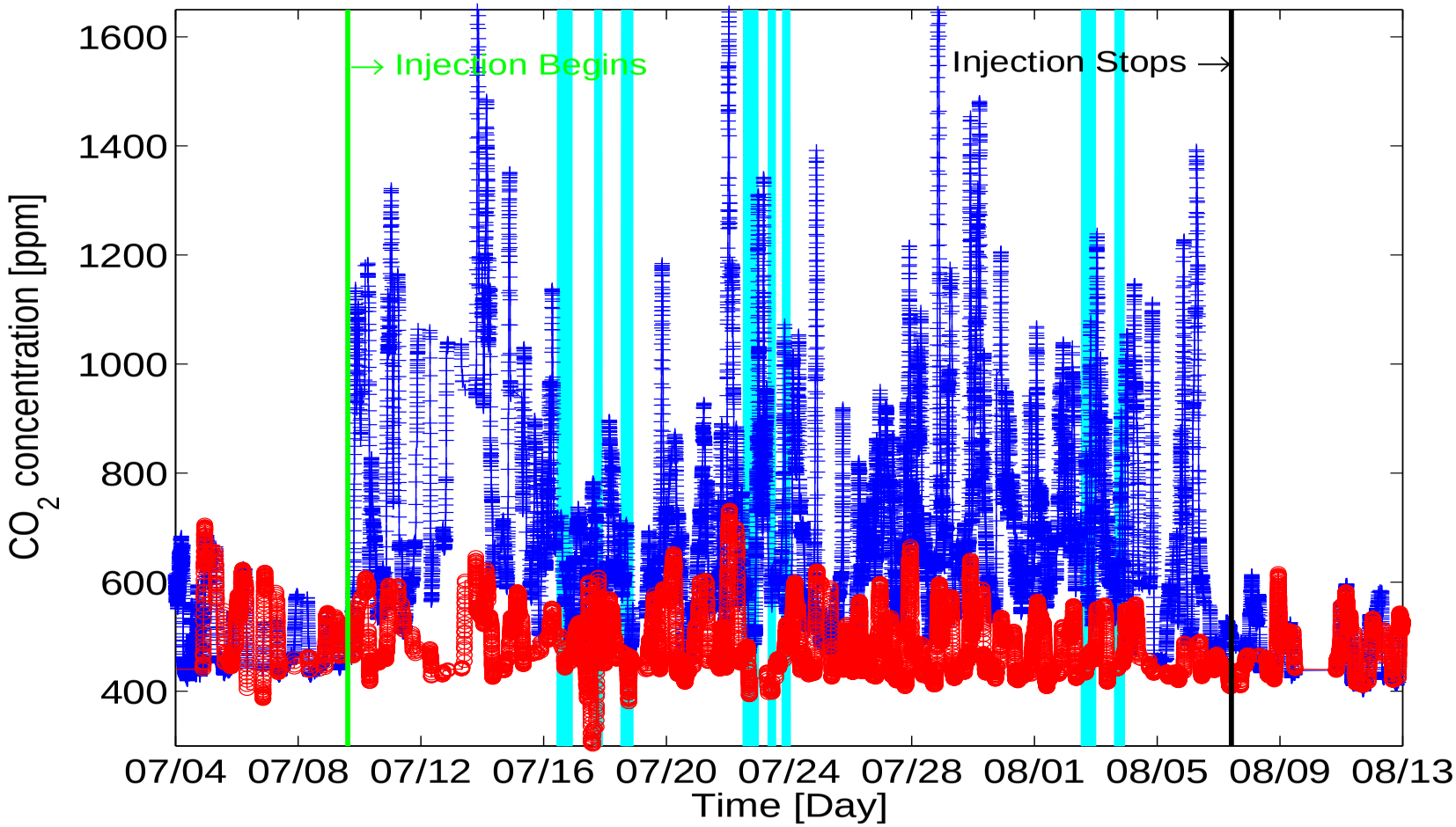


Figure 41: Smoothed data, using a +/-40 point moving average, taken during the release experiment in 2008. The data is plotted with rain marked as the light blue vertical lines. Thanks to Jennifer Lewicki for the rain information [56].

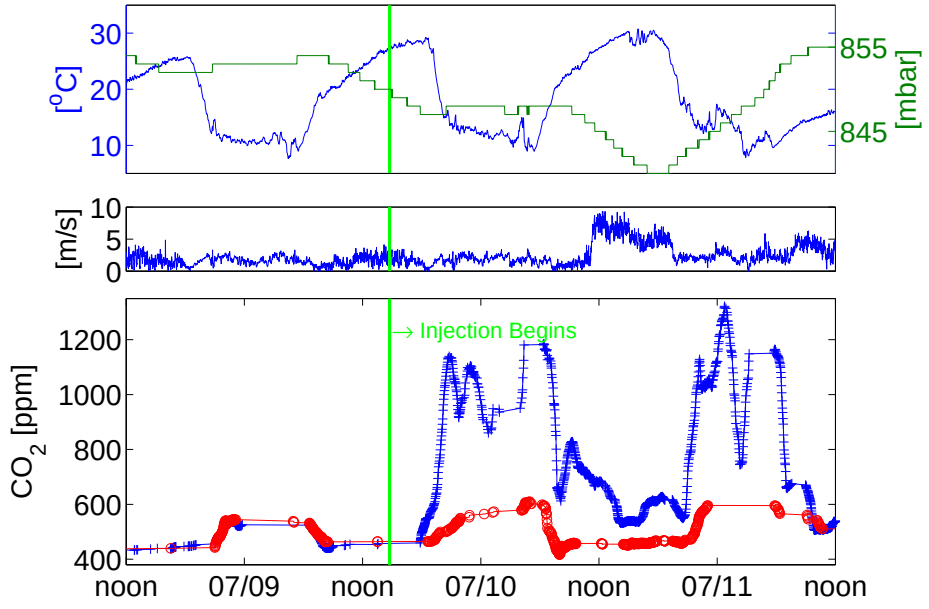


Figure 42: Plot of the CO_2 measured smoothed data and weather information [54, 56] around the time the CO_2 injection was started.

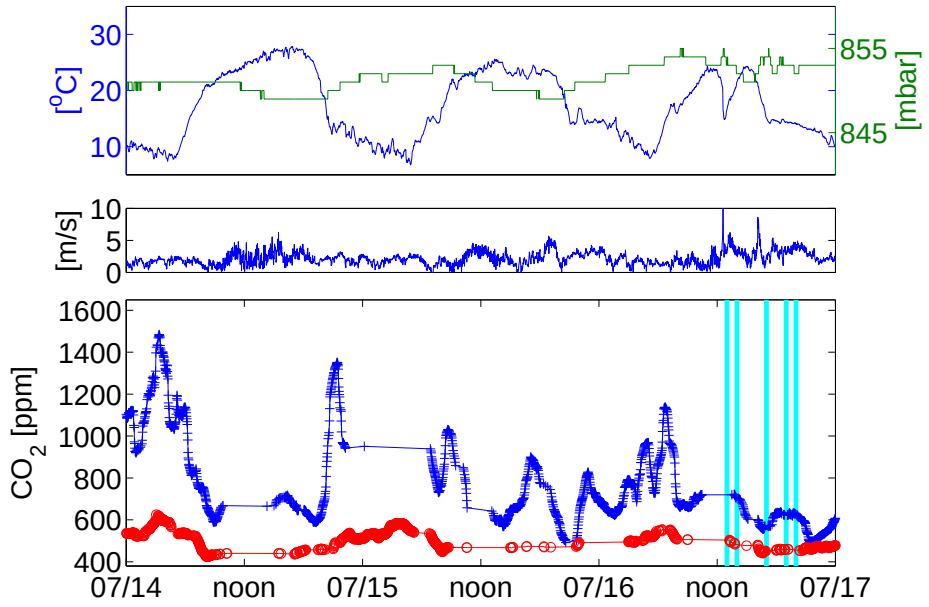


Figure 43: Plot of the CO_2 measured smoothed data and weather information [54, 56] during the CO_2 injection.

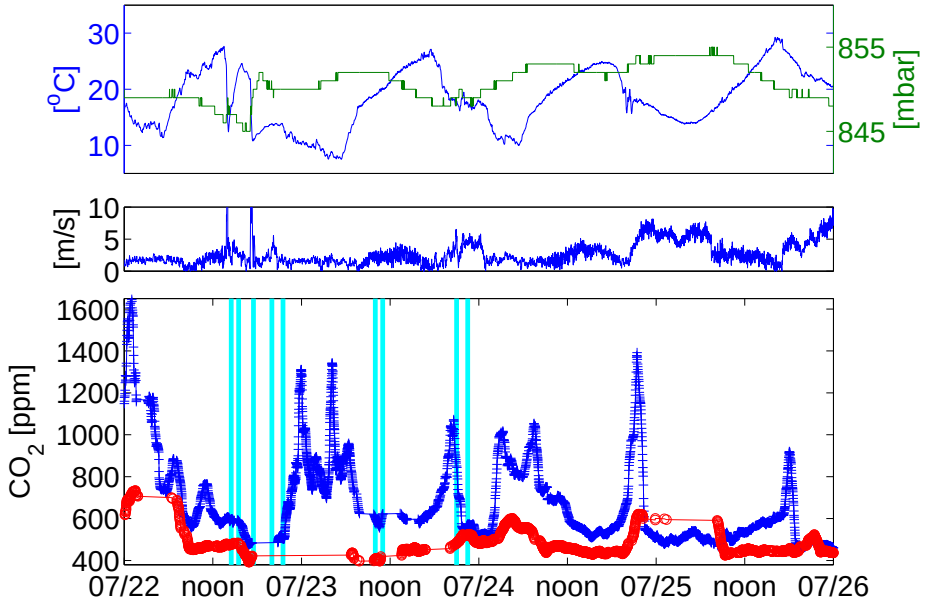


Figure 44: Plot of the CO_2 measured smoothed data and weather information [54, 56] during the CO_2 injection.

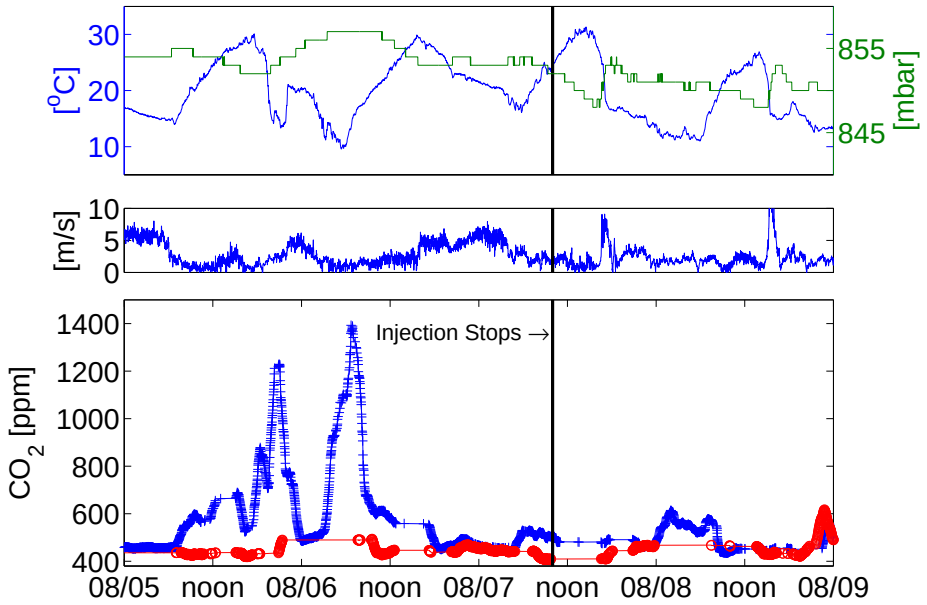


Figure 45: Plot of the CO_2 measured smoothed data and weather information [54, 56] around the time the CO_2 injection was stopped.

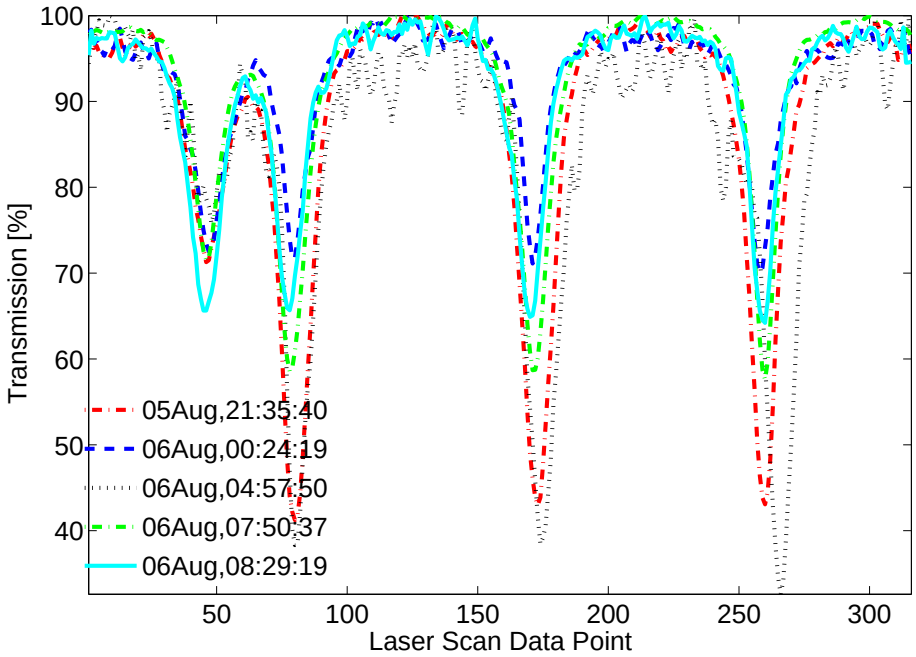


Figure 46: Plot of scan measured over the injection well suring the controlled release. These demonstrate that the large changes in measured CO_2 concentrations are real events.

show the calculations are correct. The difference between the station-measured H_2O [54] and the measured by CODDA can be attributed to the difference in measurement height above the ground. The station measurement being about 1.5 meters above the ground [54] and the CODDA measurement being about 0.1 meters. This is also plotted to show that while there are large differences in the measured CO_2 concentrations between the two directions during the injection, there is no difference in the H_2O concentrations measured. This demonstrates on one more level the correct functionality of the CODDA instrument.

Horizontal Release 2008 Conclusion

The results from this release are exciting. The difference in the CO_2 concentrations is clearly evident, showing that this instrument is capable of monitoring sequestration

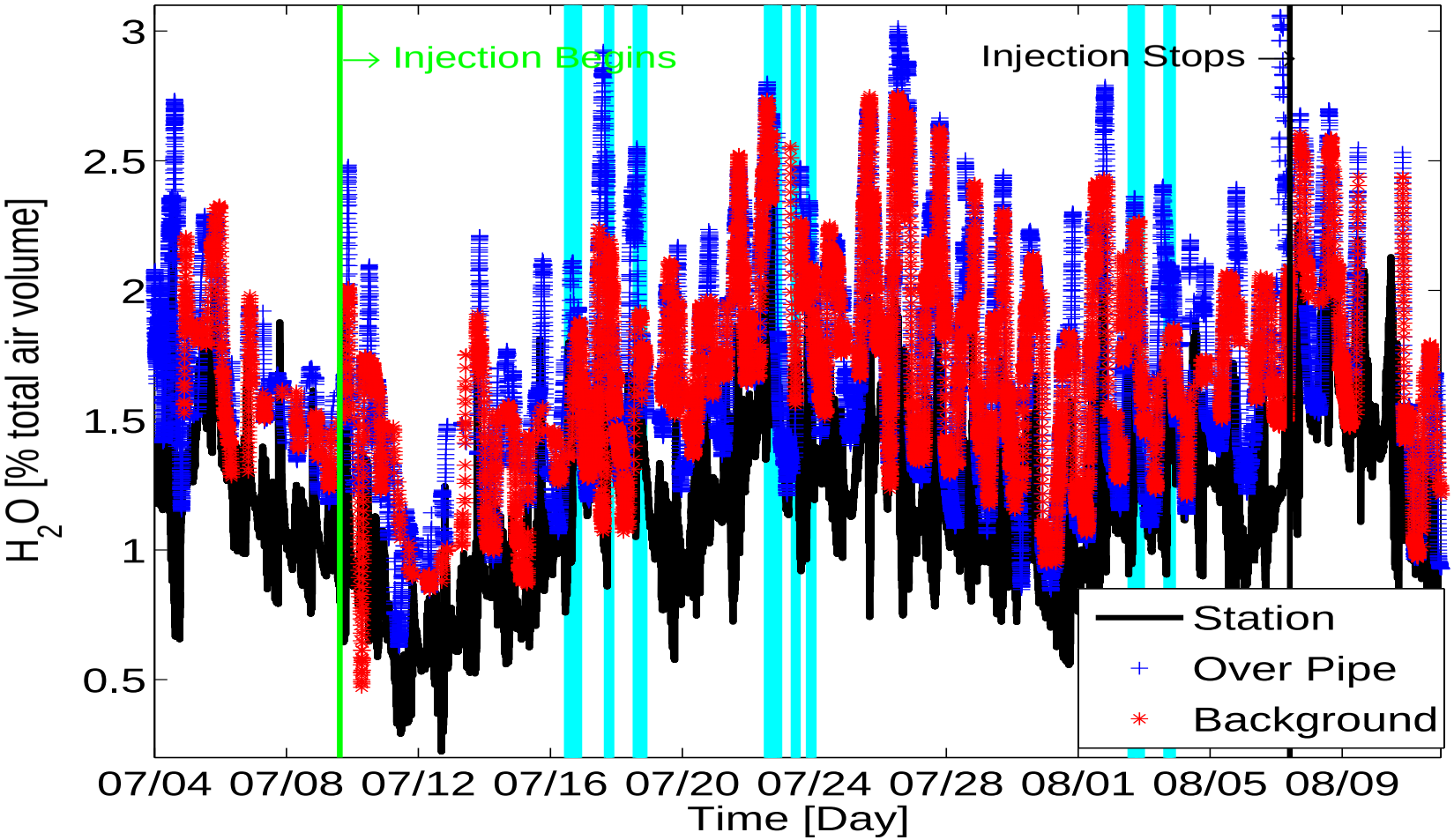


Figure 47: Data taken during the release experiment in 2008 with the moving average applied. Note that during the entire release the water vapor concentrations in both directions, over the injection pipe and away from the pipe, are the same. This measurement is closer to the ground, about 10 cm, than the weather station, about 1.5m, so the water vapor concentration measured by CODDA is higher [54, 56].

sites. However, the CODDA Instrument did not peform perfectly in the 2008 season. Heat was a big issue with the data collection. Another issue was water condensation (dew) on the retro reflector mirror surfaces. These two issues, while challenging, may be overcome to improve the instrument.

CONCLUSION

Instrument Results

The average monthly global concentration of CO_2 in the atmosphere has risen from 315 ppm in 1958 to 382 ppm in 2007 (see figure 2 on page 3) [11, 12]. This is attributed largely to the increase in fossil fuel consumption combined with deforestation [2, 17]. There is steadily growing international concern that CO_2 emissions are altering the global climate [19, 20, 14, 13, 2, 17, 15, 6]. One of many methods to prevent CO_2 emissions is through carbon capture and sequestration (CCS) [1, 23, 24, 25, 23, 24, 25]. CCS prevents CO_2 from being released to the atmosphere, but if the CO_2 is not retained in the chosen storage locations, the benefits of CCS are lost [33, 34, 35]. Sequestration sites need to be monitored to verify storage integrity.

The CODDA Instrument uses a tunable laser diode to measure CO_2 molecular absorption and thus accurate CO_2 concentration from equation 12 on page 12. The instrument achieves this by using a distributed feedback (DFB) laser diode source to tune across several CO_2 absorption features near 2.003 μm. These are strong absorption features and allow the laser path to have a good amount of absorption for a total length of about 100 m.

The instrument system has been shown to work both in the lab and in the field. The results from the field experiments in 2006 demonstrated that the instrument is functional and capable of field measurements that differentiate between an external source of CO_2 and the natural background. The field measurements from the release in 2007 show the capabilities of the instrument and also that not only a differentiation is clear but also quantitative field measurements are possible. The data plotted in figure 34 clearly demonstrates that the instrument is capable of distinguishing between

the ambient CO_2 diurnal cycle and an influx from an external source. The data collected in the 2008 experiement season further demonstrate that CODDA is able to measure CO_2 continuously yielding real time results. The results are clear that the instrument is able to distinguish between normal diurnal changes and artificially induced differences in CO_2 concentrations. This data also shows the ability of the instrument to take data in all Rocky Mountain summer weather conditions, which can range in temperature from about 0 ^{o}C to over 37 ^{o}C. This is an important step towards continuous, year round carbon sequestration site monitoring.

Future Work

The CODDA instrument worked well in the field and there has been a consistant improvement from one measurement season to the next. In working with the instrument there are several issues that become apparent that could be fixed or changed to improve the measured results.

The layout used for alternating directions forced the orthogonal direction to be dependent on the steering of the forward going laser beam. This meant that on hot afternoons marginal data could be collected with the laser passing over the pipe but with the laser passing orthogonal to the pipe the data collected was unusable. The layout of the system needs to be reconsidered and redesigned to make the quality of the return signal in each direction completely independent.

The scintillations due to changes in the air are on a visual time frame, perhaps as fast as 15 ms. In preparation for the field experiements of 2008, some testing was done to determine how fast the laser may be temperature tuned. While the laser could be temperature tuned on the order of 0.1 ms this did not produce repeatable results. As part of this project, no current tuning of the laser diode has been tested. It is

thought that perhaps current tuning over a single absorption feature is possible on a time frame shorted than scintillation effects. This should be tested to determine both repeatability and feasability. If it is possible, this will both enhance the measurement and also increase the temporal resolution. Increased temporal resolution may perhaps lead to better understanding the sharp increases and decreases in changes of CO_2 concentrations during the injection.

Another way to update the instrument would be to run on less power and with an uninteruptible power supply (UPS). With a UPS powering the diode driver and temperature drivers small flickers in the power line would not interupt the data capturing process.

The CODDA instrument can also be improved by better controlling heat produced by the sun and by the electrical equipment while at the same time preventing heat loss at night.

REFERENCES CITED

[1] B. Metz, O. Davidson, H. de Coninck, M. Loos, L. Meyer, editors. *Intergovernmental Panel on Climate Change Special Report on Carbon Dioxide Capture and Storage*. Cambridge University Press, Cambridge, U.K., 2005.

[2] Pieter T. Tans. How can global warming be traced to CO2? *Scientific American*, 295(6):124, Dec 2006.

[3] J. M. Barnola, D. Raynaud, Y. S. Korotkevich, C. Lorius. Vostok ice core provides 160,000-year record of atmospheric CO2. *Nature*, 329(6138):408–414, October 1987. doi:10.1038/329408a0.

[4] Eric Monnin, Andreas Indermühle, André Dällenbach, Jacqueline Flückiger, Bernhard Stauffer, Thomas F. Stocker, Dominique Raynaud, Jean-Marc Barnola. Atmospheric CO2 concentrations over the last glacial termination. *Science*, 291(5501):112 – 114, January 2001. doi:10.1126/science.291.5501.112.

[5] P.N. Pearson, M.R. Palmer. Atmospheric carbon dioxide concentrations over the past 60 million years. *Nature*, 406(6797):695–699, August 2000.

[6] Nicholas J. Shackleton. The 100,000-year ice-age cycle identifed and found to lag temperature, carbon dioxide, and orbital eccentricity. *Science*, 289:1897–1902, 15 September 2000. doi:10.1126/science.289.5486.1897.

[7] J. R. Petit, J. Jouzel, D. Raynaud, N. I. Barkov, J.-M. Barnola, I. Basile, M. Bender, J. Chappellaz, M. Davis, G. Delaygue, M. Delmotte, V. M. Kotlyakov, M. Legrand, V. Y. Lipenkov, C. Lorius, L. Pepin, C. Ritz, E. Saltzman, M. Stievenard. Climate and atmospheric history of the past 420,000 years from the Vostok ice core, Antarctica. *Nature*, 399(6735):429–436, June 1999. doi:10.1038/20859.

[8] K.M Cuffey, F. Vimeux. Covariation of carbon dioxide and temperature from the Vostok ice core after deuterium-excess correction. *Nature*, 412(6846):523–527, August 2001.

[9] Marten Scheffer, Victor Brovkin, Peter M. Cox. Positive feedback between global warming and atmospheric CO2 concentration inferred from past climate change. *GEOPHYSICAL RESEARCH LETTERS*, 33(L10702), 2006. doi:10.1029/2005GL025044.

[10] J. R. Petit, J. Jouzel, D. Raynaud, N. I. Barkov, J.-M. Barnola, I. Basile, M. Bender, J. Chappellaz, M. Davis, G. Delaygue, M. Delmotte, V. M. Kotlyakov, M. Legrand, V. Y. Lipenkov, C. Lorius, L. Pepin, C. Ritz, E. Saltzman, M. Stievenard. Vostok ice core CO2 data. *Nature*, 399(6735):429–436, June 1999. doi:10.1038/20859.

[11] Monthly average carbon dioxide concentration. Scripps Institute of Oceanography in colaboration with the National Oceanic and Atmospheric Administation (NOAA), May 2007.

[12] Global stations CO2 concentration trends. Scripps Institute of Oceanography in colaboration with the National Oceanic and Atmospheric Administation (NOAA), November 2007.

[13] Richard J. Norby, Yiqi Luo. Evaluating ecosystem responses to rising atmospheric CO2 and global warming in a multi-factor world. *New Phytologist*, 162(2):281–293, 2006.

[14] James Hansen. Defusing the global warming time bomb. *Scientific American*, 290(3):68, 2004.

[15] Konstantin Y. Vinnikov, Norman C. Grody. Global warming trend of mean tropospheric temperature observed by satellites. *Science*, 302:269–272, 10 October 2003. doi:10.1126/science.1087910.

[16] M. New, M. Hulme, P.D. Jones. Representing twentieth century space-time climate variability. Part 1: Development of a 1961-90 mean monthly terrestrial climatology. *Journal of Climate*, 12:829–856, 1999.

[17] Pieter T. Tans. Trends in atmospheric carbon dioxide. *National Oceanic & Atmospheric Administration*, 17, April 2006.

[18] C. D. Keeling, S. C. Piper, R. B. Bacastow, M. Wahlen, T. P. Whorf, M. Heimann, H. A. Meijer. Atmospheric CO2 and 13CO2 exchange with the terrestrial biosphere and oceans from 1978 to 2000: Observations and carbon cycle implications. *A History of Atmospheric CO2 and its effects on Plants, Animals, and Ecosystems*, pages 83–113, 2005.

[19] J. Alcamo, G.J.J. Kreileman. Emission scenarios and global climate protection. *Global Environmental Change*, 6(4):305–334, 1996.

[20] Climate Change 2001. Synthesis Report. A contribution of working groups I, II, and III to the third assessment report of the Intergovernmental Panel on Climate Change. Technical Report, Cambridge University Press, Cambridge, UK, 2001.

[21] Climate Change 2001. -Mitigation. the third assessment report of the Intergovernmental Panel on Climate Change. Technical Report, Cambridge University Press, Cambridge, UK, 2001.

[22] Howard J. Herzog. What future for carbon capture and sequestration? *American Chemical Society*, 35(7):148–153, April 2001. Massachusetts Institute of Technology.

[23] Lawrence Berkeley National Laboratory. *An Overview of Geologic Sequestration of CO2*. ENERGEX'2000: Proceedings of the 8th International Energy Forum. Las Vegas, NV, July 2000.

[24] Tianfu Xu. CO2 geological sequestration. *Lawrence Berkeley National Laboratory.*, Paper LBNL-56644 JArt, November 18, 2004.

[25] D. Mingzhe, L. Zhaowen, L. Shuliang, S. Huang. CO2 sequestration in depleted oil and gas reservoirs-caprock characterization and storage capacity. *Energy conservation and Management*, 47:1372–1382, 2006.

[26] LBNL. *Relevance of underground natural gas storage to geologic sequestration of carbon dioxide*. Sixth International Conference on Greenhouse Gas Control Technologies (GHGT-6), Kyoto (JP), October 2002.

[27] Coal: America's energy future Volume II: A technical overview. Technical Report, The National Coal Council, March 2006.

[28] R. Korbol, A. Kaddour. Sleipner Vest CO2 disposal - injection of removed CO2 into the Utsira formation. *Energy Conversion and Management*, 36:509–512, 1995.

[29] This project is described at www.bp.com.

[30] S.G. Whittaker, K. Kreis, T.L. Davis, Z. Hajnal, T. Heck, L. Penner, H. Qing, B. Rostron. Characterizing the geologic container at the Weyburn field for subsurface CO2 storage associated with enhanced oil recovery. *Proceedings of the Diamond Jubilee convention of the Canadian Society of Petroleum Geologists*, 2002.

[31] S.G. Whittaker. Geological storage of greenhouse gases: The IEA Weyburn CO2 monitoring and storage project. *Canadian Society of Petroleum and Geologists Reservoir*, 31(8):9, Sep 2004.

[32] Kevin G. Knauss, James W. Johnson, Carl I. Steefel. Evaluation of the impact of CO2, co-contaminant gas, aqueous fluid and reservoir rock interactions on the geologic sequestration of CO2. *Chemical Geology*, 217:339– 350, 2005.

[33] Elizabeth J.Wilson, Timothy L. Johnson, David W. Keith. Regulating the ultimate sink: Managing the risks of geologic CO2 storage. *Environmental Science & Technology*, 37(16):3476–3483, August 2003. doi:10.1021/es021038.

[34] *Monitoring to ensure safe and effective geologic sequestration of carbon dioxide*. Intergovernmental Panel on Climate Change. Regina, Canada, 2002.

[35] Robert P. Hepple. Implications of surface seepage on the effectiveness of geologic storage of carbon dioxide as a climate change mitigation strategy. *Lawrence Berkeley National Laboratory,*, Paper LBNL-51267, July 30, 2002.

[36] S. M. Benson, E. Gasperikova, G. M. Hoversten. Monitoring protocols and life-cycle costs for geologic storage of carbon dioxide. pages 1259–1266. Proceedings of the 7th International Conference on Greenhouse Gas Control Technologies (GHGT-7), 2005.

[37] Diego Riveros-Iregui. *Hydrologic-Carbon Cycle Linkages in a Subalpine Catchment.* Doctoral Dissertation, Montana State University, Sep 2008.

[38] D. D. Baldocchi. Assessing the eddy covariance technique for evaluating carbon dioxide exchange rates of ecosystems: past, present, and future. *Global Change Biology*, 9:479–492, 2003.

[39] D. P. Billesbach, M. L. fischer, M. S Torn, J. A. Berry. A portable eddy covariance system for measurement of ecosystem-atmosphere exchange of CO2, water vapor, and energy. *Journal of Atmospheric and Oceanic Technology*, 21:639–650, 2004.

[40] K. J. Davis, P. S. Bakwin, C. Yi, B. W. Berger, C. Zhaos, R. M. Teclaw, J. G. Isebrands. The annual cycles of CO2 and H2O exchange over a northern mixed forest as observed from a very tall tower. *Global Change Biology*, 9:1278–1293, 2003.

[41] N. T. Edwards, J. S. Riggs. Automated monitoring of soil resparation: a moving chamber design. *Soil Science Society of America Journal*, 67:1266–1271, 2003.

[42] T. J. Griffis, J. M. Baker, S. D. Sargent, B. D. Tanner, J. Zhang. Measuring field scale isotopic CO2 fluxes with tunable diode laser absorption spectroscopy and micrometeorological techniques. *Agricultural and Forest Meteorology*, 124:15–29, 2004.

[43] Bill Wilcox Jr., Dennis Killinger. *Hitran-PC: Installation and User Manual for Version 3.00*, Chapter 6. Ontar Corparation, May 2000.

[44] L. S. Rothman, A. Barbe, D. Chris Benner, L. R. Brown, C. Camy-Peyret, M.R. Carleer, K. Chance, C. Clerbaux, V. Dana, V. M. Devi, A. Fayt, J.-M. Flaud, R.R. Gamache, A. Goldman, D. Jacquemart, K.W. Jucks, W. J. Lafferty, J.-Y. Mandin, S.T. Massie, V. Nemtchinov, D.A. Newnham, A. Perrin, C.P. Rinsland, J. Schroeder, K.M. Smith, M.A.H. Smith, K. Tang, R. A. Toth, J. Vander Auwera, P. Varanasi, K. Yoshino. The HITRAN molecular spectroscopic database: Edition of 2000 including updates through 2001. *Journal of Quantitative Spectroscopy & Radiative Transfer*, 82:5–44, March 2003.

[45] Gerhard Herzberg. *Molecular spectra and molecular structure. II: Infrared and Raman spectra of polyatomic molecules*, Volume 2. D. Van Nostrand, 1949.

[46] Gerhard Herzberg. *Molecular spectra and molecular structure. III: Electronic spectra and electronic structure of polyatomic molecules*, Volume 3. Van Nostrand Reinhold, 1966.

[47] Kevin S. Repkasy, Seth D. Humphries, John L. Carlsten. Differential absorption measurements of carbon dioxide using a temperature tunable distributed feedback diode laser. *Review of Scientific Instruments*, 77(11):113107, 2006. doi:10.1063/1.2370746.

[48] Michael Drew Obland. *Water Vapor Profiling using a Widely Tunable Amplified Diode Laser Differential Absorption Lidar (DIAL).* Doctoral Dissertation, Montana State University, May 2007.

[49] Damien Weidmann, Anatoliy A. Kosterev, Frank K. Tittel, Neil Ryan, David McDonald. Application of a widely electrically tunable diode laser to chemical gas sensing with quartz-enhanced photoacoustic spectroscopy. *Optics Letters*, 29(16):1837–1839, 2004.

[50] G. C. Bjorklund, M. D. Levenson, W. Lenth, C. Ortiz. Frequency modulation (FM) spectroscopy. *Applied Physics B: Lasers and Optics*, 32(3):145–152, Nov 1983. doi:10.1007/BF00688820.

[51] Nanoplus: Nanosystems and Technologies GmbH, March 2008.

[52] H. Kogelnik, C. V. Shank. Coupled-wave theory of distributed feedback lasers. *Journal of Applied Physics*, 43(5):2327–2335, May 1972. doi:10.1063/1.1661499.

[53] J. Seufert, M. Fischer, M. Legge, J. Koeth, R. Werner, M. Kamp, A. Forchel. DFB laser diodes in the wavelength range from 760 nm to 2.5 μm. *Spectrochimica Acta Part A: Molecular and Biomolecular Spectroscopy*, 60(14):3243–3247, December 2004. doi:doi:10.1016/j.saa.2003.11.043.

[54] The weather station is operated and maintained by Dr. Joe Shaw and Nick Jurich.

[55] Seth D. Humphries, Amin R. Nehrir, Charlie J. Keith, Kevin S. Repasky, Laura M. Dobeck, John L. Carlsten, Lee H. Spangler. Testing carbon sequestration site monitor instruments using a controlled carbon dioxide release facility. *Applied Optics*, 47(4):548–555, February 2008. doi:10.1364/AO.47.000548.

[56] Rain data collected by instruments operated by Dr. Jennifer Lewicki of Berkeley National Labs.

APPENDICES

APPENDIX A

WEDGE DETAILS

A glass wedge is a piece of glass with flat surfaces but those surfaces are intended to not be parallel with each other. In this case, the two points of interest lay in the difference between the angles of the light reflected off the front surface and the light that is reflected off of the back surface and then transmitted through the front surface.

Light incident on the first surface of the glass forms some angle, θ_i, with respect to the surface normal. Some of the incident light is reflected off of the front surface at angle θ_{rf} which is known using Snell's law of reflection and is written as

$$\theta_{rf} = \theta_i \tag{14}$$

Some of the incident light is transmitted through the front surface into the glass. Using Snell's law of transmission to find the transmitted angle, θ_t, yields

$$\theta_t = sin^{-1}\left(\frac{n_1\ sin(\theta_i)}{n_2}\right) \tag{15}$$

Where n_1 and n_2 are the indices of refraction for the first and second mediums respectively.

By geometry the angle of incidence on the back surface of the glass, θ_{tbr}, with respect to surface normal, may be written as

$$\theta_{tb} = \theta_t + \alpha \tag{16}$$

where α is the angle formed by the two surfaces of the wedge.

Some of the light incident on the back surface will be transmitted at an angle, θ_{ttb}, defined by Snell's law of transmission to yield

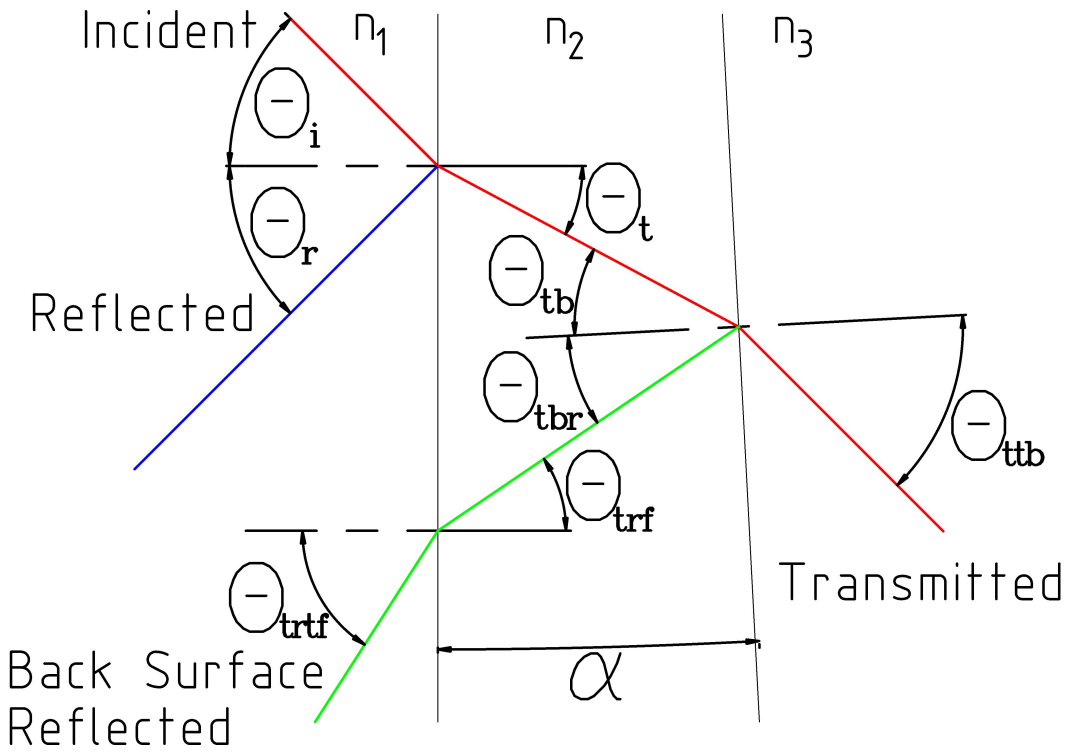


Figure 48: Detailed drawing of incident light transmission through and reflections off of a glass wedge.

$$\theta_{ttb} = sin^{-1}\left(\frac{n_2\ sin(\theta_{tbr})}{n_3}\right) \tag{17}$$

Where n_2 and n_3 are the indices of refraction for the second and third mediums respectively.

Some of the light is reflected off of the back surface towards the front surface at angle θ_{tb}. this is written as

$$\theta_{tbr} = \theta_{tb} \tag{18}$$

θ_{trf} may be rewritten with respect to the normal of the front surface as

$$\theta_{trf} = \theta_{tbr} + \alpha = \theta_t + 2\alpha \tag{19}$$

Some of this light is then transmitted through the glass forming an angle, θ_{trtf}, defined by Snell's law of transmission. This is written as

$$\theta_{trtf} = sin^{-1}\left(\frac{n_2\ sin(\theta_{trf})}{n_1}\right) \tag{20}$$

Figure 48 shows the incident light transmitted into and through the glass wedge. The figure includes only first reflections. There are more reflections that, depending on the amount reflected, may be a significant portion of the incident light.

The glass wedge in use in the CODDA System is made of BK7 and has about a 3^o wedge angle to it. So, if we assume the glass has index of refraction of $n_2 = 1.5$, that $n_1 = n_3 = 1$, $\alpha = 3^o$ and θ_i=45^o, that results in θ_t=28.13^o, $\theta_{trf} = 34.13^o$, and finally $\theta_{trtf} = 57.3^o$. This is 12^o greater than the reflection off of the front surface, $\theta_{rf} = 45^o$.

APPENDIX B

EXTERNAL DRAWINGS AND SCHEMATICS

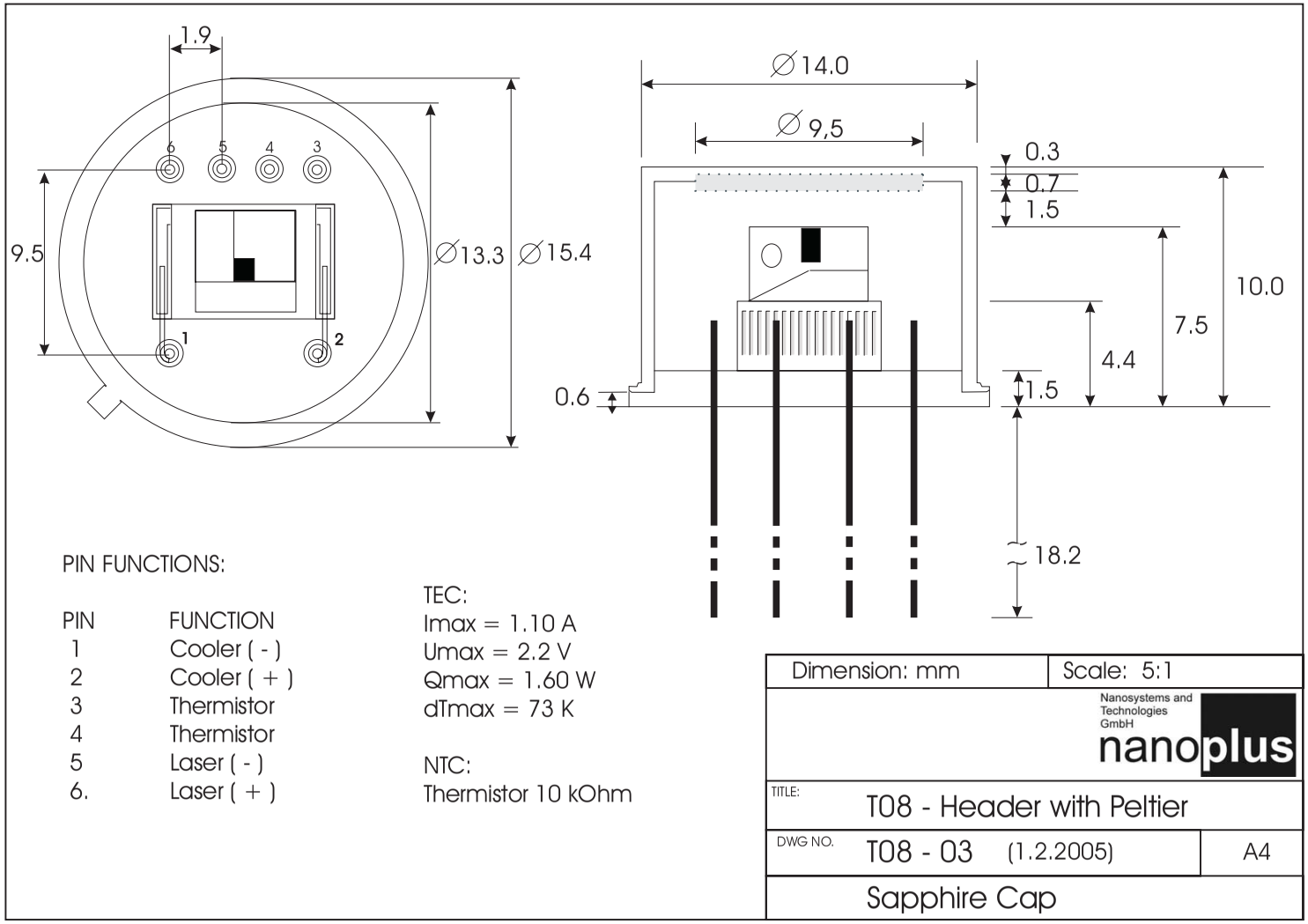


Figure 49: Drawing of the TO-8 can holding the DFB laser diode which is mounted on the TEC.

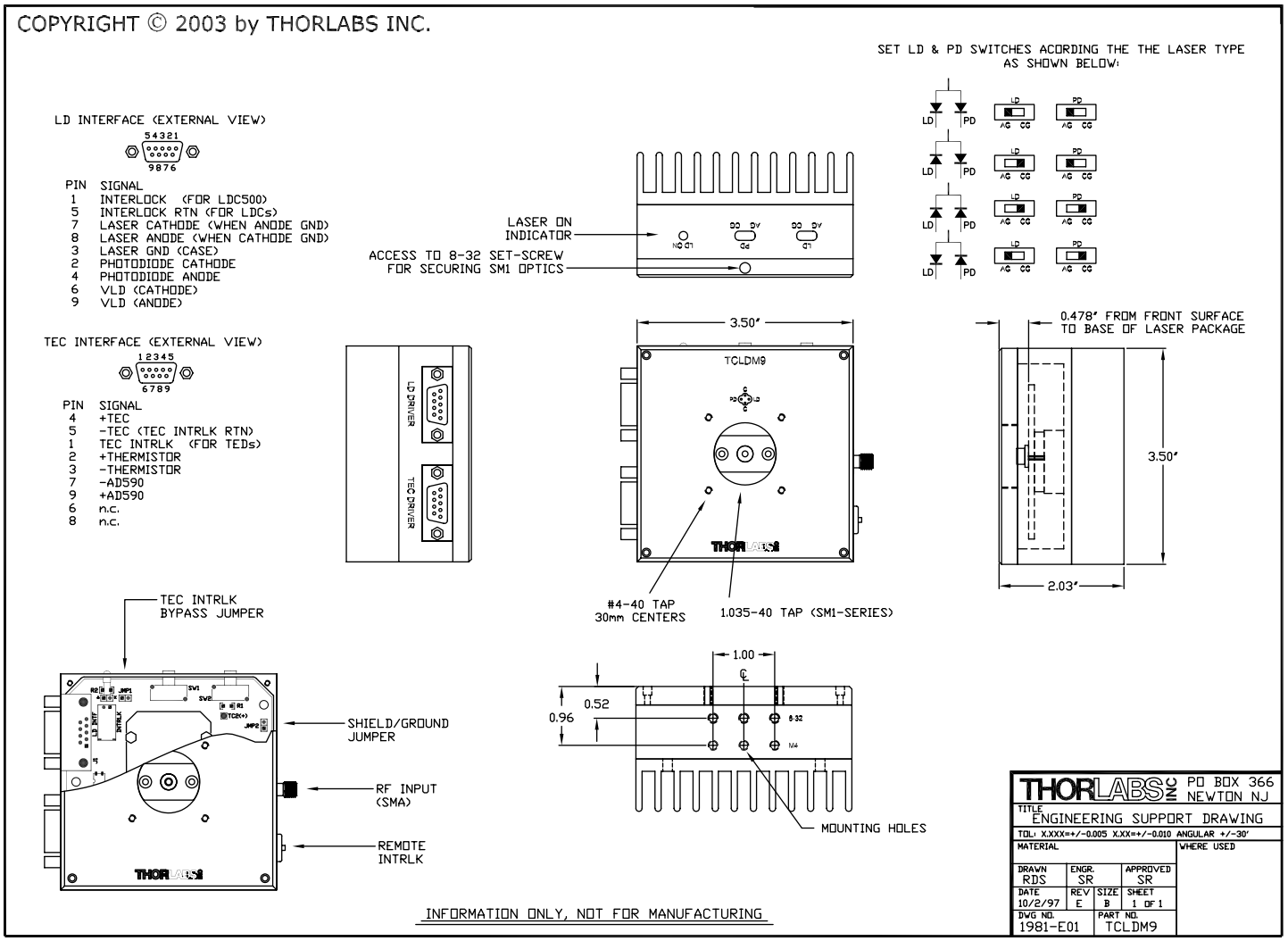


Figure 50: Drawing of the laser mount used to hold the laser diode. The mount has an internal TEC that holds the temperature of the DFB laser diode more stable.

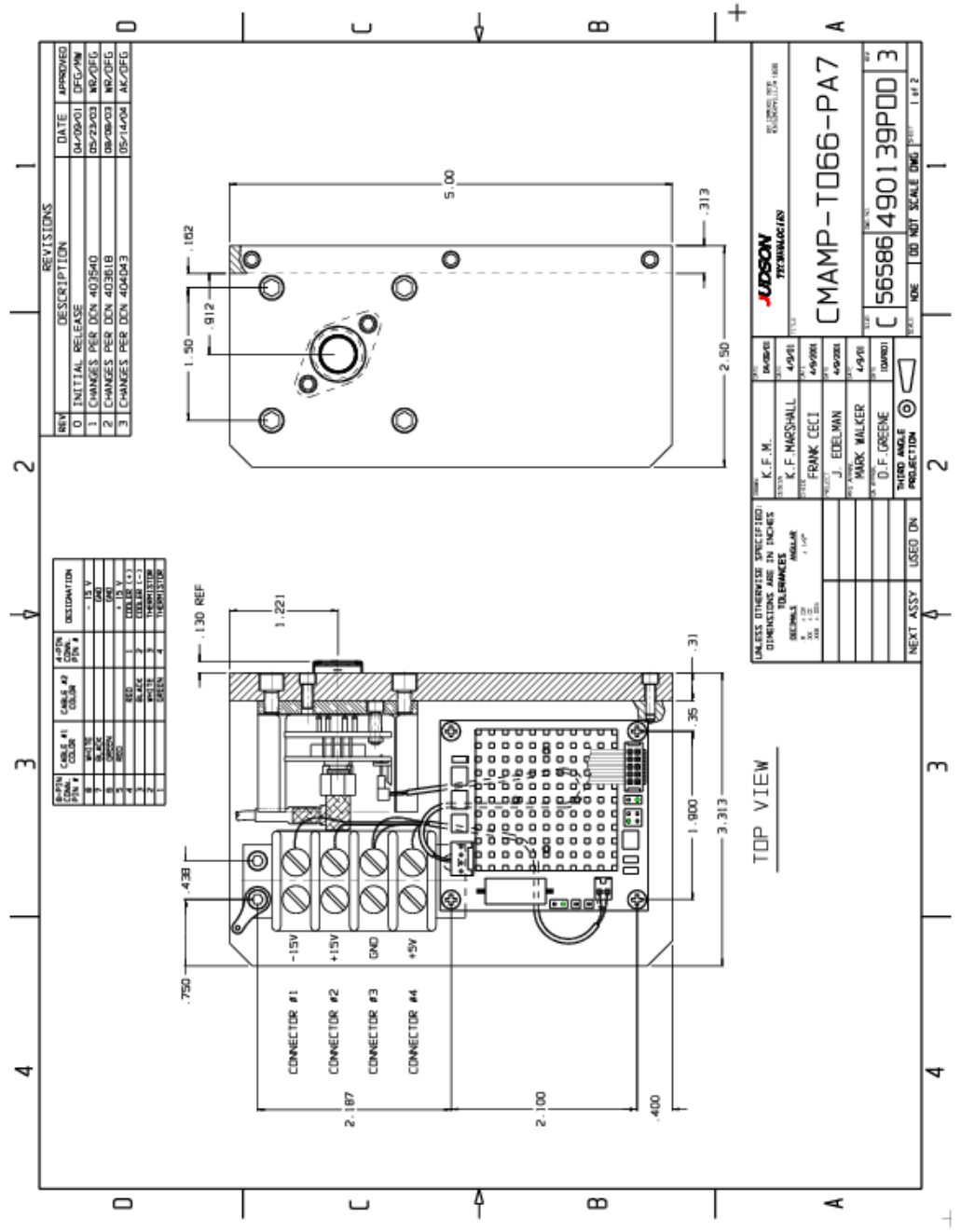


Figure 51: Drawing and specifications for the Judson 2.2 μm detector mount.

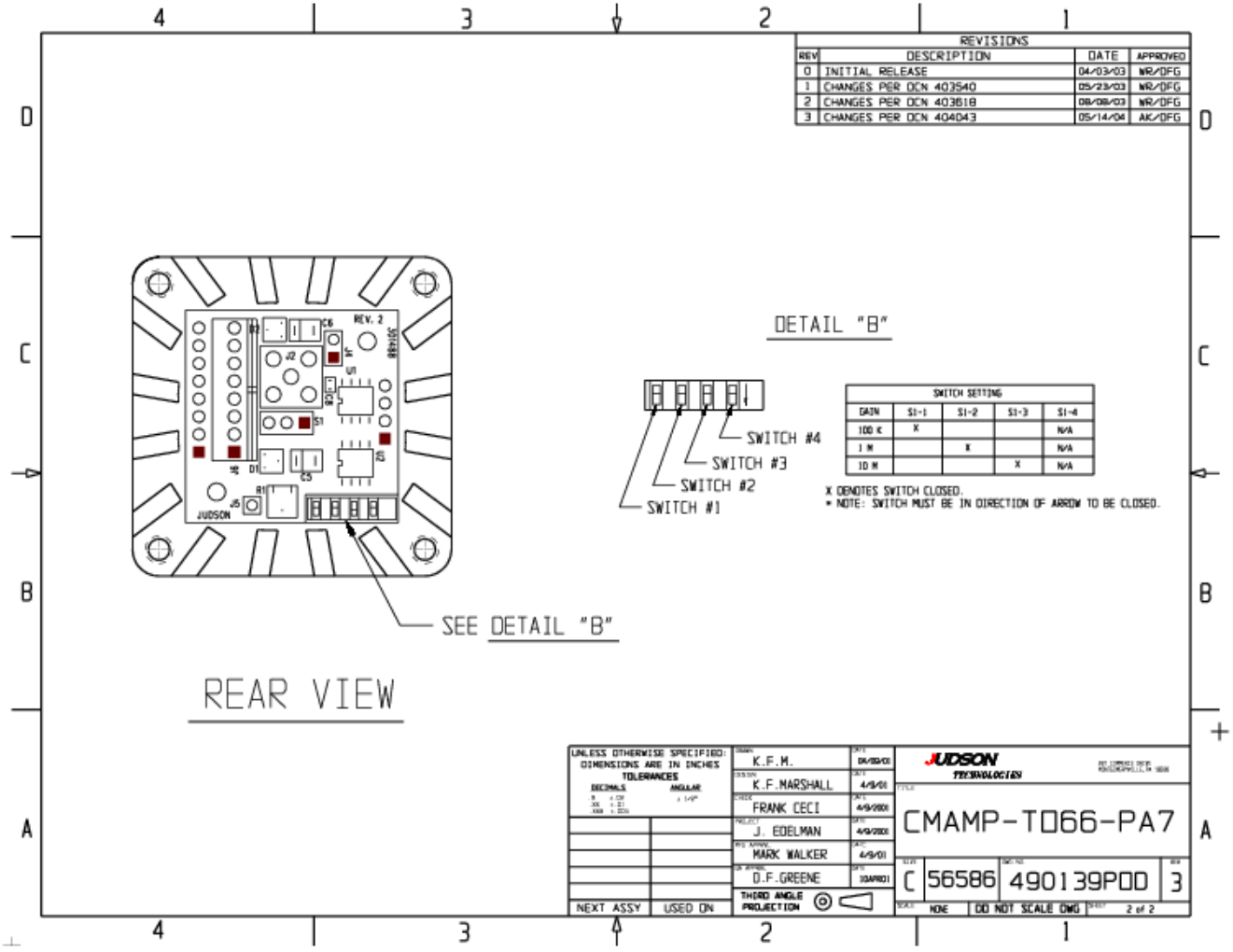


Figure 52: Drawing and specifications for the TEC controller that is mounted with the Judson 2.2 μm detector.

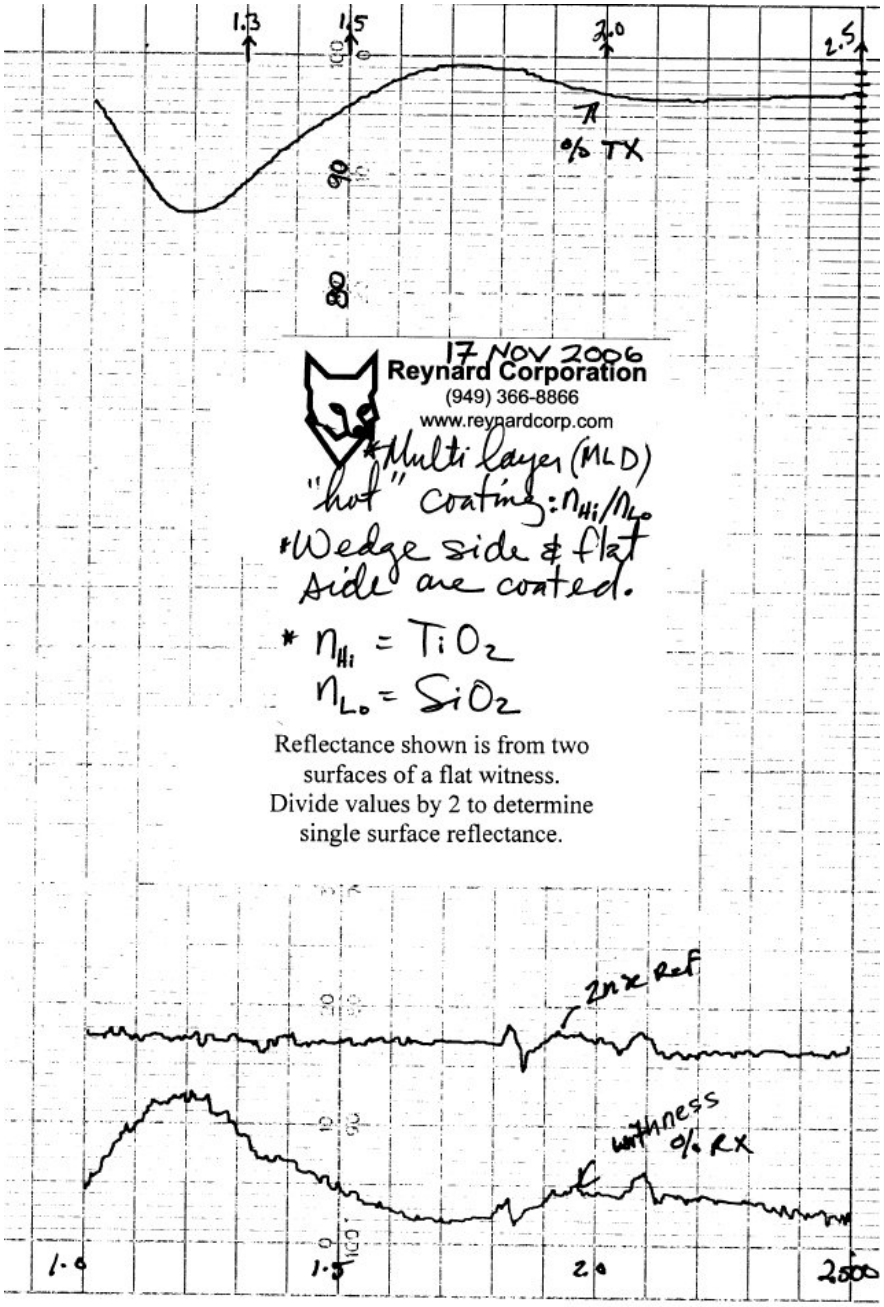


Figure 53: Judson 2.2 μm detector sapphire window coating information.

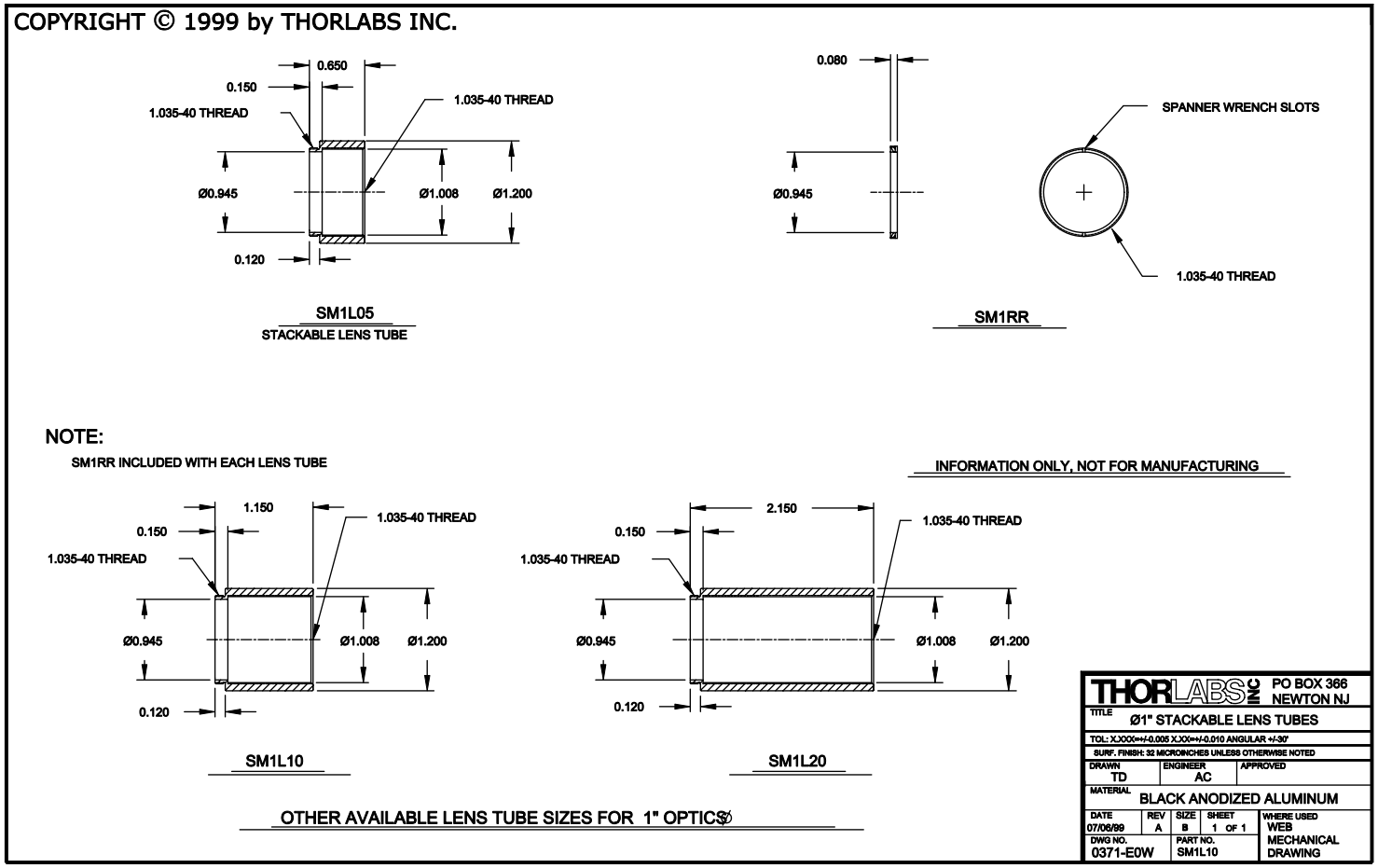


Figure 54: Drawing of the mount for the focusing lens.

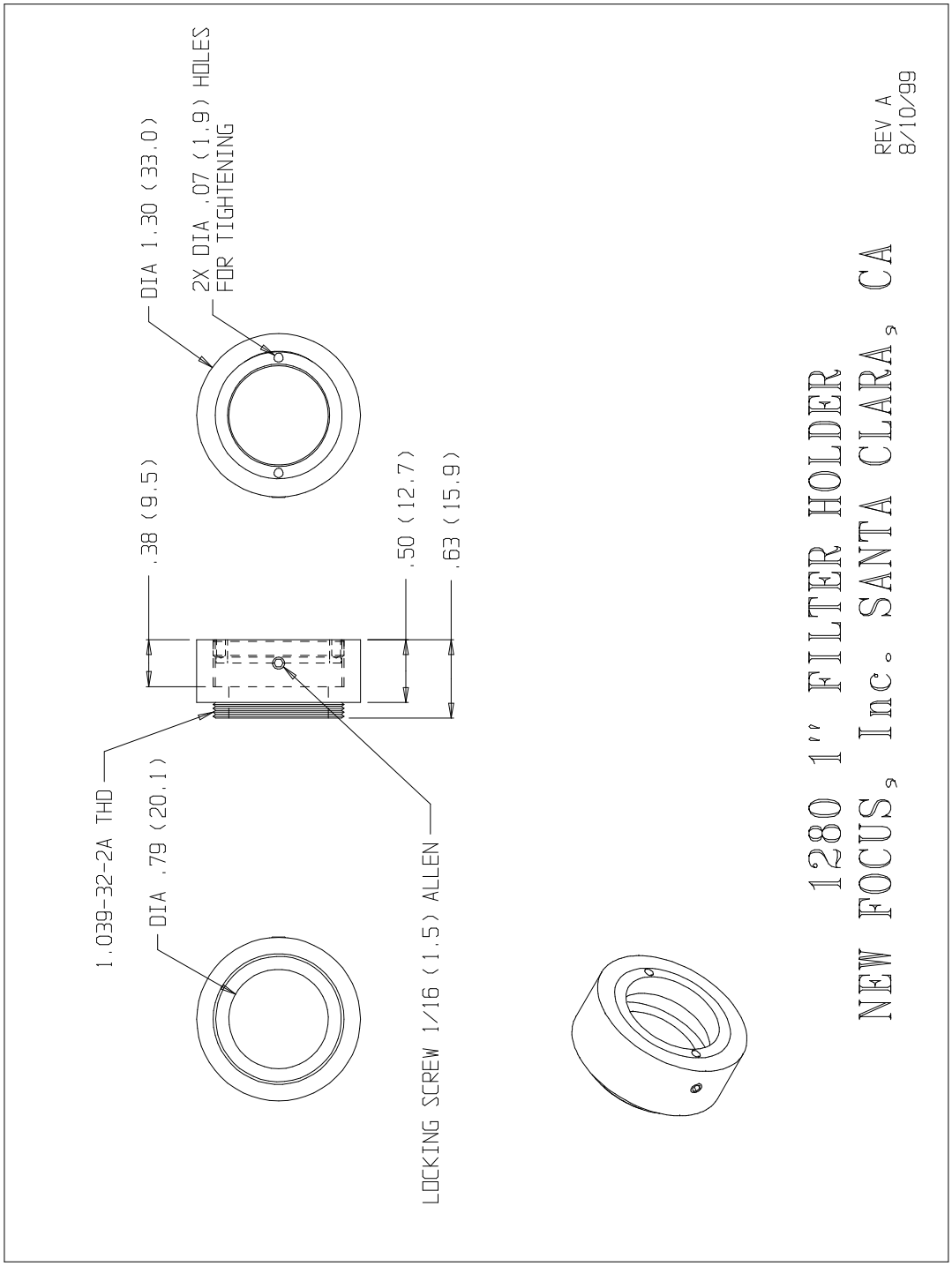


Figure 55: Drawing of the mount for the filter.

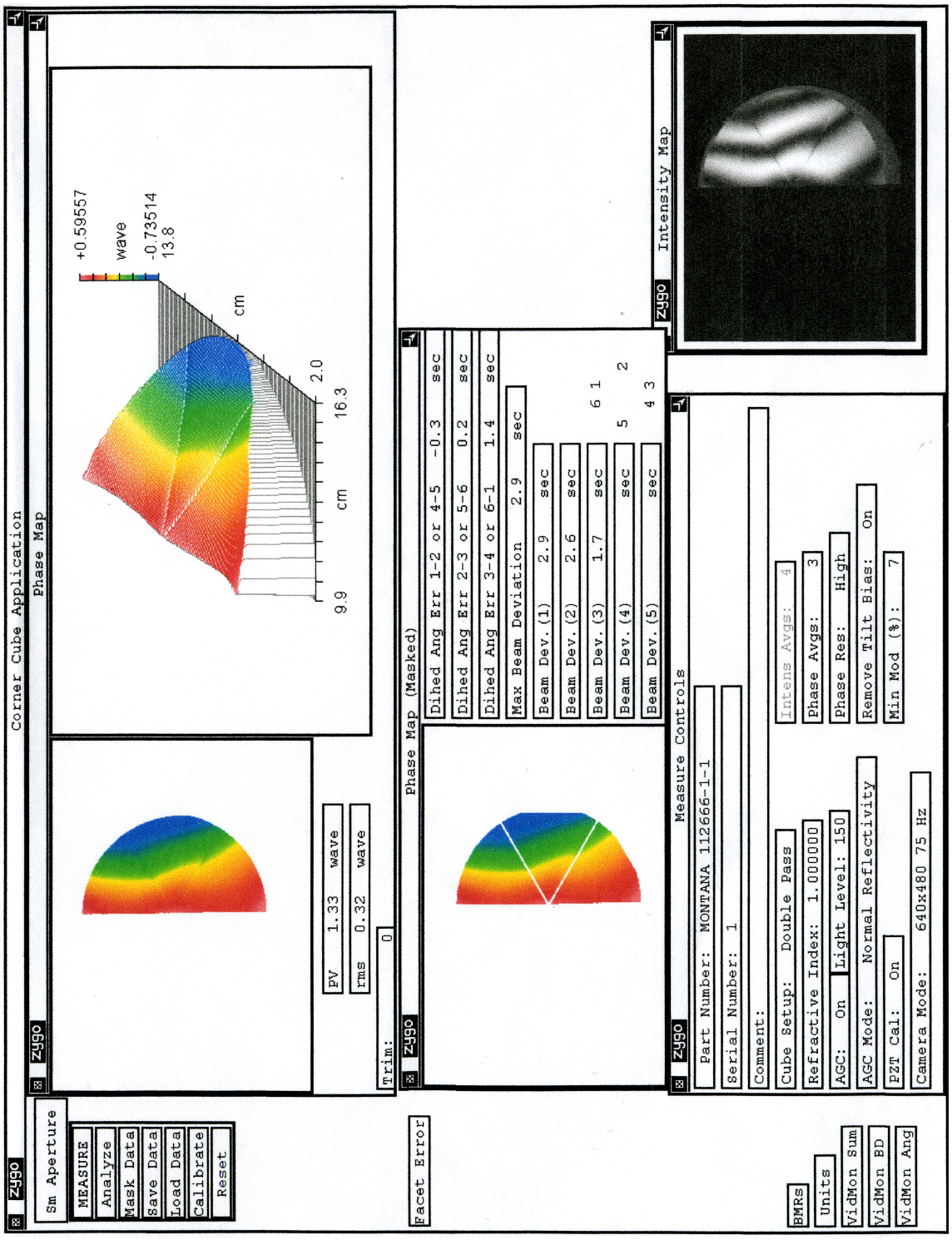


Figure 56: Manufacturer information about the first 5 inch retro-reflector.

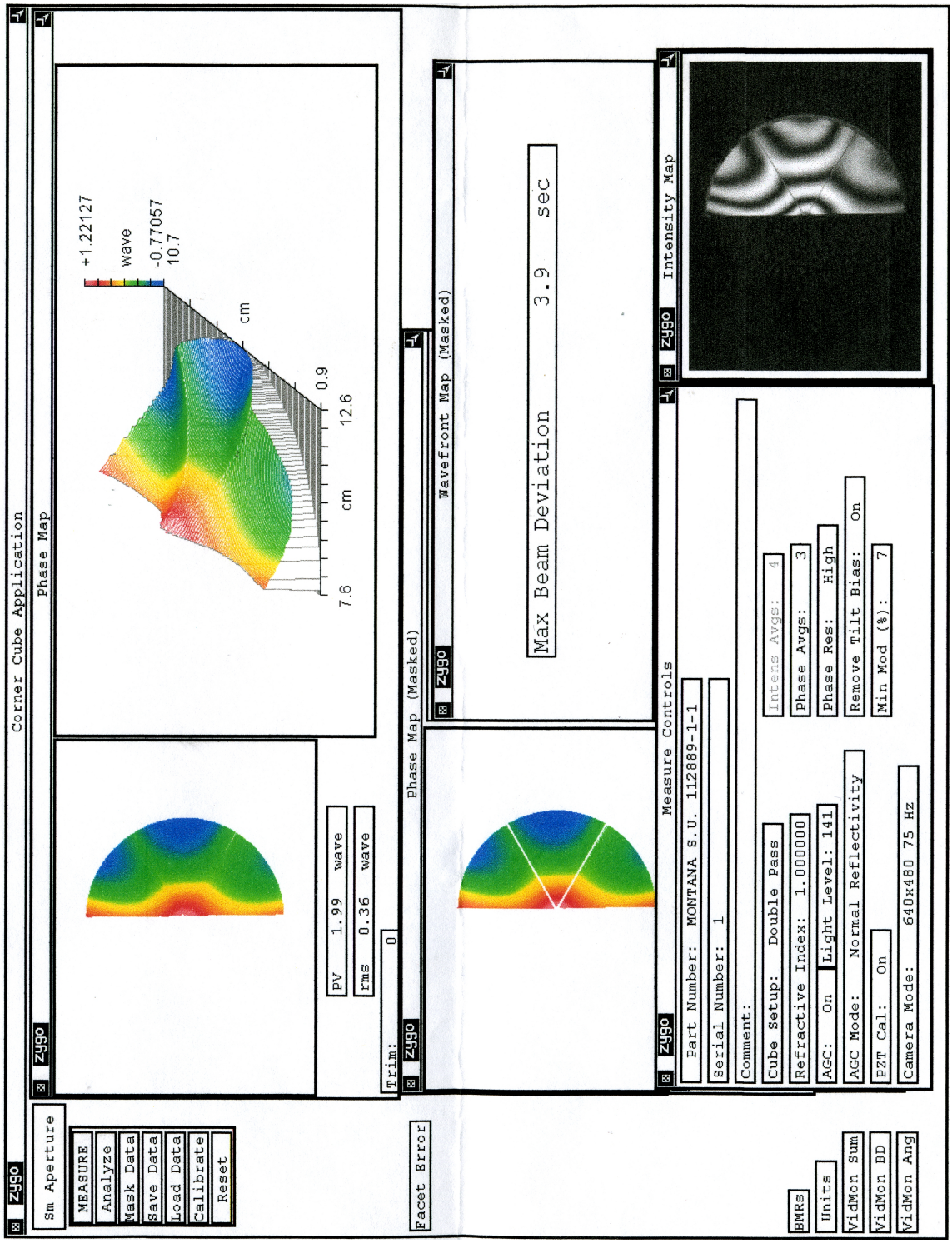


Figure 57: Manufacturer information about the second 5 inch retro-reflector.

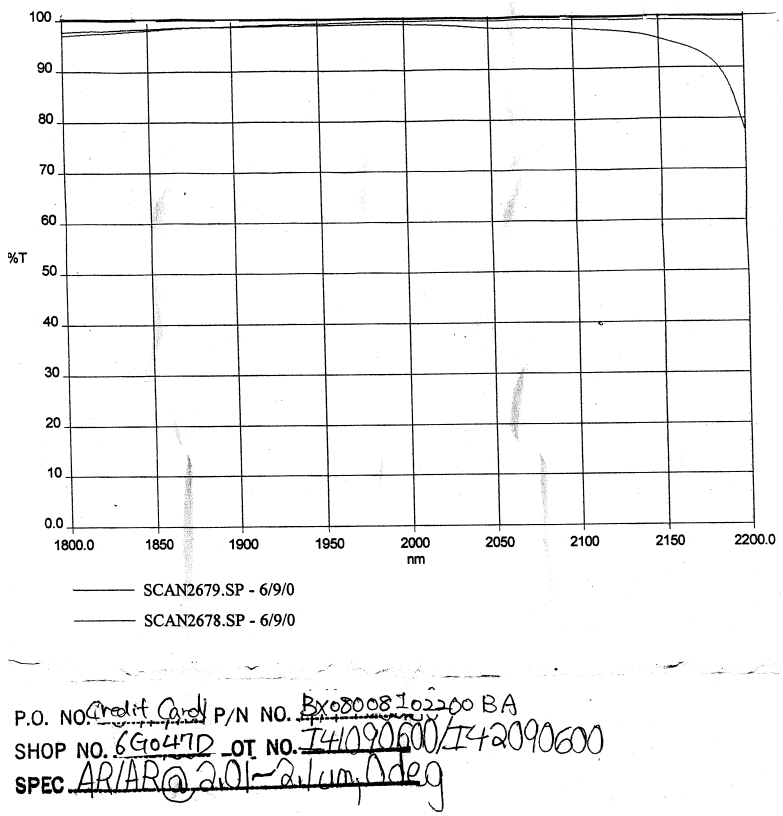


Figure 58: Anti-Reflection coatings on spherical, F/1, 20 mm collimation lens.

APPENDIX C

ANALYSIS ALGORITHMS

Analysis Code

Code for Analyzing Scans



Code for GUI



Code to perform actual Scanning

Code for DAQscanning.m



Code for Making Noise



GUI Figure

 The Matlab GUI to operate the code in Section C

GUI Screenshots

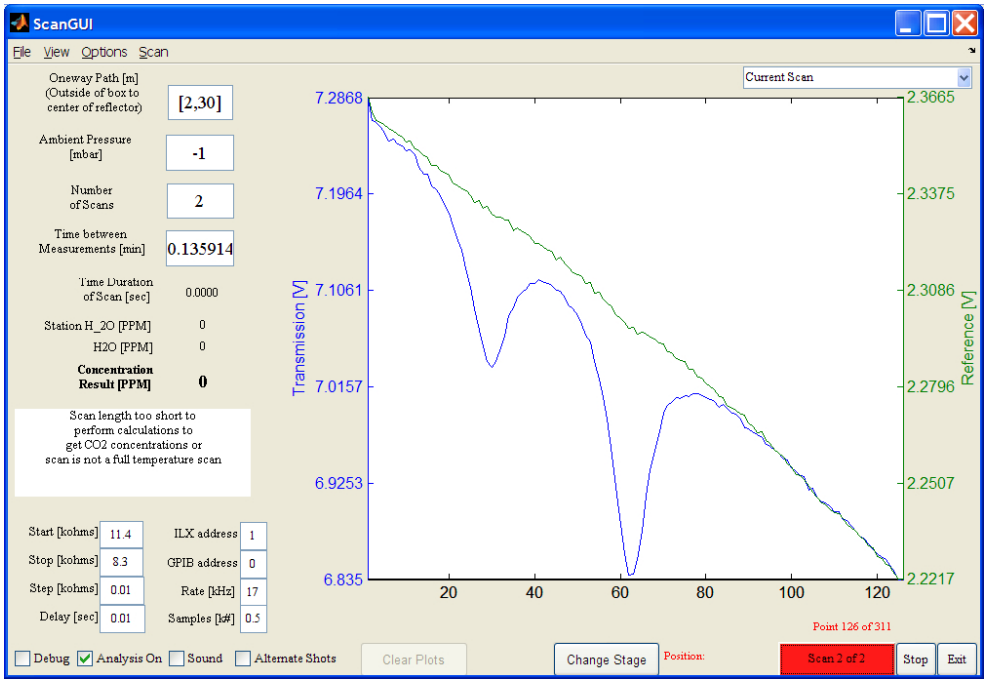


Figure 59: MATLAB GUI screenshot performing a scan.

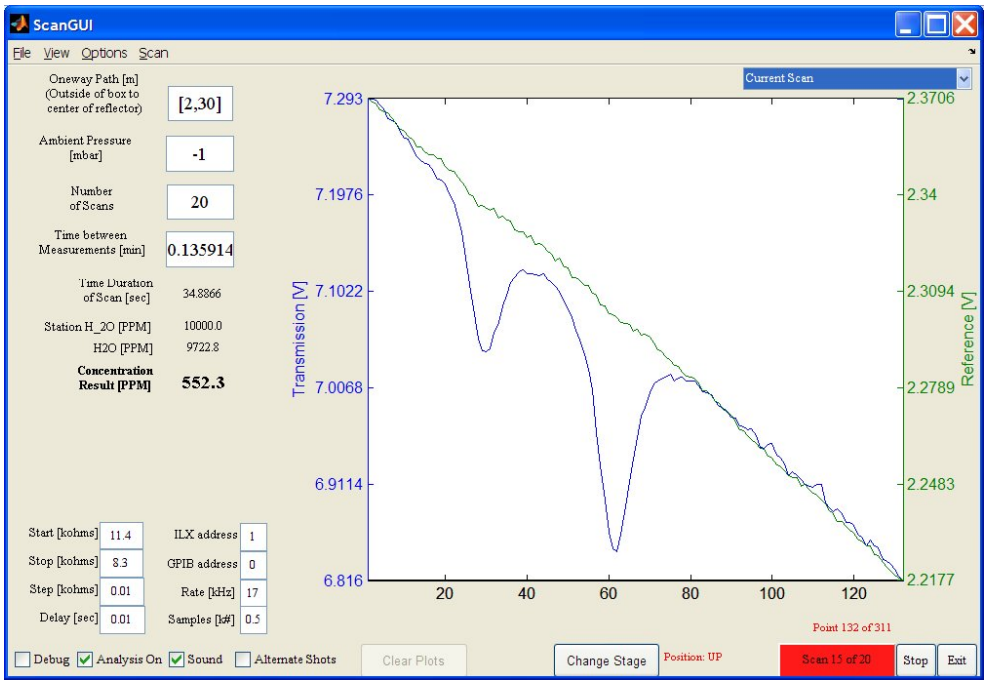


Figure 60: MATLAB GUI screenshot performing a scan.

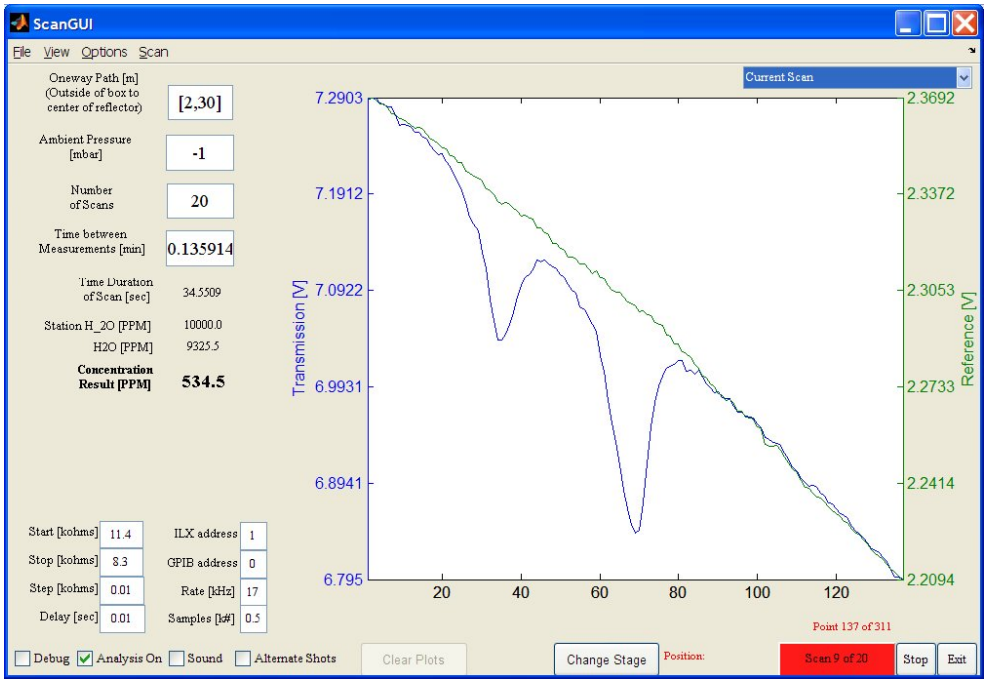


Figure 61: MATLAB GUI screenshot performing a scan.

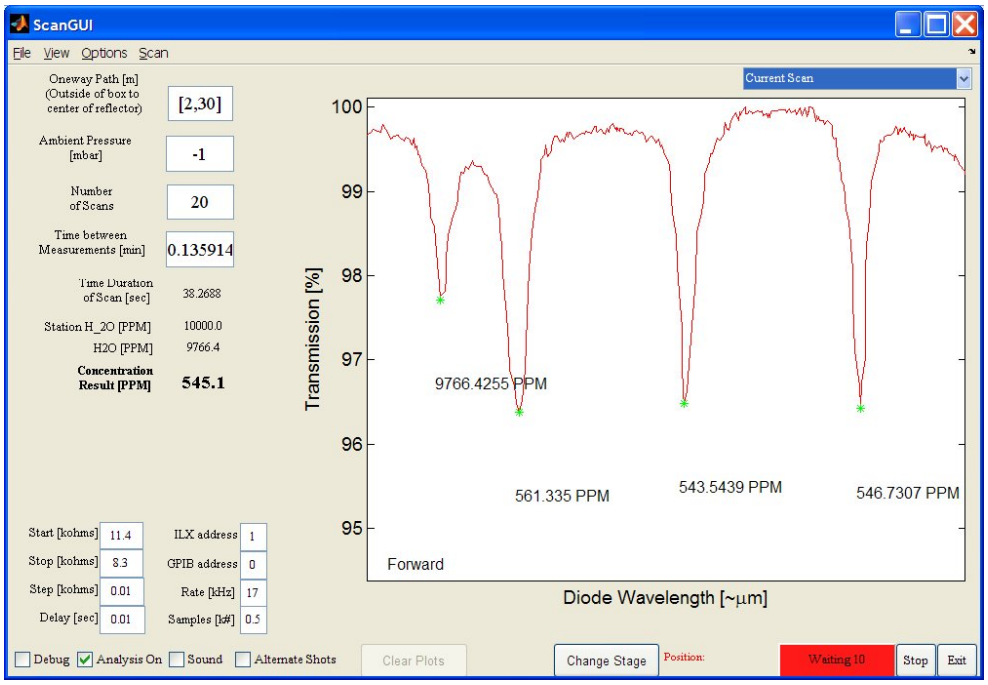


Figure 62: MATLAB GUI screenshot of a completed scan.

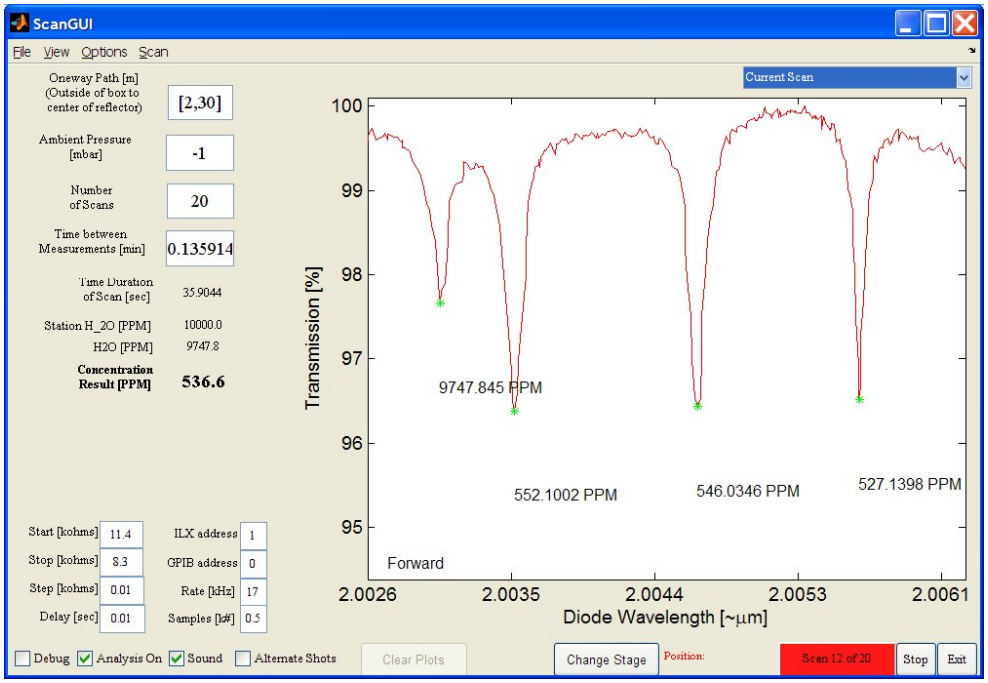


Figure 63: MATLAB GUI screenshot of a completed scan.

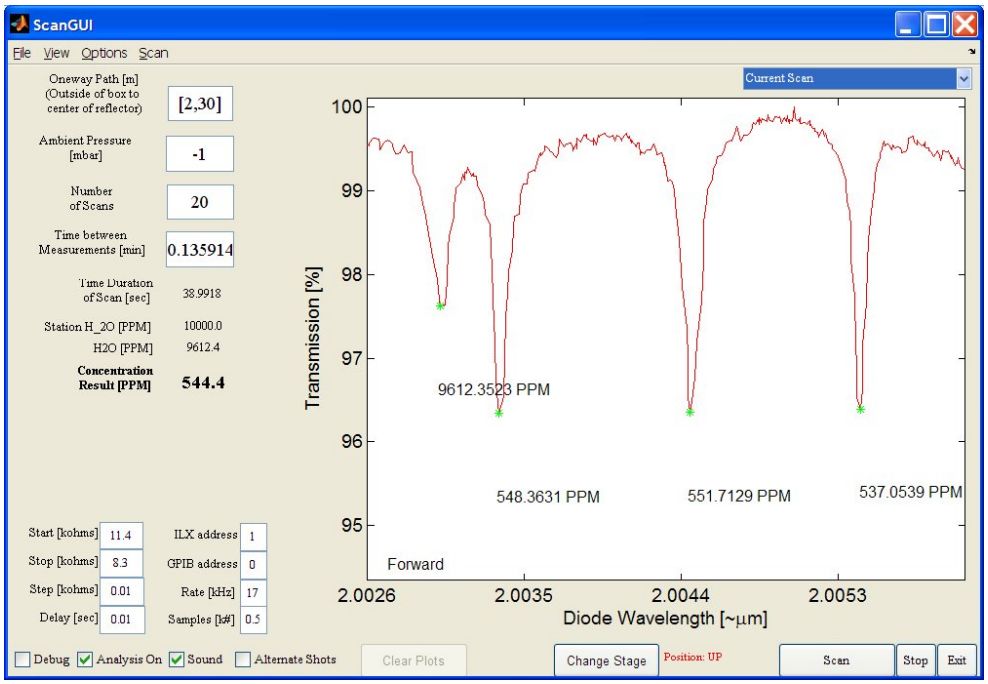


Figure 64: MATLAB GUI screenshot of a completed scan.



Figure 65: MATLAB GUI screenshot of a completed scan.

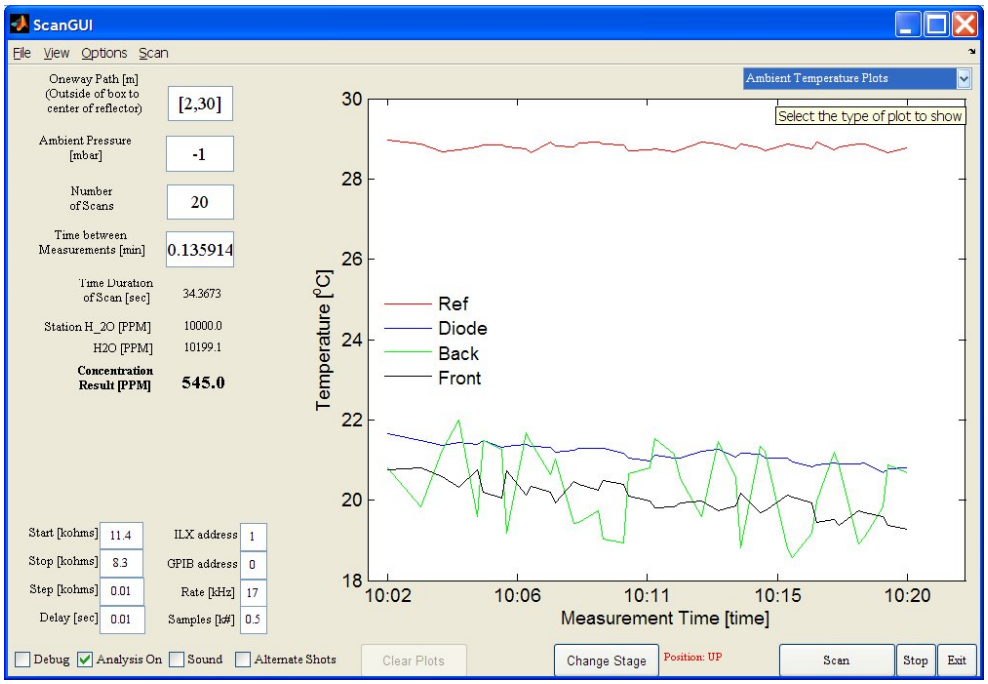


Figure 66: MATLAB GUI screenshot of plotted temperature measurements.

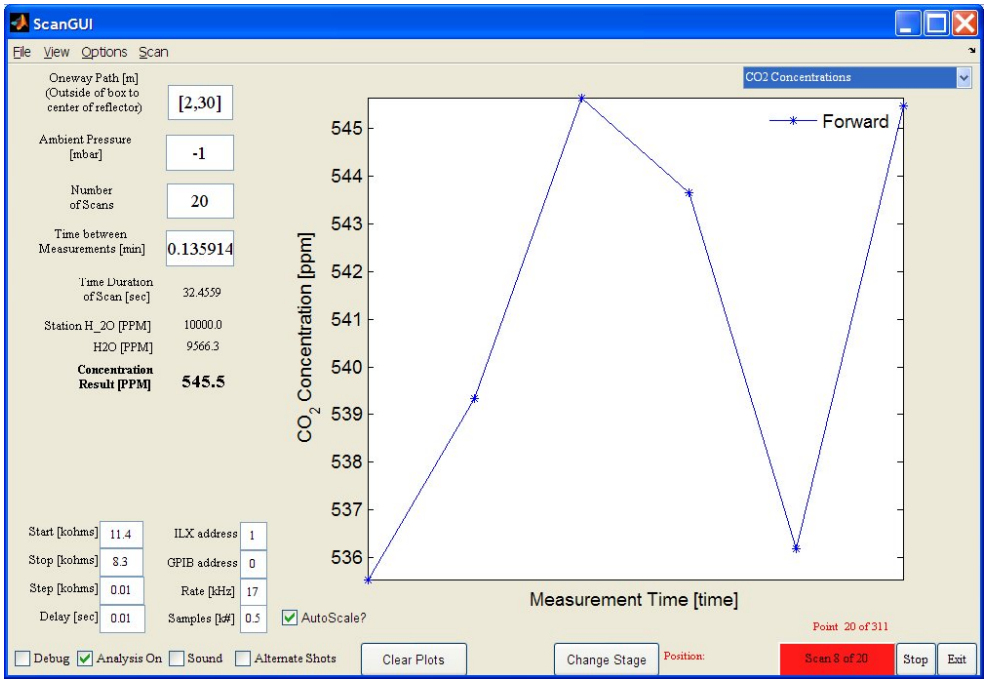


Figure 67: MATLAB GUI screenshot of plotted CO_2 concentration measurements.

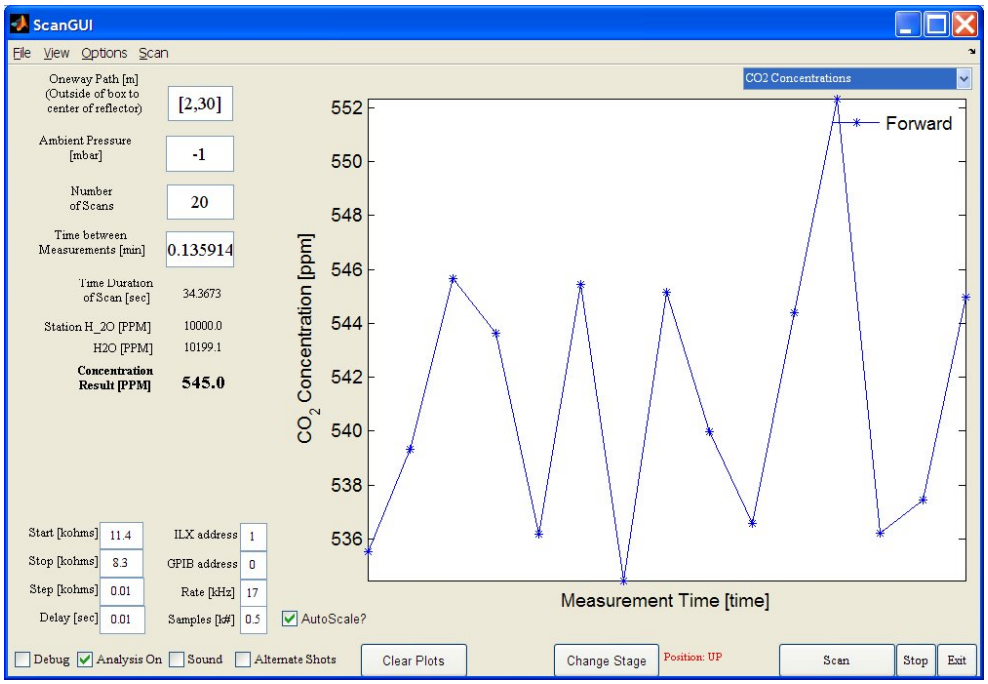


Figure 68: MATLAB GUI screenshot of plotted CO_2 concentration measurements.